Spring 2-2011

A VIRTUAL SUPPLY AIRFLOW RATE METER IN ROOFTOP AIR CONDITIONING UNITS

Daihong Yu
University of Nebraska-Lincoln, daisy.yu926@gmail.com

A VIRTUAL SUPPLY AIRFLOW RATE METER IN ROOFTOP AIR CONDITIONING UNITS

By

Daihong Yu

A THESIS

Presented to the Faculty of

The Graduate College at the University of Nebraska

In Partial Fulfillment of Requirements

For the Degree of Master of Science

Major: Architectural Engineering

Under the Supervision of Professor Haorong Li

Lincoln, Nebraska

Feb, 2011

A VIRTUAL SUPPLY AIRFLOW RATE METER IN ROOFTOP AIR CONDITIONING UNITS

Daihong Yu, M.S.

University of Nebraska, 2011

Adviser: Haorong Li

Virtual sensing technology aims to estimate difficult to measure, expensive, or new quantities by using multifarious mathematical models along with non-invasive and low-cost measurements. Such embedded intelligence is a key to improving the performance of building systems in terms of functionality, safety, energy efficiency, environmental impacts, and costs. Considering the progress that has been achieved over many various fields (e.g., process controls, automobiles, avionics, autonomous robots, telemedicine) within the last two decades, numerous intelligent features have been incorporated and enabled that would otherwise not be possible or economical.

To identify the potential opportunities and research/development needs of virtual sensing technology in building systems,

First, this thesis reviews the major milestones of virtual sensing development in other emerging fields and its formulation of development methodologies.

Second, the state-of-the-art in virtual sensing technology in building systems is summarized as a starting point for its future developments and applications.

After that, a cost-effective virtual supply airflow (SCFM) meter for rooftop air-conditioning units (RTUs) is created by using a first-principle model in combination with accurate measurements of virtual or virtually calibrated temperature sensors (a virtual mixed air temperature sensor and a virtually calibrated supply air temperature

sensor) as a supplementary example. Modeling of the virtual meter, uncertainty analysis, and experimental evaluation are performed through a wide range of laboratory testing in the development. The study reveals that the first-principle based virtual SCFM meter could accurately predict SCFM values for RTUs (uncertainty is ± 6.9%). This innovative application is promising with a number of merits, such as high cost-effectiveness, ease-of-implementation, long-term availability after one-time development, and generic characteristics for all RTUs with gas heating.

Significant research and developments are needed before virtual sensors become commonplace within buildings. It is believed a wealth of virtual sensing derived applications would facilitate the sustainable management and optimize the advanced controls in building systems. It is hoped that this study can provide a resource for future developments.

COPYRIGHT

I hereby declare that I am the sole author of this thesis.

I authorize University of Nebraska-Lincoln, Lincoln, Nebraska, to lend this thesis to other institutions or individuals for the purpose of scholarly research.

I authorize University of Nebraska-Lincoln, Lincoln, Nebraska, to reproduce this thesis by photocopying or by other means, in total or in part, at the request of other institutions or individuals for the purpose of scholarly research.

AUTHOR'S ACKNOWLEDGEMENTS

First and foremost, I would like to gratefully acknowledge Professor Haorong Li for his tireless guidance in my study, research, and personal development. He is knowledgeable, perseverant, and passionate in life and career.

It is also a great honor for me to have Professor James E. Braun as the key committee member who offered much advice and insight throughout my work on virtual sensing technology with his patience and knowledge.

I also sincerely thank my committee members Dr. Siu Kit Lau and Dr. Tian Zhang for their instruction and help. Thank you all!!

TABLE OF CONTENTS

LIST OF TABLES

LIST OF FIGURES

NOMENCLATURE

Roman Letter Symbols

A	area, ft^2 (m^2)
a,c	empirical coefficient
C	discharge coefficient, specific heat, Btu/(lbm·°F) (kJ/(kg·K));
C_{min}	the smaller of C_g and C_a, Btu/(hr·°F) (kW/K)
C_{max}	the bigger of C_g and C_a, Btu/(hr·°F) (kW/K)
C_r	a capacity ratio as C_{min}/C_{max}
D	duct diameter, in (m); discharge dew point temperature, °C (°F)
e	error between $SAT_{lab,meas}$ and $SAT_{mfr,meas}$ (°F, °C)
$e_{C,eva}$	relative error between $\dot{V}_{C,meas}$ and $\dot{V}_{C,model}$
e_{eva}	error between $SAT_{mfr,cal}$ and $SAT_{exp,eva}$ (°F, °C)
e_H	error between $SAT_{th,pred}$ and $SAT_{mfr,meas}$ (°F, °C)
$e_{H,eva}$	relative error between $\dot{V}_{H,meas}$ and $\dot{V}_{H,model}$
EAT	exhaust air temperature (°F, °C)
ET	entering air temperature, °C (°F)
h	enthalpy, kJ/kg (Btu/lbm), heat transfer coefficient, Btu/(h·ft^2·°F) ($kW/(m^2 \cdot K)$)
H	height, ft (m); pump head, fan head, inch H_2O (Pa)
Hstage	heating stage status
h_1	enthalpy of air before the thermal equipment Btu/lbm (kJ/kg)

h_2	enthalpy of air after the thermal equipment Btu/lbm (kJ/kg)
k	slope of the best-fit line geometry constant, thermal conductivity, Btu/h·ft·°F (kW/(m·K))
L	length, ft (m)
LMTD	logarithmic mean temperature difference
m	mass of charge, lbm(kg)
$\dot{m}$	mass flow rate, lbm/min (kg/s)
MAT	mixed air temperature, °C (°F)
MAT_{wb}^{0}	critical point of the mixed air wet bulb temperature, °F (°C)
MOAT	measurement of the manufacturer-installed OAT sensor, ºF (ºC)
MRAT	measurement of the manufacturer-installed RAT sensor, ºF (ºC)
MSAT	measurement of the manufacturer-installed SAT sensor, ºF (ºC)
n	the number of right angle bends
N	number of suction strokes per unit time
NTU	number of transfer units
Nu	Nusselt number
OARH	outside air relative humidity
OAT	outside air temperature, °C (°F)
OADst	outside air damper position
P	pressure
Pr	Prandtl number
$\dot{Q}$	capacity, Btu/hr (kW)

Q	volumetric flow rate, m^3/s
RAT	return air temperature, °C
Re	duct Reynolds number
S	suction dew point temperature, °C (°F)
SHR	sensible heat ratio
SAT	Supply air temperature, °C (°F)
T	temperature, °C (°F)
U	heat transfer coefficient, Btu/(hr·°F·ft²) (kW/(m^2·K))
v	specific volume, ft^3/lb (m^3/ kg), kinematic viscosity, ft^2/s (m^2/s)
V	displacement volume, cfm (m^3), linear velocity, ft/s (m/s)
$\dot{V}$	supply airflow rate, cfm (m^3/s)
w	humidity ratio, speed
W	width, m
$\dot{W}$	compressor power consumption, Btu/h (kW)
X	mass flow rate, power consumption, current, coefficient of performance or compressor volumetric efficiency
ZARH	zoon air relative humidity
ZAT	zoon air temperature, °C (°F)
ΔP	pressure drop
ΔT_{fan}	supply fan temperature rise, ºF (ºC)
$\Delta T_{oa\text{-}ra}$	difference between outdoor and return-air temperature

Greek symbols

β	outside fresh air ratio

ε	heat exchanger effectiveness
η	efficiency
μ	dynamic viscosity of air, lbm/ft·s ($N \cdot s/m^2$)
ρ	density, lb/ft^3 (kg/m^3)

Subscripts

a	air
aie	air stream in the inlet of evaporator
aic	air stream in the inlet of condenser
amb	ambient
aoe	air stream in the outlet of evaporator
aoc	air stream in the outlet of condenser
B	bypasing
c	cooling
ca	condenser air
cal	calibration
ch	charge
comp	compressor
cond	condenser
cycle	refrigerant cycle
d	design
db	dry bulb
dis	discharge
down	downstream

error	bias error
eva	evaluation
evap	evaporator
exp	experimental
fan	supply air fan
g	gas
G	grid
i	inlet
lab	lab-installed
ll	liquid line
loss	heat loss
LCV	leaky check valve
LRV	leaky reversing valve
mfr	manufacturer
max	maximum
meas	measured
min	minimum
model	modeling
normal	normal condition
o	outlet
P	constant pressure
pred	predicted
pump	heat pump

r	ratio
ref	refrigerant
s	supply air, sensible
sc	subcooling
sh	superheat
sp	set point
suc	Suction line
th	theoretical
total	total value
rated	nominal value at rated conditions
up	upstream
v	volumetric
vir	virtual
wb	wet bulb
wb	wet bulb

Abbreviations

AHU	Air handling unit
ANN	Artificial Neural Networks
ARMAX	auto-regressive moving-average time-series model
BF	bypass factor
CAV	Constant air volume
COP	coefficient of performance

DDC	direct digital control
DF	decoupling feature
DX	direct expansion
EMCS	energy management control system
EER	energy efficiency ratio
FDD	fault detection and diagnoses
FP	First principle
FXO	fixed orifice
HVAC	Heating, ventilation and air-conditioning system
IAQ	indoor air quality
MLP	Multi-layer Perceptron
NTU	number of transfer units
PAFM	physical airflow meter
PCA	Principle Component Analysis
RTU	rooftop air conditioning unit
SCFM	supply airflow rate
SVM	Support Vector Machine
TXV	thermal expansion valve
TXV	thermostatic expansion valve
VAV	variable air volume
VHC	virtual heating capacity

Chapter 1 INTRODUCTION

1.1 Background on virtual sensing technology in building systems

Embedded intelligence is a key to improving the performance of systems in terms of functionality, safety, energy efficiency, environmental impacts, and costs. Consider the progress that has been achieved with automobiles within the last two decades. Modern automobiles incorporate many intelligent features, including anti-lock brakes, electronic stability control, tire pressure monitoring, and feedback on fuel efficiency and the need for service. If a car is in need of service, then a technician has access to on-board diagnostic information. In many cases, these advanced features have been enabled through the development of virtual sensors. A virtual sensor estimates a difficult to measure or expensive quantity using one or more mathematical models along with lower cost physical sensors. Fifty years ago, most automobiles provided fuel level and some warning lights using four physical sensors, on average. Today, about 40 relatively low-cost embedded physical sensors are employed along with virtual sensors to optimize driving performance, safety, functionality, and reliability of vehicles (Healy, 2010).

In contrast, building systems rarely provide feedback on energy efficiency or the need for service and generally do not provide optimized controls. In fact, typical information provided to a building owner and occupants, even with a direct digital control (DDC) energy management control system (EMCS), is not significantly better than what was provided 50 years ago. Although the energy efficiency of individual building components has improved significantly (e.g., the rated efficiency of new residential cooling equipment has nearly tripled), the operating efficiency is typically degraded by 20% to 30% due to improper installation/commissioning and inadequate maintenance/repair (CEC, 2008).

One of the reasons that building applications are slower to adopt more automation and intelligent features than automobiles may be that they are not mass produced in factories. For automobiles, automated features are part of an integrated design and their development costs can be spread out over millions of vehicles. For buildings, the cost threshold for advanced features is much higher because buildings tend to be individually engineered. Also, building systems can be very large and complex, serving hundreds of zones with individual controllers and often requiring thousands of sensors to adequately characterize and monitor performance. Therefore, a key to realizing more intelligent features in buildings should be to reduce the cost threshold. Lowering the cost of sensing through the availability of virtual sensors helps in attacking this problem with the potential for providing high level performance monitoring information (e.g., energy efficiency) at significantly less cost. It would also make sense if advanced features were embedded within individual manufactured devices (air handling units, compressors, etc.) rather than being engineered within the control system during the building design phase. In order to realize widespread application, advanced features should be commodities rather than individual engineering projects.

Practically every device within a building could serve as a virtual sensor in addition to providing its intended function. For instance, a fan/motor package could incorporate a model that provides virtual sensing for air flow rate and power consumption using only measurements of static pressure difference and inlet temperature. A compressor could incorporate a map for refrigerant flow rate and input power using physical measurements of inlet and outlet pressure, along with inlet temperature. Valves or dampers could also output flow measurements based on differential pressure and inlet temperature measurements. A “smart” lighting fixture could provide power, lighting, and heat gain outputs based on the input control signal. A “smart” window could provide estimates of heat gain and even solar radiation based on low-cost measurements and a model.

The availability of a rich set of high value sensor information would enable a level of building optimization and improvement not previously possible. Virtual sensors for capacity and power consumption at the device level would allow real-time monitoring of device, subsystem, and whole-building efficiencies. This information could be used along with other virtual sensors to enable diagnosis, tracking, and economic impact evaluation of specific faults. The virtual sensor outputs and embedded models could also be employed within a control optimizer that determines setpoints that minimize operating costs at each operating condition. If all devices incorporated embedded intelligence then there would undoubtedly be a significant amount of redundant information that could use to diagnose sensor faults (e.g., faults within devices providing virtual sensor outputs).

Some might argue that all of the data necessary to provide monitoring, diagnostics, and optimal control could be provided more reliably and robustly using physical sensors. However, virtual sensors have several advantages in addition to lower cost. For example, virtual sensors could be more easily added as retrofits in a number of important applications, such as measurement of refrigerant flow rate or pressure. A physical sensor for refrigerant mass flow would require opening up the system, recovering the refrigerant, installing the sensors, and then recharging the system. The installation of refrigerant pressure sensors would require access to threaded service ports on the equipment, which can cause refrigerant leakage over time (Li and Braun, 2009a). The same refrigerant-side sensor information could be obtained using non-invasive surface mounted temperature sensors along with models.

In some cases, it is very difficult to install physical sensors that can accurately measure a desired quantity. For example, it is very difficult to obtain accurate mixed air temperature measurements at the inlet of cooling coils or evaporators because the compactness of the mixing chamber creates highly non-uniform flow and temperature characteristics. However, an accurate effective mixed air temperature is readily obtained using a model and measurements obtained at other more uniform locations (e.g., coil outlet and/or return and ventilation air streams). In other

cases, it can be impossible to measure some quantities directly. For example, it is currently not possible to directly measure the amount of refrigerant charge within an air conditioner or heat pump.

Virtual sensors have been developed in other fields to obtain measurements indirectly in a cost-effective, non-invasive or/and practical manner, but are only recently the subject of development for building systems. There is no widely accepted definition of virtual sensing. In the context of this thesis, virtual sensing is considered to include any indirect method of determining a measureable quantity that utilizes outputs from other physical and/or virtual sensors along with process models and/or property relations. The primary goals of this thesis are to review the state-of-the-art in virtual sensing in other fields and as applied to building systems, to newly develop a virtual supply air flow (SCFM) meter in rooftop air-conditioning units (RTUs), and to provide some perspective regarding open issues and possible next steps as a starting point for future development and implementation. First, this chapter reviews the major milestones of virtual sensing development in other emerging fields and its formulation of development methodologies.

1.2 Major milestones in virtual sensing development

There has been a rapid development of virtual sensing technology over the past decade within a number of different domains, including avionics, autonomous robots, telemedicine, traffic, automotive, nature and building monitoring and control (Dorst, et al.1998; Hardy and Ahmad, 1999; Hardy and Maroof, 1999; Oosterom and Babuska, 2000; Kestell, et al. 2001; Oza,et al 2005; Srivastava, et al. 2005; Gawthrop 2005; Kabadayi, et al. 2006; Bose, et al. 2007; Ibarg¨uengoytia, et al. 2008; Said, et al. 2009; Raveendranathan, et al. 2009; et al.). In particular, virtual sensing has found widespread applications in process controls and automobiles, so here focuses on these two fields in providing a brief history of notable developments.

1.2.1 Virtual sensing in process controls

"Virtual sensors", also termed "soft sensors", have found widespread applications in process control engineering since the early 1980s. Researchers in process control engineering (Venkatasubramanian et al., 2003a, 2003b, 2003c; Fortuna et al, 2007; Kadlec et al., 2009) use the term virtual sensors to characterize software that includes several interacting measurements of characteristics and dynamics that are processed (fused) together to calculate new quantities that need not be measured directly. Under this definition, well-known software algorithms that are considered to be soft sensors include Kalman filters and state observers or estimators such as electric motor velocity estimators. In process control engineering, virtual sensing is focused on estimating system dynamics or state variables through construction of state observers. Accordingly, virtual sensor development involves representing the whole control system using a mathematical transient model through ordinary or partial differential equations, and then constructing state observers or estimators to estimate non-measured states using mathematical transformation techniques. The transformed estimators or observers are considered to be virtual sensors.

1.2.2 Virtual sensing in automobiles

There have been a large number of virtual sensing developments for automobiles during the past decade. Unlike applications in process control engineering where system dynamics or transient states are of primary interest, the focus for virtual sensing in automobiles has primarily been on determination of steady-state variables. The methods for constructing virtual sensors have been more fragmented and component-oriented. Steady-state models represented by algebraic equations are often used to relate the quantity that is not measured directly to one or more quantities that are directly measured using physical sensors. These steady-state models can be considered to be virtual sensors.

Figure 1 depicts a vehicle that employs ten virtual sensors that have been developed in the past decade to provide increased functionality, safety, and reliability. Table 1 describes the corresponding physical sensor and references for each virtual sensor. For example, virtual sideslip angle and velocity of the centre of gravity sensors play important roles in reducing the potential dangers associated with loss of control of a vehicle. These quantities would be difficult and expensive to measure directly and are estimated using a hyperbolic tangent switching function (Zhang, et al. 2009; Shraim, et al. 2006) that combines available vehicle information (e.g. mass of vehicle, friction coefficient). Another example is the virtual tire pressure sensor. Conventionally, tire air pressure is measured directly using a pressure responsive element located within the tire. However, this construction is complicated and costly. There have been a number of different developments related to tire pressure indication, reflected in more than 40 patents (Gustafsson et al. 2001; Yoshihiro 1998; Takeyasu 1997). A widely studied approach utilizes a Kalman filter to estimate tire pressure in a simple model that uses wheel speed and road friction that are also sensed using virtual observers (Zhang, et al. 2009; Shraim, et al. 2006; Gustafsson, 1997; 1998; 2001). On-vehicle sensors alone do not provide sufficient quality and quantity of information to fulfill all of the evolving vehicle requirements (Röckl, et al. 2008). Virtual sensors have also been developed that utilize car-to-car communication within an intelligent automotive system for a variety of purposes, including cooperative collision and traffic jam warnings. The convergence of multiple virtual sensors has significantly upgraded the intelligence of automobiles over time.

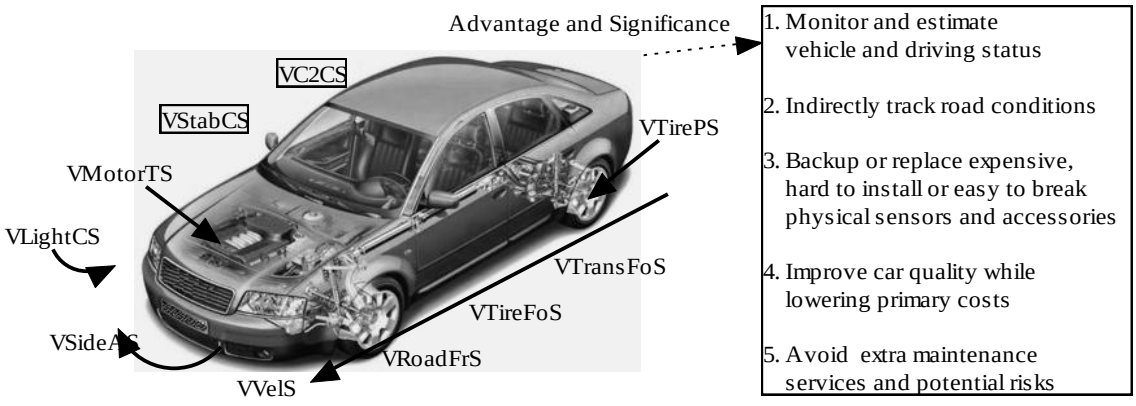

VTirePS-Virtual vehicle tire-air pressure sensor
VTireFoS-Virtual vehicle tire-road forces sensor
VTransFoS-Virtual vehicle transversal forces sensor
VRoadFrS-Virtual vehicle road friction sensor
VSideAS-Virtual vehicle sideslip angle sensor
VVelS-Virtual vehicle velocity sensor
VC2CS-Virtual vehicle car-2-car communication sensor
VMotorTS-Virtual motor combustion timing sensor
VLightCS-Virtual vehicle enhanced lighting preview control sensor
VStabCS-Virtual vehicle stability control sensor

Figure 1: A virtual sensing systemized vehicle

Table 1: Virtual sensing developments in vehicles

Domain	Title of Virtual Sensor	Counterpart	Reference
Automotive: Vehicle	Virtual vehicle tire-air pressure sensor	Pressure sensor, such as piezoelectric	(Gustafsson et al. 2001); (Yoshihiro 1998); (Takeyasu 1997) et al. (more than 40 patents)
	Virtual vehicle tire-road forces sensor	Force sensor, such as strain gauge	(Doumiati, et al. 2009); etc.
	Virtual vehicle transversal forces sensor	Force sensor, such as strain gauge	(Stephant, et al. 2004b)
	Virtual vehicle road friction sensor	Force sensor, such as strain gauge	(Gustafsson, 1997; 1998); (Gustafsson, et al. 2001); etc
	Virtual vehicle sideslip angle sensor	without a corresponding physical sensor	(Zhang, et al. 2009); (Milanese , et al. 2007); (Stephant, et al. 2004a, 2004b, 2007); etc
	Virtual vehicle velocity sensor	Speed sensor, originally developed as virtual sensors	(Zhang, et al. 2009) ,(Shraim, et al. 2006); etc
	Virtual vehicle car-2-car communication sensor	without a corresponding physical sensor	(Röckl, et al. 2008)
	Virtual motor combustion timing		(Holmberg and Hellring 2003)
	Virtual vehicle enhanced lighting preview control sensor		(Lauffenburger 2007)
	Virtual vehicle stability control sensor		(Canale, et al. 2008a, 2008b); (Wenzel, et al. 2007); etc

1.2.3 Use of virtual sensing in other emerging fields

Virtual sensing techniques are penetrating other emerging fields in recent years, including wireless communication, sensor networks, active noise control, and data fusion (Raveendranathan, et al. 2009; Kestell, et al. 2001; Said, et al. 2009). Similar to applications in

automobiles, the primary focus for virtual sensing developments in these emerging fields has been on estimating steady-state variables. However, transient-state variables are also utilized in many virtual sensing schemes, notably in active noise control which uses mechanistic models similar in nature to the process control field. Data-driven modeling methods are more frequently used in the fields of wireless communication, sensor networks and data fusion because the amount of data and information in these fields are very rich. Also, researchers in these fields are more accustomed to applying data processing techniques and less skilled in developing physical models.

Another emerging area for adoption of virtual sensing is the building industry. The development of virtual sensors for building components has lagged other fields, probably because of the fragmented nature of the industry and the emphasis on initial costs. In fact, the concept and potential for "virtual sensing" has only recently been considered for building applications leading to some initial developments (Li and Braun, 2007a; 2007b; 2009a; 2009b).

1.3 Formulation of development methodology for virtual sensing

Virtual sensors are the embodiment of virtual sensing techniques. For the sake of simplicity, the term virtual sensor is used interchangeably with virtual sensing to present development methodology. Although many different types of virtual sensors have been developed, there is no widely accepted definition and no systematic virtual sensing development methodology. It is useful to categorize virtual sensors before attempting to describe general approaches for their development.

1.3.1 Categorization of virtual sensors

Virtual sensors can be categorized, as shown in Figure 2, according to three interrelated criteria that affect development approaches: 1) measurement characteristics, 2) modeling methods, and 3) application.

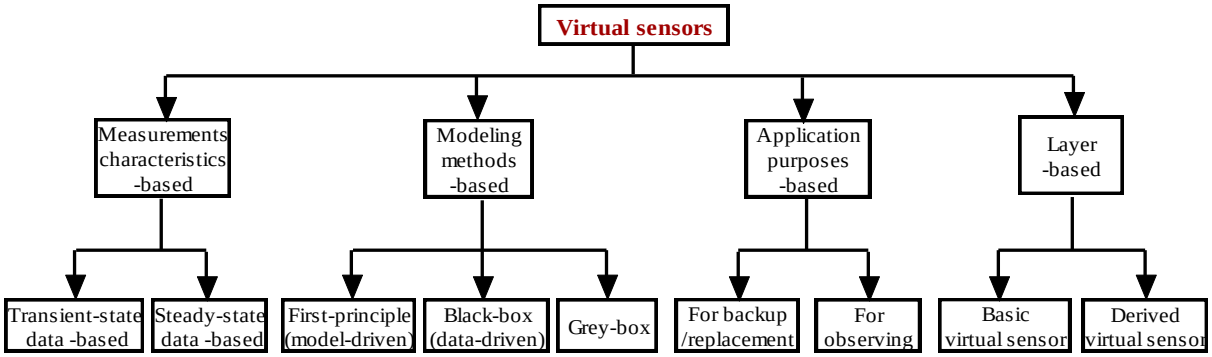

Figure 2: A categorization scheme for virtual sensors

The measurement characteristic category refers to whether the desired virtual sensor outputs are transient or steady-state variables. A transient virtual sensor incorporates a transient model to predict the transient behavior of an unmeasured variable in response to measured transient inputs. This type of sensor would be necessary for feedback control or if transient information were useful in fault identification. For performance monitoring or fault identification it is often adequate and/or desirable to assume that the modeled process is quasi-static. In this case, steady-state models (i.e., with no dynamic terms) are utilized. This modeling is appropriate when the measured input quantities change slowly or the modeled process responds very "quickly" to changes in inputs. Many processes in the food and biochemistry industry, like fermentation processes, utilize transient-state virtual sensors (Rotem, et al. 2000; Kampjarvi, et al. 2008). Transient-state virtual sensors are also very common in the specialty chemistry field (Bonne and Jorgensen 2004). However, steady-state virtual sensors represent the majority of the applications in different fields (Qin 1997; Casali, et al. 1998; Park and Han 2000; Jos de Assis and Maciel Filho 2000; Meleiro and Finho 2000; Radhakrishnan and Mohamed 2000; Devogelaere, et al. 2002; James, et al. 2002.et al.).

With respect to modeling methods, virtual sensors can be divided into three types: first-principle (model-driven), black-box (data-driven), and grey-box virtual sensors. First-principle (physical or white-box) virtual sensors are most commonly derived from fundamental physical

laws and have parameters with some physical significance. For example, DeWolf et al. (1996) developed a virtual slurry polymerization reactor sensor based on a Kalman filter and Prasad, et al. (2002) applied a multi-rate Kalman filter to the control of a polymerization process. For the same application, Doyle (1998) utilized a non-linear observer method. In contrast to first-principle virtual sensors, black-box (data-driven) approaches utilize empirical correlations without any knowledge of the physical process. Examples include multivariate Principle Component Analysis (Gonzalez, 1999; Warne et al. 2004), Partial Least Squares (Frank and Friedman, 1993; Kourti, 2002), Artificial Neural Networks (Poggio and Girosi, 1990; Bishop, 1995) and so on. A grey-box virtual sensor utilizes a combination of physical and empirical models in estimating the output of an unmeasured process (Casali et al. 1998; Meleiro and Finho 2000; James, et al. 2002).

According to application, virtual sensors can be divided into backup/replacement and observing virtual sensors. Backup/replacement virtual sensors are used either to back up or replace existing physical sensors. A backup virtual sensor can provide a check on the accuracy of an installed sensor and even enable virtual calibration. For example, the reliability of temperature sensors is affected by incorrect installation, hostile environmental conditions, or natural drift (ASHRAE, 2009). A replacement application is dictated by cost and reliability considerations, such as the virtual tire-air pressure sensor studied for automobiles (Gustafsson, et al. 2001; Yoshihiro 1998; Takeyasu 1997; et al.). A physical pressure sensor located within the tire is expensive and exposed to high rotational speeds and vibration which over time can lead to unreliable measurements and failure. Within automotive applications, the majority of the existing virtual sensors either back up or replace physical counterparts. In contrast, observing virtual sensors estimate quantities which are not observable (or measurable) directly using existing physical sensors. For example, typically there is no physical sensor to directly determine engine performance. Mihelc and Citron (1984) proposed a virtual engine-performance monitor for determining the relative combustion efficiencies of each cylinder within a multiple cylinder

internal combustion engine using available information (e.g. the position of engine crankshaft). This performance index allows evaluation of test engine fuel distribution stem and ignition system control strategies.

Either backup/replacement or observer sensors can be used for a variety of end-use applications, including performance monitoring, control, and fault detection and diagnostics (FDD). FDD virtual sensors allow flagging of a fault and "measurement" of the fault severity. For instance, a virtual air flow sensor could be a cost-effective replacement for a physical sensor and be used to directly identify a fan or heat exchanger fouling fault. Alternatively, diagnostic fault indicators could be energy rates or other variables that have no physical sensor counterpart. Since the early 1990s, a number of FDD virtual sensors have been studied, such as FDD virtual sensors for a turbo generator (Gomez, et al. 1996) and an ethylene cracking process (Kampjarvi, et al. 2008).

1.3.2 Approaches for developing virtual sensors

Transient-state virtual sensors are typically developed using measurements associated with responses to rapid control changes (e.g. system shut-down or turn-on). The models could be physical, grey-box, or black-box models. Transient physical or grey-box models could be sets of linear or non-linear ordinary differential equations or time-series equations. System identification techniques are employed to determine model order and estimate parameters. Neural networks are sometimes employed as a black-box modeling approach for transient representations, requiring time series data as inputs. A significant amount of training data is typically required to train a transient neural network model. Transient training approaches need to handle batch-to-batch data variations (Nomikos and MacGregor, 1995) that account for the finite and varying duration of the processes, the time variance of the particular batches described by the batch trajectory, the often high batch-to-batch variance, and the starting conditions of the batches (Champagne, et al. 2002). An example of a grey-box transient model is an auto-

regressive moving-average time-series model with deterministic input terms (ARMAX). An ARMAX model was proposed by Casali et al. (1998) for characterizing particle size in a grinding plant. Meleiro and Finho (2000) presented a grey-box transient virtual sensor that is part of a self-tuning adaptive controller of a fermentation process and that utilizes a Multi-layer Perceptron (MLP) approach which is trained using simulated data based on a phenomenological model.

Steady-state virtual sensors are developed using measurements collected while a system is running in an uninterrupted, continuous way. Steady-state virtual sensors use algebraic equations rather than differential or time-series equations and respond instantaneously to time-varying inputs to provide quasi-steady outputs. This is appropriate for many applications and can be combined with steady-state detectors so that the outputs are only utilized under appropriate operating conditions. Steady-state virtual sensors can use physical, grey-box, or black-box models. Steady-state first principle models might incorporate mass balances, force balances, energy balances, and/or rate equations that describe a mechanical, thermal, or chemical process. Black-box models are often multi-variable polynomials or neural networks. An example of a grey-box virtual sensor is a biomass concentration sensor developed for a biochemical batch process (James, et al. 2002) that combines a physical model of a portion of the process with an artificial neural network model.

Black-box models have the potential to provide a more accurate representation than a physical or grey-box model because they have several degrees of freedom to map the measured behavior. However, they require significantly more training data and generally do not extrapolate well beyond the range in which they were trained. There are a number of statistical tools that can be used during the development of black-box models for any application, including Principle Component Analysis (PCA), or more precisely on Hotelling's T2 (Hotelling, 1931) and Q-Statistics (Jackson and Mudholkar, 1979). PCA is one of the most popular tools for developing black-box models for virtual sensors (Jolliffe, 2002). Another popular method is the Self

Organizing Maps or Kohonen Map (Kohonen, 1997), which is a type of artificial neural network. Specific examples of black-box virtual sensors that have been developed include single or multi-regression models (Kresta, et al.1994; Park and Han, 2000), Partial Least Squares (Wold, et al. 2001), Artificial Neural Networks (ANN) (Qin and McAvoy, 1992; Bishop, 1995; Radhakrishnan and Mohamed, 2000; Principe, et al. 2000; Hastie, et al. 2001), Neuro-Fuzzy Systems (Jang,et al. 1997; Lin and Lee, 1996) and Support Vector Machines (SVMs) (Vapnik, 1998).

1.3.3 General steps in developing virtual sensors

A number of studies have been done to define procedures for developing virtual sensors (Park and Han, 2000; Han and Lee, 2002; Warne et al., 2004). In general, the process can be defined in terms of three steps as illustrated in Figure 3 and described in the following paragraphs: (i) data collection and pre-processing, (ii) model selection and training and (iii) sensor implementation and validation.

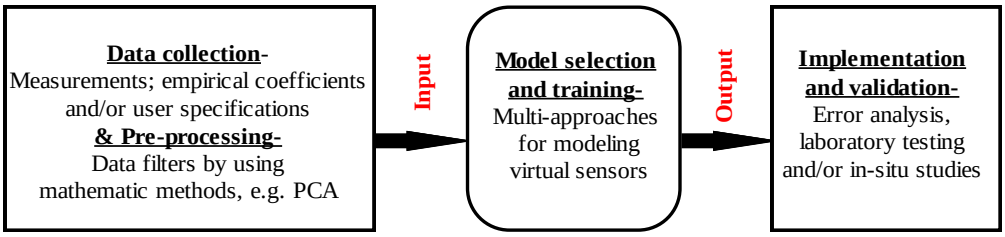

Figure 3: General steps in developing virtual sensors

Proper data collection and pre-processing (pre-filtering or data outliers) is fundamental in the development of accurate and reliable virtual sensor models. The type and range of test data depends on the modeling approach. Transient sensors require transient test data, whereas transient data should be filtered for steady-state modeling approaches. A "steady-state detector" may be used as a pre-processor (Li and Braun 2003b, Wichman and Braun 2009) to eliminate transient data. For black-box models, Principle Component Analysis is a popular approach for pre-processing data in order to aid in the model selection (Serneels and Verdonck, 2008, Stanimirova, et al. 2007 and Walczak and Massart, 1995).

Model selection and training are the most difficult and critical steps in the process of developing a virtual sensor. There are many model types to choose from and each requires a process of determining the proper model order, estimating parameters, and then redefining the model selection/order. The previous section provided an overview of possible modeling approaches. However, there is a bit of an art involved in identifying an appropriate model.

A virtual sensor could be implemented as part of a control or monitoring system or as a standalone sensor with its own hardware, embedded software, and input/output channels. In either case, the virtual sensor implementation needs to be tested in both laboratory and in-situ studies to validate performance and evaluate robustness (e.g., error analysis). Statistical approaches can be used to validate accuracy (e.g., student's t-test Gosset, 1908). It is important to assess the performance using independent data (Hastie et al., 2001; Weiss and Kulikowski, 1991).

With the review of virtual sensing technology development and formulization accomplished above, the state-of-the-art in virtual sensing technology in building systems are studied in Chapter 2 as a starting point for its future developments and applications in building systems. In the meantime, a first-principle (FP) based virtual supply airflow (SCFM) meter for RTUs is created using a white-box model in combination with accurate measurements of low-cost virtual or virtually calibrated temperature sensors (virtually calibrated supply air temperature sensor and a virtual mixed air temperature sensor) as a supplementary example of the study.

1.4 Background on development of a virtual SCFM meter in RTUs

RTUs are widely used for air conditioning retail, residential and industrial premises, covering from small to medium sizes of spaces. The U.S. Department of Energy estimates that RTUs including unitary air-conditioning equipments account for about 1.66 quads of total energy consumption for commercial buildings in the United States (Westphalen and Koszalinski 2001). Knowledge of SCFM through RTUs is certainly of great importance for a number of reasons. For instance, low SCFM directly impairs temperature distribution and causes poor indoor air quality

(IAQ). ASHRAE standard 62.1-2007 specifies ventilation and circulation airflow rate based on the occupancy and floor area. In some cases, low SCFM across the RTUs makes the heating equipment to run on the high temperature limit, leading to intensive heating cycling and energy losses.

In the last two decades, a number of studies have focused on finding good solutions for measuring SCFM (e.g., ASHRAE 41.2, 1987; Howell and Sauer. 1990a, 1990b; Riffat. 1990, 1991; ASHRAE 110, 1995; Palmiter and Francisco, 2000; etc). In terms of physical airflow measuring and monitoring devices, the most popular techniques are based on air dynamic pressure measurements by using a pitot traverse or on air velocity by vane anemometer. However, in general

- *A physical airflow monitoring meter (PAFM) is fragile*

The main disadvantage of PAFM is its flimsy reliability. Periodical calibration is required but rarely followed in real applications. Credibility of measurements would be compromised dramatically after long-term use in adverse duct work surroundings.

- *Implementing and maintaining a PAFM are expensive*

PAFMs are costly in the regards of procurement and installation, ranging from hundreds to thousands dollars. Much more expenses emerge along for maintenance, repair or rebuild, due to the hostile operating environment.

- *Additional pressure loss is incurred*

In order to get accurate measurement, a high air velocity across the instrument is desired for a spread of different airflow rate. To achieve this, a piece of duct work is throttled and it causes additional pressure loss to the fan.

Besides, installing PAFMs in RTUs is even more unrealistic,

- *It is hard to install a PAFM in RTUs.*

RTUs usually have compact structure and duct work. The originally efficient configuration leaves barely any space for a physical meter. PAFMs require more space than is available to measure the true value of SCFM.

- *Relative price of PAFMs over RTUs is high*

The majority of light commercial RTUs falls in the range of 5 tons to 15 tons of cooling capacity and only cost several thousand dollars. However, a decent air flow station plus installation could cost up to one thousand dollars per unit and eat up the cost advantage of RTUs.

Despite the importance of SCFM, it is tough to justify installation of PAFMs in RTUs. To beat the costly and vulnerable PAFMs, a low-cost but accurate virtual SCFM meter is highly needed to solve the dilemma for RTUs. In fact, the SCFM values by indirectly using equipment capacity in combination with temperature change across equipment (an energy balance) have been of great concern over the past decades (ACCA, 1995). However, this method is known to be problematic. For gas furnaces, erratic temperature measurement errors in the supply plenum exist due to non-uniform temperature distribution and intensive thermal radiation, with the resulting estimate of SCFM having a big potential spread (Wray et al. 2002; Yu et al. 2011). Instead, this study develops the virtual SCFM meter which utilizes newly developed low-cost virtual or virtually calibrated temperature sensors to access accurate SCFM values. The primary merit of the proposed virtual SCFM meter is its cost-effectiveness and long-standing accuracy and stability.

Utilizing the virtual SCFM meter as an innovative automated FDD application to enhance the real-time monitoring, control and diagnosis of RTUs is promising. Badly maintained, degraded, and improperly controlled equipment wastes about 15% to 30% of energy used in commercial buildings (Katipamula and Brambley 2005). Based on economic evaluations (Li and Braun 2003a) by applying the automated FDD technique for RTUs to a number of California sites, significant savings: around 70% of the original service cost savings and $5 to $51/kW·year

operating cost savings, were observed. What is more, the payback period of the automated FDD technique mainly derived from low-cost temperature sensors is less than one year (Li and Braun 2007a, 2007b).

1.5 Outline of the thesis

The introductory part, Chapter 1, gives the background on virtual sensing technology in building systems. Major milestones of its notable developments in other fields and the formulation of virtual sensor development are included. After that, background about the general steps in developing a virtual SCFM meter in RTUs is addressed.

In Chapter 2, unique opportunities for virtual sensing in buildings are elaborated firstly. The state-of-the-art in virtual sensing technology in building systems are presented herein covering over thirty virtual sensors for building mechanical systems, building envelope, and occupied zones as a starting point for its future developments and applications in building systems.

A newly developed virtual SCFM meter for RTUs is studied in Chapter 3. The basic mechanism of a virtual SCFM meter is briefly described at first. Modeling of the virtual meter, uncertainty analysis, and experimental evaluation are then systematically conducted for both cooling- and heating-based approaches by using a wide span of laboratory testing data. Comparisons of the two approaches are made based on the involved measurements and calculations. It reveals that the latter one excels the former one in several aspects. After that, detailed implementation issues incorporating measuring and processing the parameters and a graphical implementation flowchart of the heating-based virtual SCFM meter are provided. The study concludes that the non-intrusive virtual SCFM meter can accurately predict the SCFM for RTUs with high robustness.

Chapter 4 provides some perspective regarding open issues of implementation and maintenance of virtual sensing technology in buildings. Meanwhile, future steps of developing an improved virtual SCFM meter are illustrated including improving the virtual calibration method of a SAT sensor in RTUs. After that, conclusions about the virtual sensing technology in buildings and the virtual SCFM meter in RTUs is made.

Chapter 2 VIRTUAL SENSING TECHNOLOGY IN BUILDING SYSTEMS

2.1 Unique opportunities for virtual sensing in building systems

Within a building's life cycle, the majority of the human effort (~90%) is placed on initial design, selection and purchase whereas the majority of the costs (more than 75%) occur during operation. Problems that develop during operation are often ignored as long as comfort is satisfied, leading to inefficient operation (Cisco, 2005). According to CEC (2008), the widespread lack of quality system installation and maintenance can increase the actual HVAC system energy use by 20% to 30%. A number of other investigations have shown energy penalties from 15% to 50% due to faults or non-optimal operations (Katipamula, 2005; Liu et al. 2004). In addition, up to 70% reduction in service costs have been estimated for improved maintenance scheduling (Li and Braun 2007c).

One current approach for improving operational performance is to utilize a manual process of "continuous commissioning". However, this approach has disadvantages compared to continuous monitoring and automated fault detection and diagnostics. First, it is very costly in that it entails bringing specialized engineers to the field to perform inspection, measurement, and evaluation. Second, it is not continuous and is only performed periodically (e.g., every 3-5 years). There has been an increasing trend towards remote monitoring of building systems. However, these monitoring systems do not include intelligence that could provide automated continuous commissioning with automated diagnoses of faults and reports for building operators or service contractors with recommendations and priorities for fixing problems.

Most of the approaches that have been developed for automated diagnostics require a number of measurements that are typically not available within existing monitoring systems or not accurate. For example, for light commercial RTUs with economizers, only zone temperature, outdoor air temperature (and humidity for enthalpy economizers), discharge air temperature, and return air temperature sensors are installed which is not sufficient for typical diagnostic methods (Rossi and Braun, 1997; Li and Braun, 2003b). Furthermore, the return and outdoor air temperature sensors are not typically very accurate and often result in faulty operation of the economizer. The requirement for additional and more accurate sensors has limited the deployment of automated diagnostics because of the additional costs.

Virtual sensing techniques could facilitate the development of more cost-effective and robust diagnostic systems and optimal control. Recently, Li and Braun (2007a, 2007b) proposed some virtual sensors for vapor compression cycle equipment for use as part of fault detection and diagnosis methods. The virtual sensors use low-cost temperature sensors together with manufacturers' rating data to derive measurements which otherwise would be either very expensive or impractical/impossible to obtain directly. The following section provides a review of these virtual sensors along with examples of other developments for buildings that can be considered to be virtual sensors.

2.2 State-of-the-art in virtual sensing in buildings

Table 2 presents a summary of virtual sensor developments with each sensor classified according to the categories previously presented and organized regarding the type of building system component. All of these virtual sensor developments are based on steady-state models using either first-principle or grey-box approaches. In many cases, the authors did not explicitly utilize the terminology virtual sensor, but the models were well developed and meet the criteria for virtual sensors.

Table 2: Virtual sensors in buildings

Building Systems Category			Title of Virtual Sensor	Measurement Characteristics	Modeling Methods	Application	Layer	Reference
Building mechanical systems	Vapor compression air conditioner		Virtual refrigerant charge sensor	Steady-state	Grey-box	Observing	Basic	(Li and Braun 2009a)
			Virtual liquid line pressure sensor		First-principle	Replace /backup		(Li and Braun 2009b)
			Virtual suction line pressure sensor					
			Virtual evaporator pressure sensor					
			Virtual condensing pressure sensor					
			Virtual compressor discharge pressure sensor					
			Virtual refrigerant flow rate sensor		First-principle and Grey-box	Replace /backup	Derived	Li (2004), (Li and Braun 2007a), (Li and Braun 2007b)
			Virtual compressor power consumption sensor		Grey-box	Replace /backup	Basic	
			Virtual equipment energy ratio sensor		First-principle		Derived	
			Virtual compressor coefficient of performance sensor					
			Virtual supply air humidity sensor		First-principle	Replace /backup	Basic	
	Chiller		Virtual overall condenser heat loss coefficient	Steady-state	First-principle	Observing	Basic	(Wang and Cui. 2006; Mclntosh , et al. 2000; (Reddy 2007a,2007b)
			Virtual overall evaporator heat loss					
			Virtual polytropic efficiency of the					
			Virtual reduced evaporator water flow		First-principle	Observing		
			Virtual reduced condenser water flow					
	Heat pump		Virtual check valve leakage for fixed orifice expansion (FXO) device	Steady-state	First-principle	Observing	Derived	(Li and Braun. 2009c)
			Virtual check valve leakage for thermal expansion valve (TXV)device				Basic	
			Virtual reversing valve leakage indicator				Derived	
	Air handling unit	General	Virtual mixed air temperature sensor	Steady-state	Grey-box	Replace /backup	Basic	(Wichman and Braun 2009)
		Cooling/heating coil	Virtual DX cooling coil capacity sensor	Steady-state	Grey-box	Observing	Basic	(Yang and Li, 2010)
			Virtual DX cooling coil sensible heat ratio					
			Virtual DX cooling coil sensible cooling capacity					
		Filter	Virtual filter efficiency sensor	Steady-state	Grey-box	Observing	Basic	(Ward and Siegel 2005)
			Virtual filter bypass low drop sensor					
		Fan/ pump	Virtual supply fan airflow meter	Steady-state	First-principle	Observing	Basic	(Liu, et al. 2007a)
			Virtual return fan airflow meter					
		Other	Virtual pump water flow meter	Steady-state	First-principle	Observing		(Joo, et al. 2007)
	Building envelop and zone systems		Virtual frequency of hot and cold complaints sensor	Steady-state	Grey-box	Observing	Basic	(Federspiel 2000); (Friedman 2004)
			Virtual hot and cold complaints impact sensor					
			Virtual total solar radiation sensor	Steady-state	Grey-box	Observing	Basic	(Seo, et al. 2008)
			Virtual direct solar radiation sensor					
			Virtual diffuse solar radiation sensor					

2.2.1 Virtual sensors used in building mechanical systems

2.2.1.1 Virtual sensors for vapor compression air conditioners

Li and Braun (2007a, 2007b, 2009a, and 2009b) introduced the concept of virtual sensing for application to buildings. Eleven virtual sensors were developed and validated for vapor compression air conditioners with the main purpose of reducing costs for a fault detection and diagnostic method. Figure 4 depicts an air conditioner that employs these eleven virtual sensors. For the most part, the virtual sensors are organized according to the four major components of a typical vapor compression system: compressor, condenser, evaporator and expansion valve. In addition, there is piping between these components, including a discharge line between the compressor and condenser, a liquid line connecting the condenser to the expansion device, and a suction line between the evaporator and compressor. The expansion device is usually located in close proximity to the evaporator with small feeder tubes that distribute refrigerant to individual evaporator flow circuits. The following subsections provide brief descriptions of the development and application of the virtual sensors depicted in Figure 4.

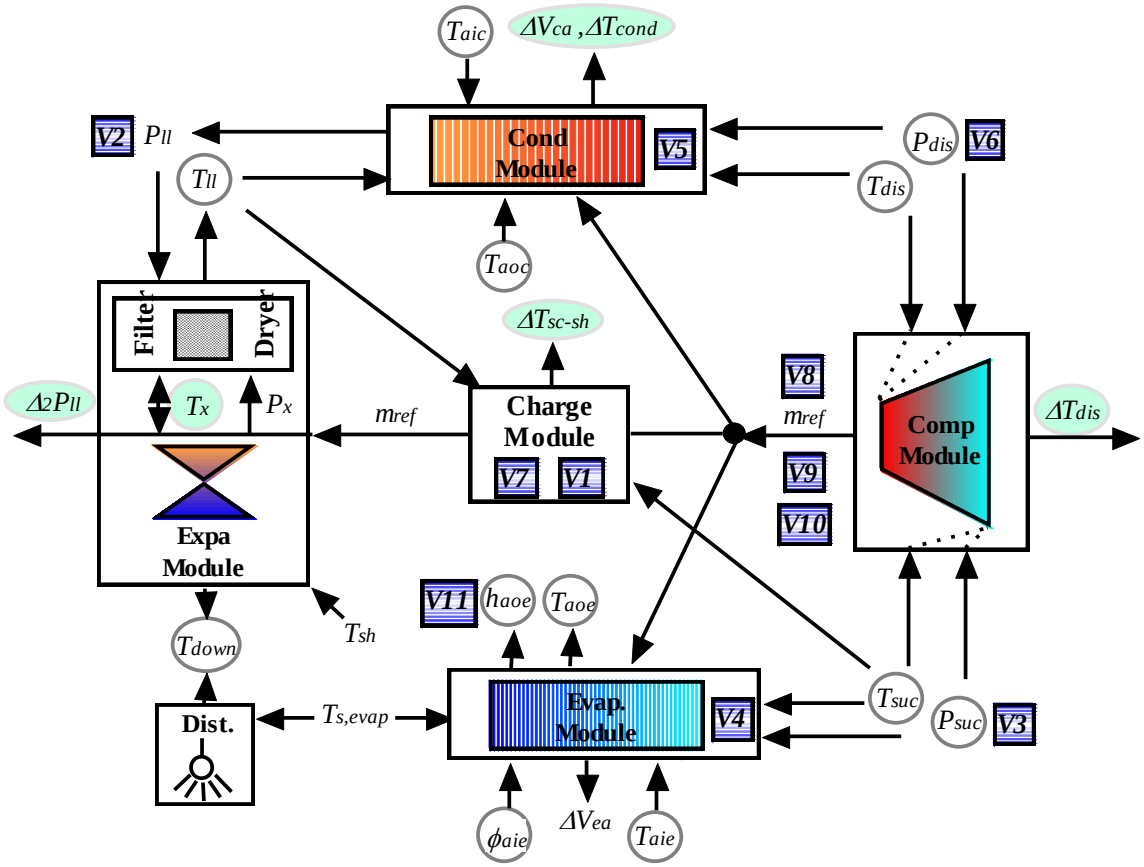

ΔT_{cond}-condenser temperature residual	T_{aoe}-evaporator outlet air temperature
V_{ca}-condenser volumetric air flow rate residual	h_{aoe}-evaporator outlet air humidity
V_{ea}-evaporator volumetric air flow rate residual	T_{down}-expansion device down stream pressure
m_{ref}-refrigerant mass flow rate	T_{suc}-suction temperature
P_{suc}-suction pressure	ΔT_{sc-sh}-charge level feature
T_{aic}-condenser inlet air temperature	ΔT_{dis}-discharge temperature residual
T_{aoc}-condenser outlet air temperature	$\Delta_2 P_{ll}$-liquid line pressure drop residual
T_{dis}-discharge temperature	P_{ll}-liquid line pressure
T_{sh}-suction superheat	ϕ_{aie}-evaporator inlet air humidity
P_{dis}-discharge pressure	T_{ll}-liqid line temperature
P_x-expansion device upstream pressure	T_x-expansion device upstream temperature

Virtual sensors:

V1-Virtual refrigerant charge sensor
V2-Virtual liquid line pressure sensor
V3-Virtual suction line pressure sensor
V4-Virtual evaporating pressure sensor
V5-Virtual condensing pressure sensor
V6-Virtual compressor discharge pressure sensor
V7-Virtual refrigerant flow rate sensor
V8-Virtual compressor power consumption sensor
V9-Virtual system coefficient of performance sensor
V10-Virtual compressor volumetric efficiency sensor
V11-Virtual supply air humidity sensor

Figure 4: Intelligent air conditioner enabled through multiple virtual sensors

Virtual refrigerant charge sensor

Proper refrigerant charge level is critical for a vapor compression system to operate efficiently and safely. A number of studies conducted by separate investigators (Proctor and Downey1995; Cowan 2004) have concluded that more than 50% of the packaged air-conditioning systems in the field have improper refrigerant charge due to improper commissioning, service, or leakage. There is no direct measurement of refrigerant charge besides removing all of the charge and weighing it. Charge tuning is typically accomplished in the field using manufacturers' charge tables that are expressed in terms of measured superheat at the evaporator outlet (T_{sh}) and sub-cooling at the condenser outlet (T_{sc}). However, these specifications are not applicable when faults are present (e.g., low indoor airflow) or under certain operating conditions (e.g., low or high ambient and high or low mixed-air wet-bulb temperatures). In addition, these approaches typically specify utilization of compressor suction and discharge measurements (P_{suc} and P_{dis}) to indirectly determine T_{sh} and T_{sc}. This requires the installation of gauges or transducers, which for a permanent installation could be a potential source of refrigerant leakage.

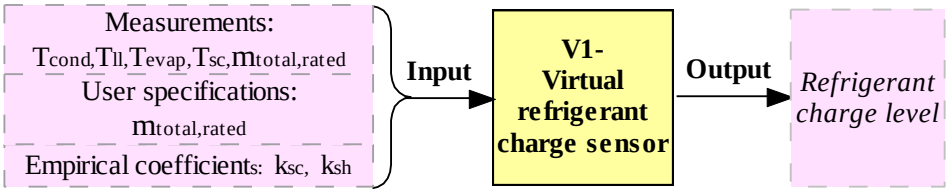

Figure 5: Virtual refrigerant charge sensor

To allow continuous monitoring of refrigerant charge using non-invasive measurements, Li and Braun (2009a) proposed a virtual sensor (depicted in Figure 5) that uses four surface mounted temperature measurements (condensing, liquid-line, evaporating, and suction-line temperature) that are obtained while the system is operating at steady state. The algorithm for estimating refrigerant charge from temperature measurements is given in equations 1 and 2:

$$\frac{m_{total} - m_{total,rated}}{m_{total,rated}} = \frac{1}{k_{ch}} \left\{ (T_{sc} - T_{sc,rated}) - \frac{k_{sh}}{k_{sc}} (T_{sh} - T_{sh,rated}) \right\} \quad (1)$$

$$k_{ch} = \frac{m_{total,rated}}{k_{sc}} \quad (2)$$

Where m_{total} is the total refrigerant charge, the subscript rated denotes rating operating conditions, k_{sc} is a constant that depends on the condenser geometry, and k_{sh} is a constant that depends on the evaporator geometry. The constants k_{sc} and k_{sh} can be estimated using a small amount of experimental data.

The virtual refrigerant charge sensor algorithm has been validated for a range of different systems and over a wide range of operating conditions with and without other faults. In general, the charge predictions are within about 8% of the actual charge. The algorithm could be easily implemented at relatively low cost as part of a permanently installed control or monitoring system to indicate charge level and/or to automatically detect and diagnose low or high levels of refrigerant charge.

Virtual refrigerant pressure sensors

Refrigerant pressures are useful for monitoring, control and diagnostics in a vapor compression system. For several diagnostics algorithms, refrigerant pressures are used to determine evaporating and condensing temperatures, liquid line sub-cooling, and suction line superheat. However, both the hardware and installation are expensive for permanent installations. Installation requires a brazed connection. For field installations, the refrigerant has to be evacuated and recharged, which is costly. Moreover, if the connection is made using available threaded service ports on the compressor, then it is likely that refrigerant will leak over time. Virtual refrigerant pressure sensors (Li and Braun, 2009b) have significantly lower hardware and installation costs and are non-invasive.

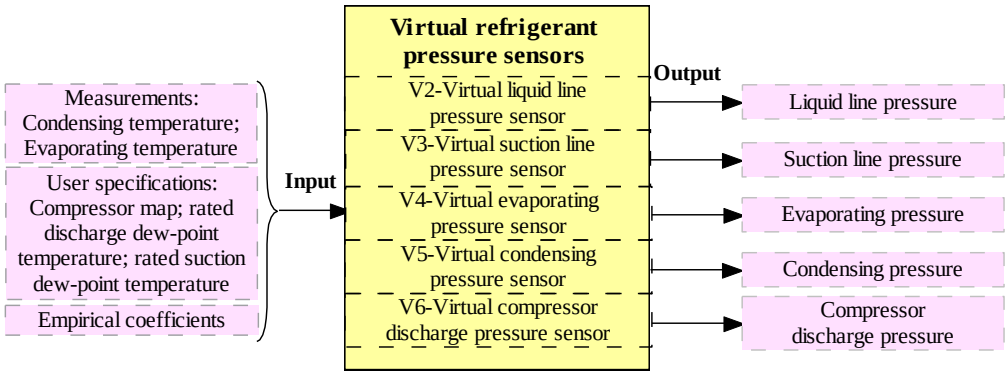

Figure 6: Virtual refrigerant pressure sensors

Figure 6 shows the inputs and outputs for the virtual sensors. The only physical measurements that are required are saturation temperatures in the evaporator and condenser. These measurements should be located in the middle of these heat exchangers where the refrigerant is two-phase at all expected operating conditions. The sensors could be attached to return bends and insulated. Virtual pressure measurements for these locations are determined using refrigerant property relations. Virtual sensors for refrigerant pressures at the inlets and outlets to the heat exchangers are then determined using models for pressure drop. Therefore, the development of virtual pressure sensors requires testing to identify the appropriate locations for saturation temperature measurements and to develop specific correlations for pressure drop. Extensive laboratory data has been collected for a range of different systems to validate the accuracy of virtual refrigerant pressure sensors. Typically, virtual pressure sensor outputs are within an uncertainty of ±4.4 % when properly calibrated.

Virtual pressure sensor outputs can be used in combination with other virtual sensors to provide a wealth of information for monitoring and diagnostics. For instance, virtual suction and discharge pressure sensors can be used along with suction temperature and compressor maps to estimate compressor flow rate and power. This information can be used to estimate real-time capacity and COP information.

Virtual refrigerant flow rate sensor

Refrigerant flow rate is a very valuable measurement for performance monitoring and diagnostics. However, it is too expensive to measure directly and can be unreliable when the condenser exit condition is a two-phase mixture. Li and Braun (2007a) proposed two approaches for estimating refrigerant flow rate from other measurements that are part of the virtual sensor as illustrated in Figure 7.

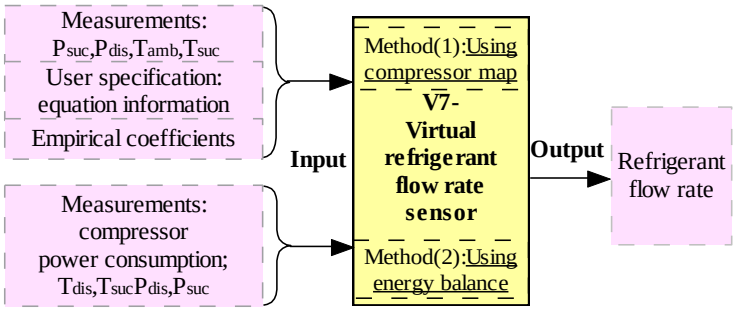

Figure 7: Virtual refrigerant flow rate sensor

The method 1 illustrated in Figure 7 uses data from a compressor manufacturer to determine a correlation for volumetric efficiency and uses it to determine mass flow rate according to:

$$\dot{m}_{ref,normal} = \eta_v \frac{NV}{v_{suc}} \tag{3}$$

Where N is the number of suction strokes per unit time, V is the displacement volume, v_{suc} is the suction line refrigerant specific volume, and η_v is volumetric efficiency. Li and Braun (2002) proposed the following empirical form for correlating volumetric efficiency

$$\eta_v = a_0 + a_1 \frac{P_{dis}}{P_{suc}} + a_2 \left(\frac{P_{dis}}{P_{suc}}\right)^2 + a_3 (T_{amb} - T_{suc})^{a_4} \tag{4}$$

Where the a's are empirical coefficients, P_{suc} and P_{dis} are suction pressure and discharge pressure that can be measured using virtual refrigerant pressures, T_{suc} is suction temperature, T_{amb} is compressor ambient temperature. Additionally, T_{aoc} (when the compressor is located in the

condenser outlet air stream) or T_{aic} (when the compressor is not directly in the condenser outlet air stream) can be used to replace T_{amb}, if it is not directly measured.

Mass flow rate determined using a compressor map is only valid if the compressor is working properly. However, a redundant mass flow measurement can be determined using the following energy balance on the compressor (method 2)

$$\dot{m}_{ref} = \frac{\dot{W} - \dot{Q}_{loss}}{h_{dis} - h_{suc}} \tag{5}$$

Where $\dot{Q}_{loss}$ is compressor heat loss rate (J/kg) is, $\dot{W}$ is measured compressor power consumption (kW), h_{dis} (T_{dis}, P_{dis}) and h_{suc} (T_{suc}, P_{suc}) are the discharge line and suction line refrigerant enthalpy (J/kg). This method was shown to work well for both normal and faulty compressor operation.

The map-based method is more accurate when the compressor is operating normally and can be used to calibrate the energy-balance method. If a fault is identified for the compressor, then the energy-balance approach can be used. Neither approach will work well if a two-phase refrigerant condition exists at the inlet to the compressor.

Virtual compressor power consumption sensor

Compressor power consumption is a very useful index in monitoring, control and diagnostics for vapor compression cycle systems. However, physical measurements for it would be expensive. Figure 8 depicts a virtual compressor performance sensor that only requires temperature measurements.

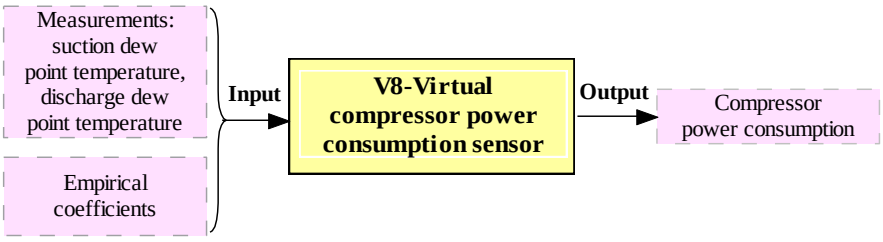

Figure 8: Virtual compressor power consumption sensor

According to ANSI/ARI Standard 540-1999, compressor manufacturer's map can be represented as a 10-coefficient polynomial equation in the form of

$$X = c_1 + c_2 S + c_3 D + c_4 S^2 + c_5 SD + c_6 D^2 + c_7 S^3 + c_8 DS^2 + c_9 SD^2 + c_{10} D^3 \quad (6)$$

Where the c's are empirical coefficients, S is suction dew point temperature, D is discharge dew point temperature, and X can be mass flow rate, power consumption, current, coefficient of performance (COP) or compressor volumetric efficiency (η_v).

These compressor map models are developed with the compressor operating under fault-free conditions. However, Li and Braun (2007a) found that the predictions of compressor power consumption using this model format match measurements within ± 5% even in the presence of multi-faults (e.g. compressor leakage, condenser fouling, evaporator fouling). This model can be used as a virtual compressor power consumption sensor.

Virtual system performance sensors

The evaluation of system performance degradations using energy efficiency ratio (EER) or coefficient of performance (COP) is crucial. However, so far, no such physical "efficiency" sensor has been developed and produced. Li (2004) proposed a method to obtain EER and COP using virtual sensors illustrated in Figure 9.

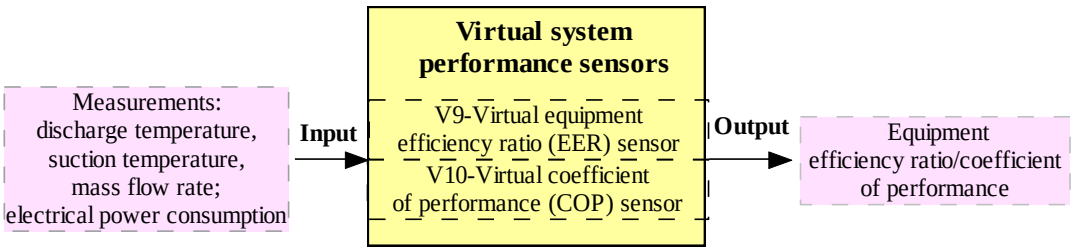

Figure 9: Virtual system performance sensors

EER and COP are equivalent parameters that differ by a unit conversion factor, with either quantity expressed as

$$EER = \frac{\dot{Q}_c(\dot{m}_{ref}, T_{dis}, T_{suc})}{\dot{W}} \quad (7)$$

Where $\dot{Q}_c$ is equipment cooling load that is determined using measurements of $\dot{m}_{ref}$, T_{dis} and T_{suc}, and $\dot{W}$ is the equipment electrical consumption. The quantities $\dot{m}_{ref}$ and $\dot{W}$ can be determined using the virtual mass flow rate sensor and virtual compressor power consumption sensor described previously. Both virtual sensors work very well (Li 2004; Li and Braun 2007a) under most realistic conditions.

Virtual supply air humidity sensor

Supply air humidity is rarely measured in building applications but is useful in estimating coil latent loads and as input for fault detection and diagnostic methods. Li and Braun (2007a) presented a virtual supply air humidity senor that is based on the use of a simple bypass factor model. Figure 10 shows an input/output flow diagram for the sensor.

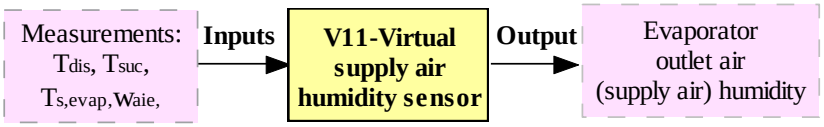

Figure 10: Virtual supply air humidity sensor

The bypass factor, BF, is defined as follows

$$BF = \frac{h_{aoe} - h_{s,evp}}{h_{aie} - h_{s,evp}} = \frac{w_{aoe} - w_{s,evp}}{w_{aie} - w_{s,evp}} \quad (8)$$

Where h_{aoe}, h_{aie}, and $h_{s,evap}$ are evaporator outlet air (supply air) enthalpy, evaporator inlet air (mixed air) enthalpy and saturated air enthalpy at the evaporator surface temperature ($T_{s,evap}$), respectively; w_{aoe}, w_{aie}, and $w_{s,evap}$ are supply air humidity ratio, evaporator inlet air (mixed air) humidity ratio and saturated air humidity ratio at the evaporator surface temperature ($T_{s,evap}$), respectively. Figure 11 illustrates the bypass factor analysis on a psychrometric chart. It can be shown that,

$$\frac{w_{aoe} - w_{s,evap}}{w_{aie} - w_{s,evap}} = \frac{T_{aoe} - T_{s,evap}}{T_{aie} - T_{s,evap}} \quad (9)$$

Where T_{aoe} and T_{aie} are supply air temperature and mixed air temperature, respectively. Substituting Equation (9) into (8),

$$BF = \frac{T_{aoe} - T_{s,evap}}{T_{aie} - T_{s,evap}} \quad (10)$$

With measurements of T_{aoe}, T_{aie}, and $T_{s,evap}$, BF can be calculated for wet coil conditions using Equation (10) and then outlet humidity ratio can be estimated according to:

$$w_{aoe} = BF(w_{aie} - w_{s,evap}) + w_{s,evap} \quad (11)$$

Where w_{aie} is measured and $w_{s,evap}$ is derived from a measurement of evaporator surface temperature $T_{s,evap}$.

Generally, evaporator inlet (mixed) air humidity sensors tend not to be permanently installed in building mechanical systems because of issues of cost, accuracy, and reliability. Direct measurements of a mixed air humidity can be very inaccurate due to non-uniform air conditions caused by mixing within a small chamber of return and ventilation air that are at very different conditions. In addition, humidity sensors are sensitive to dust and dirt and can often fall out of calibration. As a result, there is a need for a virtual sensor for mixed air humidity. Wichman and Braun (2009) presented a virtual mixed air temperature sensor (described later in this study) that could be the basis for the development of a virtual mixed air humidity sensor.

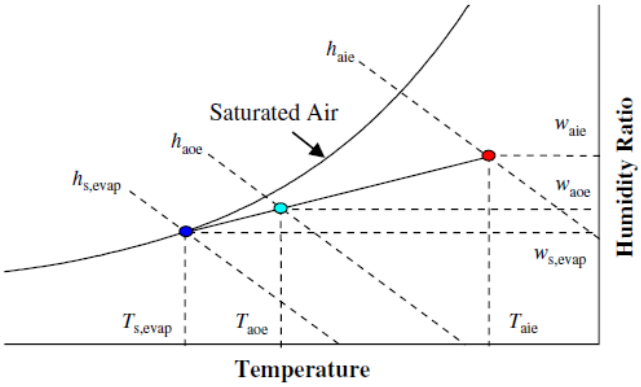

Figure 11: Illustration of bypass factor analysis

2.2.1.2 Virtual sensors for chillers

A number of independent studies (Wang and Cui. 2006; Mclntosh , et al. 2000; Reddy 2007a,2007b; et al.) have focused on identifying common faults occurring in chillers using low-cost measurements. A number of virtual sensors were developed that are listed in Figure 12.

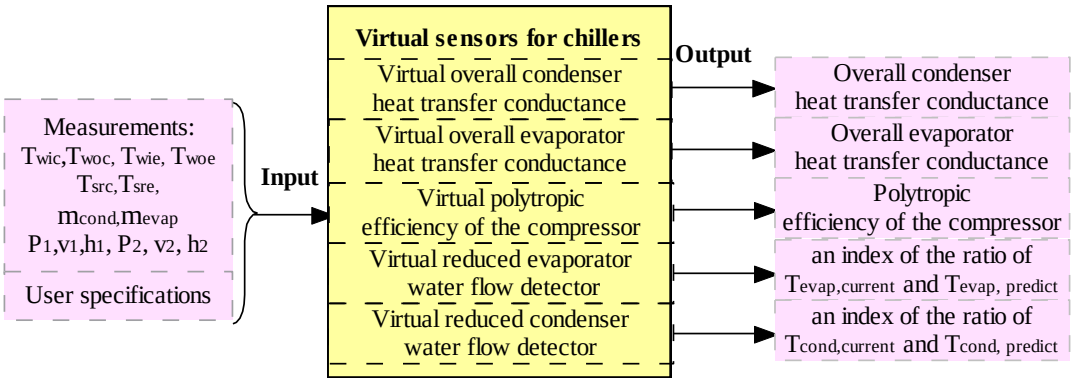

Figure 12: Virtual sensors for chillers

The sensor outputs could be useful for monitoring and as part of a fault diagnoses scheme. For instance, the evaporator and condenser heat transfer conductances could be used to monitor overall performance of the heat exchangers. In order to utilize these indices for fault identification, it would be necessary to correlate normal conductance values in terms of operational conditions (e.g., flow rates) and to establish thresholds for faulty performance. For water side fouling, virtual indices for relative reduction in water flow could be used directly to indicate a change from normal performance. Compressor performance could be monitored using

a virtual polytropic efficiency determined from inlet and outlet state measurements. However, in order to utilize this performance index in a fault detection scheme, it would be unnecessary to correlate normal performance and set appropriate thresholds. There are many more opportunities to develop virtual sensors and related fault detection and diagnosis schemes for chillers.

2.2.1.3 Virtual sensors for heat pumps

Virtual sensors that have been developed for air conditioners (Li and Braun, 2007a, 2007b, 2009a, 2009b) generally apply to heat pumps and can be used to diagnosis faults. However, there are some additional faults that are exclusive to heat pumps, such as reversing valve leakage and check valve leakage that require unique virtual sensors. Li and Braun (2009c) proposed and tested virtual sensors (shown in Figure 13) for identifying these two faults. Equation (12) represents a virtual check valve leakage sensor for systems that incorporate a fixed orifice expansion (FXO) device,

$$DF_{LCV,FXO} = \frac{\dot{m}_{cycle}}{[CA_{FXO}]\sqrt{\rho(P_{up} - P_{down})}} - 1 \tag{12}$$

Where $DF_{LCV,FXO}$ is the ratio of the leaky check valve opening to the FXO opening, C is a discharge coefficient, A_{FXO} is the FXO throat area, A_{LCV} is the opening of the leaky check valve, $\dot{m}_{cycle}$ is the refrigerant mass flow rate which can be measured using a virtual refrigerant mass flow rate sensor , ρ is refrigerant density, P_{up} is the upstream pressure, and P_{down} is the downstream pressure.

For systems having a thermal expansion valve (TXV), Equation (13) applies for determining a check valve leakage indicator.

$$DF_{LCV,TXV} = \frac{T_{sh,sp} - T_{sh}}{T_{sh,sp}} \tag{13}$$

Where $DF_{LCV,TXV}$ is a unique function of the check valve leakage fault level and can be calculated using a measurement of T_{sh} and manufacturer's information for $T_{sh,sp}$.

A reversing valve leakage indicator can be estimated using Equation (14).

$$DF_{LRV} = \frac{(T_{suc,comp} - T_{suc,coil}) - [(T_{dis,comp} - T_{dis,coil}) - (UA/C_p)(LMTD/\dot{m}_{comp})]}{T_{dis,comp} - T_{suc,comp}} \quad (14)$$

Where $\dot{m}_{comp}$ is the mass flow rate through the compressor which can be estimated using a virtual sensor, C_p is the refrigerant vapor specific heat, $T_{dis,coil}$ is the reversing valve high-side outlet temperature to the cycle (to the condenser), $T_{suc,coil}$ is the low-side inlet temperature from the cycle (from the evaporator), $T_{dis,comp}$ is the high-side inlet temperature from the compressor, $T_{suc,comp}$ is the temperature of the low-side outlet to the compressor, and LMTD is a logarithmic mean temperature difference calculated by

$$LMTD = \frac{(T_{suc,comp} - T_{amb}) - (T_{dis,coil} - T_{amb})}{\ln(((T_{suc,comp} - T_{amb}) - (T_{dis,coil} - T_{amb}))} \quad (15)$$

The different leakage indicators ($DF_{LCV,FXO}$, $DF_{LCV,TXV}$, DF_{LRV}) can be used to identify faults through comparison to appropriate predefined thresholds.

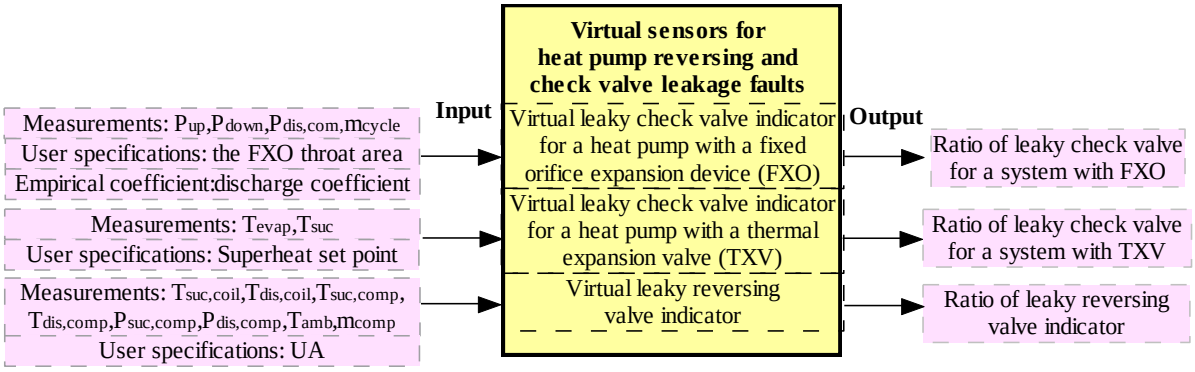

Figure 13: Virtual sensors for heat pump reversing and check valve leakage faults

Some laboratory evaluations were performed to evaluate diagnostic performance using these leakage indicators in heating mode and it was found that faults could be identified before

heating capacity degraded more than 5% for a system with an FXO and 3% for the same system retrofit with a TXV.

2.2.1.4 Virtual sensors for air handling units

Virtual mixed air temperature sensor

Mixed air temperature (MAT) is a useful measurement for control and diagnostics for economizers and vapor compression cycles. However, it can be very difficult to accurately measure MAT because of space constraints and the use of small chambers for mixing outdoor and return air in packaged ACs. Highly non-uniform temperature and velocity distributions at the inlet to the evaporator can cause significant bias errors when employing single-point and averaging temperature sensors (Avery 2002; Carling and Isakson 1999; Robinson 1999). The mixing process changes significantly as the damper position varies with economizer operation. Wichman (2007) suggested that a measurement grid of at least four temperature sensors mounted symmetrically on the duct centerline provides reasonable estimates under most conditions. However, this is a costly approach. Lee and Dexter 2005 and Tan and Dexter (2005, 2006) proposed a method for correcting the bias error associated with a single-point sensor using CFD simulations. However, this is also costly and difficult to implement in practice.

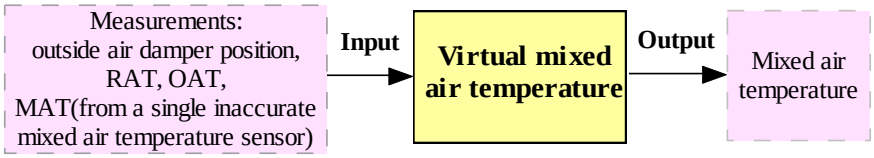

Figure 14: Virtual mixed air temperature sensor

Wichman and Braun (2009) proposed and demonstrated a scheme for adjusting a single-point measurement of MAT (virtual MAT sensor) that is based on in-situ measurements and self calibration. The approach is based on correlating the bias error in terms of damper control signal and difference between outdoor and return-air temperature. The correlation could be determined using a self-calibration procedure with only four temperature measurements: mixed, outdoor,

return, and supply air temperatures. A system was tested in a laboratory over a wide range of outdoor conditions and damper positions in a typical air-side economizer and mixing chamber integrated within a small commercial rooftop air conditioner. The scheme involves determining mixed air temperature using

$$MAT = MAT_{meas} - MAT_{error} \tag{16}$$

Where MAT_{meas} is measured mixed air temperature, and MAT_{error} is bias error corresponding to different damper control signals (OADst) and difference between outdoor and return-air temperature (ΔT_{oa-ra}),

$$MAT_{error} = f(OADst, \Delta T_{oa-ra}) \tag{17}$$

The virtual MAT sensor proposed by Wichman and Braun (2009) overcomes a typical technical barrier of using costly measurement grids or simulation software.

Virtual sensors for AC sensible and total cooling capacity

Figure 15 presents a model proposed by Yang and Li (2010) for estimating cooling coil total and sensible capacity that is based on manufacturers' rating data. The model covers all the operating conditions of the cooling system and requires four measurements (evaporator entering wet bulb temperature, evaporator entering dry bulb temperature, ambient temperature and supply air flow rate) as illustrated in Equation (18).

$$(ET_{wb}, ET_{db}, OAT, \dot{V}) \begin{cases} ET_{wb} > ET_{wb}^{0} \begin{cases} \dot{Q}_C = (ET_{wb}, OAT, \dot{V}) \\ SHR = f(ET_{wb}, ET_{db}, OAT, \dot{V}) \\ \dot{Q}_S = \mathrm{SHR} \times \dot{Q}_C \end{cases} \\ ET_{wb} \le ET_{wb}^{0} \begin{cases} \dot{Q}_C = \dot{Q}_S = \mathrm{f}(\mathrm{ET}_{\mathrm{wb}}^{0}, \mathrm{OAT}, \dot{\mathrm{V}}) \\ SHR = 1 \end{cases} \end{cases} \tag{18}$$

Where $\dot{Q}_C$ is cooling capacity, $\dot{Q}_S$ is sensible cooling capacity, SHR is sensible heat ratio, ET_{wb} is entering wet bulb temperature, ET_{wb}^{0} is critical point of the entering wet bulb temperature (Yang

and Li 2010), ET_{db} is entering dry bulb temperature, OAT is ambient temperature and $\dot{V}$ is supply air flow rate, which can be measured using a virtual air flow rate sensor.

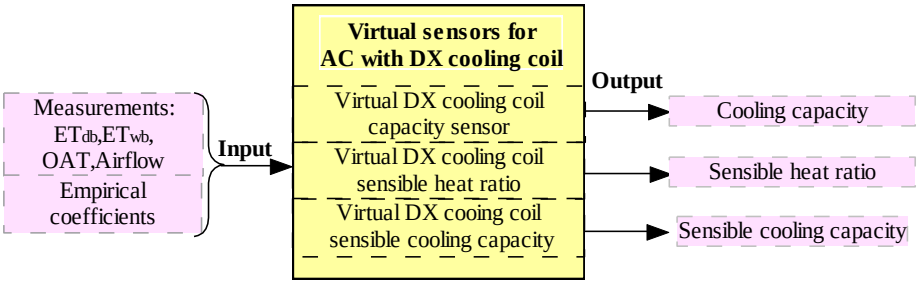

Figure 15: Virtual sensors for AC cooling coil

The performance of the virtual sensors has been evaluated using a wide range of data. Overall predictions of cooling capacity are within 10% for both wet-coil and dry-coil conditions. Additional work is necessary to evaluate accuracy when faults are present.

Virtual sensor for filters

Filtration in HVAC systems is often used for prevention of airborne diseases (Ottney et al.1993) and to protect coils from fouling (Braun, 1986). There are several standards associated with HVAC filtration efficacy, such as ASHRAE Standard 52.1, Gravimetric and Dust-Spot Procedures for Testing Air-Cleaning Devices Used in General Ventilation for Removing Particulate Matter (ASHRAE 1992) or ASHRAE Standard 52.2, Method of Testing General Ventilation Air-Cleaning Devices for Removal Efficiency by Particle Size (ASHRAE 1999). Most of the previous studies related to filtration have focused on testing of filter media, rather than on systems having installed filtration devices. A few investigators have attempted to establish models and test methods for determining in-situ filter efficiency that are based on ignoring filter bypass, the air that circumvents filters due to gaps around the filter pan or filter housing. Recently, Ward and Siegel (2005) proposed models for monitoring overall filter efficiency (a virtual filter efficiency sensor) and the air flow bypassing the filter (virtual filter bypass flow sensor) that are depicted in Figure 16.

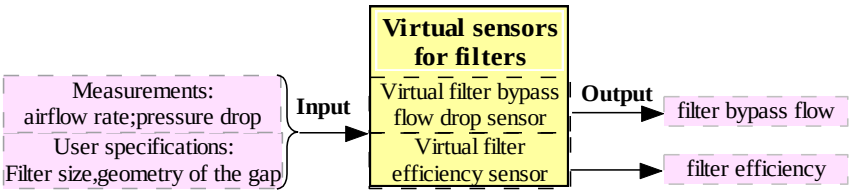

Figure 16: Virtual sensors for filters

The virtual filter sensors require specification of the size and geometry of the gaps around the filter and measurements of air flow rate and pressure drop. The flow bypassing the filter is estimated according to

$$Q_B = \frac{[-\frac{12\mu L}{WH^3} + \sqrt{(\frac{12\mu L}{WH^3})^2 + \frac{2(1.5+n)\rho\Delta P}{W^2H^2}}\,]}{(\frac{2(1.5+n)\rho\Delta P}{W^2H^2})} \tag{19}$$

Where Q_B is the flow rate of air bypassing the filter, ΔP is the pressure drop across the filter which can be measured, μ is the dynamic viscosity of air, and ρ is the density of the air, L is the length of the crack longitudinal to the flow, W is the width of the crack perpendicular to flow, H is the height of the crack, n is the number of right angle bends in the path of bypass flow.

The method of estimating bypass flow has only validated using simulation for a variety of common filters. Additional work is necessary to perform experimental validation using laboratory and field studies.

Virtual water flow rate sensor

Liu et al. (2007a) proposed a pump water flow station (virtual water flow rate meter) depicted in Figure 17 that uses pump head (H_{pump}), pump speed (w_{pump}), and empirical coefficients to determine pump performance according to

$$Q = \frac{-a_1 \cdot \overline{w}_{pump} - \sqrt{a_1^2 \cdot \overline{w}_{pump}^{\,2} - 4 \cdot a_2 \cdot (a_0 \cdot \overline{w}_{pump}^{\,2} - H_{pump})}}{2 \cdot a_0} \tag{20}$$

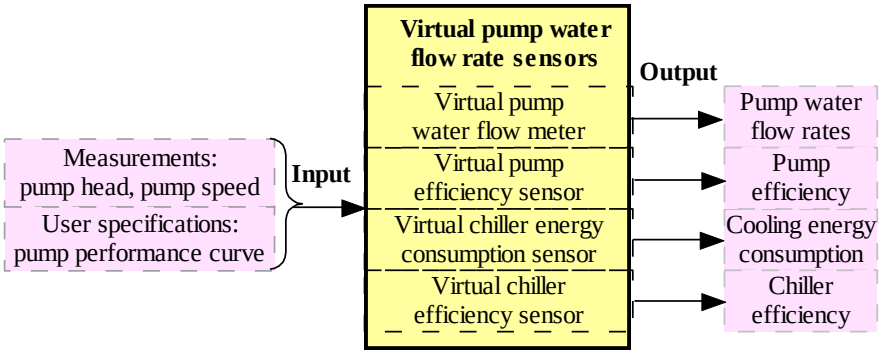

Figure 17: Virtual pump water flow rate sensor

The virtual sensor could be used along with other measurements to estimate pump efficiency, cooling energy consumption and chiller efficiency and used within a building energy management and control system. A case study was performed in a building having a chilled water system and demonstrated that the low-cost virtual sensor can accurately measure water flow rate and be used along with other measurements to monitor energy consumption. In addition to performance monitoring, the virtual flow meter could be applied for optimized pump speed control (Liu, et al. 2007b). However, the method described in this paper is not applicable for all pump characteristics. More work is needed to generalize the approach.

Virtual fan air flow rate meter

Joo et al. (2007) proposed a fan flow station (virtual fan air flow rate meter) for measuring supply and/or return fan air flows and that is illustrated in Figure 18. The model for flow rate is similar to the approach used for the pump flow sensor and is expressed as

$$Q^{'} = \frac{-a^{'}_{1}\overline{w}_{fan} - \sqrt{a^{'2}_{1}\cdot\overline{w}_{fan}^{\,2} - 4\cdot a^{'}_{2}\cdot(a^{'}_{0}\cdot\overline{w}_{fan}^{\,2} - H_{fan})}}{2\cdot a^{'}_{0}} \qquad (21)$$

Where H_{fan} is fan head, w_{fan} is fan speed, and the a's are empirical coefficients that are determined using regression applied to a fan performance curve provided by the manufacturer. The algorithm was shown to provide accurate estimates of supply and return fan air flow rate for a variable-air-volume (VAV) system.

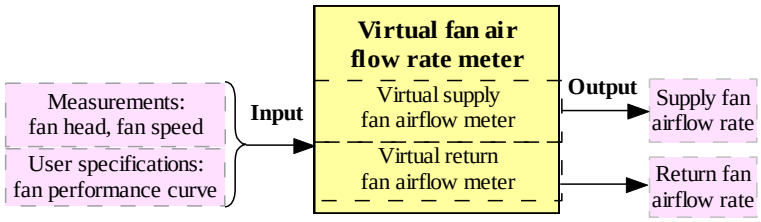

Figure 18: Virtual fan air flow rate meter

Virtual air flow measurement could be used along with other measurements to determine real-time air-side capacity measurements. In addition, they could be used for building pressure control based on supply and return air fan flow rate tracking. In this application, a positive building pressure is maintained by setting a return air fan flow rate setpoint slightly lower than the supply flow. The virtual air flow sensor was only applied to VAV AHUs. However, constant-air-volume (CAV) AHUs are very popular in light commercial buildings. It is anticipated that the method could be readily adapted to CAV RTU systems.

2.2.2 Virtual sensors for building envelopes and occupied zones

Virtual occupant complaint sensor

Federspiel (2000) developed a model for estimating the frequency of occupant complaints due to zone temperature deviations from normal setpoints. The model was derived from complaint histories and coincident time histories of zone temperature measurements. As depicted in Figure 19, the model predicts frequency of hot and cold complaints using measurements of zone air temperature and thresholds for the high-temperature and low-temperature levels at which a hot and cold complaints occur. The mathematical model was developed using level-crossing theory of stochastic processes. The predictions of virtual frequency of complaints can be combined with labor rates associated with responding to complaints and then used to estimate cost impacts. This type of virtual sensor for occupant costs could be integrated within energy management and control systems in order to optimize setpoints to minimize complaints.

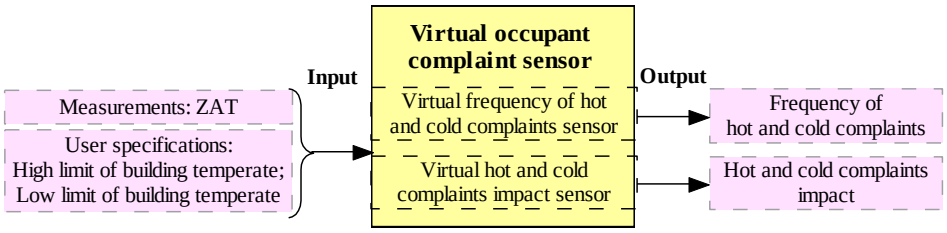

Figure 19: Virtual occupant complaint sensor

Virtual sensor for solar radiation

Solar radiation is an important measurement for use in models that predict building loads. However, it is expensive to measure on site and is rarely available. Recently, Seo, et al. (2008) evaluated a number of different models for estimating solar radiation from other available measurements and identified some simplifications that result in reasonable performance. Performance was statistically evaluated using measured solar radiation for several locations around the world. Figure 20 depicts virtual sensors for total, direct normal, and diffuse solar radiation sensor based on the simplified model. The algorithms are empirical and only require inputs of hourly cloud cover information, dry bulb temperature, relative humidity, and wind speed.

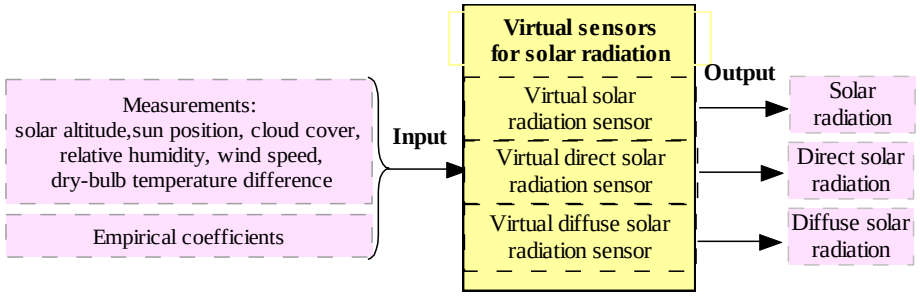

Figure 20: Virtual sensor for solar radiation

Chapter 3 DEVELOPMENT OF A VIRTUAL SCFM METER IN RTUS

The supply airflow in RTUs accompanies energy transmission from thermal components to the air. According to ASHRAE handbook of fundamental 2009, for a typical air-conditioning process shown in Figure 21, an energy balance exists across an air-handling unit in steady-flow conditions:

$$\dot{Q} = \dot{m}(h_2 - h_1) \tag{22}$$

Where $\dot{Q}$ = rate of heat flow in Btu/hr (kJ/s), $\dot{m}$ = mass flow rate in lbm/hr (kg/s), h_1, h_2 = enthalpy of air before and after the thermal equipment in Btu/lbm (kJ/kg).

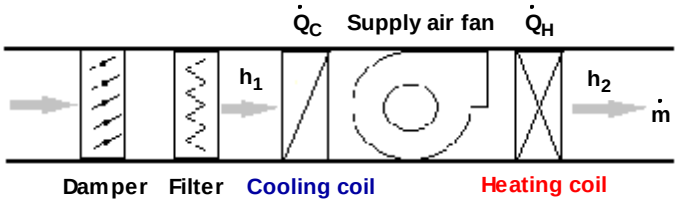

Figure 21: A typical air-conditioning process

With constant specific volume of conditioned air, SCFM can be calculated based on the mass flow rate:

$$\dot{V} = \dot{m}\, v \tag{23}$$

Where $\dot{V}$ = supply airflow rate in cfm (m^3/s), v = specific volume of air in ft^3/lbm (m^3/kg).

By combining Equations (22) and (23), the value of SCFM can be obtained as,

$$\dot{V} = \frac{\dot{Q}}{h_2 - h_1} v \tag{24}$$

To avoid using expensive measurements such as relative humidity, only sensible capacity across the cooling or heating coil is adopted in the development of a virtual SCFM meter. Equation (25) thus can be represented by and a virtual SCFM meter prototype is obtained as,

$$\dot{V} = \frac{\dot{Q}_s}{C_p \times |SAT - MAT|} v \tag{25}$$

Where $\dot{Q}_s$ = sensible capacity in Btu/hr (kJ/s), SAT = supply air temperature in ºF (ºC), and MAT= mixed air temperature in ºF (ºC)

For a typical RTU, cooling and heating are two opposite energy transmissions related to SCFM and air status change. Accordingly, there are two approaches (cooling mode- and heating mode-based approaches) to obtain the sensible capacity in Equation (25). The reliable values of $\dot{Q}_s$, which may involve other implicit variables, and SAT, MAT are needed in the cooling or heating process to make the virtual SCFM meter work.

The remaining challenge is to evaluate the two candidates (cooling mode- and heating mode-based approaches) and develop an implementation method which satisfies the following features of a feasible virtual SCFM meter: *(1) using a simple while reliable mechanism; (2) characteristic of small uncertainty and robust against faults; and (3) easy-to-obtain parameters or measurements*.

Without the presence of simultaneous cooling and heating, individual cooling mode- and heating mode-based approaches are studied in the next two subsections. The inputs and basic measurements are verified and adopted from the referred literature. The critical measurements are reiterated in detail in the section of implementation issues.

3.1 Modeling and evaluations of cooling-based approach

3.1.1 Modeling of cooling-based approach

To simplify the analysis of air-conditioning components and reduce the cost for model development, certain studies have attempted to develop generic models as virtual sensors by using rating data from manufacturers. For example, as reviewed previously, Yang and Li (2010) proposed a generic rating-data-based virtual cooling capacity sensor for direct-expansion (DX) coils with four parameters (mixed air wet bulb temperature MAT_{wb}, MAT, OAT and SCFM) in Equation (18). The detailed calculation procedure of virtual cooling capacity sensor and its calculation case is provided in the Appendix A (Yang and Li 2010). Since this virtual cooling capacity sensor has been demonstrated to be very simple and accurate, it is utilized in this study for obtaining cooling capacity.

The model can be rearranged as one expression for the gross sensible cooling capacity:

$$\dot{Q}_{C,s} = \dot{Q}_C \times SHR = f(OAT, MAT, MAT_{wb,} \dot{V}_C) \tag{26}$$

Besides, considering the effect of supply fan heat loss in cooling mode, the energy balance expressed in Equation (25) can be reduced to

$$\dot{V}_C = \frac{\dot{Q}_{C,s}}{C_p \times (MAT + \Delta T_{fan} - SAT)} v \tag{27}$$

Where ΔT_{fan} = supply fan temperature rise in ºF (ºC).

By combining Equations (26) and (27), the cooling-based approach formulation for a virtual SCFM meter can be expressed as

$$\dot{V}_{C,model} = f(OAT, MAT, MAT_{wb}, SAT, \Delta T_{fan}) \tag{28}$$

Observed from Equation (28), to develop a cooling-based SCFM meter $\dot{V}_{C,model}$, four dry bulb temperatures (OAT, MAT, SAT, ΔT_{fan}) and one wet bulb temperature (MAT_{wb}) should be used.

3.1.2 Evaluations of cooling-based approach

3.1.2.1 Experiment preparation of cooling-based SCFM meter

System description: Experiments for evaluating the cooling-base virtual SCFM meter were performed in a 7.5 ton RTU equipped with two constant speed compressors in an environmental chamber. Figure 22 illustrates the basic setting (Yu et al., 2011) in the lab. The nominal supply airflow rate is 2,400 cfm (1.13 m^3/s) with standard speed option. Together with another RTU outside of the building, artificial indoor and outdoor air physical conditions can be created and maintained.

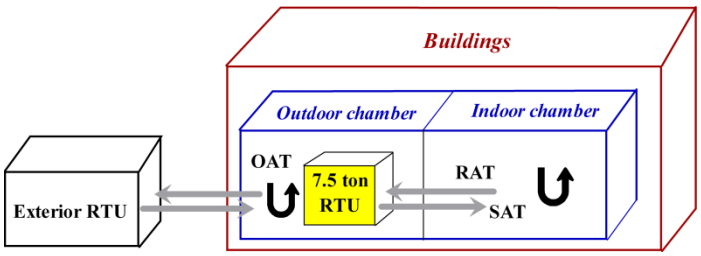

Figure 22: Illustration of machine layout in the lab

Experimental designs: Data used for evaluation here are adopted from the study by Yang and Li (2010). About 110 sets of tests plotted in Figure 23 were performed with OADst at 30%, cooling running stage at 2, and a wide span of OAT (70.0~110.0 ºF [21.1~43.3ºC]) and measured SCFM $\dot{V}_{meas}$ (about 1800~2600 cfm [0.76~1.23 m^3/s]) to cover the most real operation combinations. Each test was conducted around 20 minutes preparation, followed by 10 to 15 minutes steady status data. Average readings of each test were collected and utilized in the evaluation. All temperature sensors have been tuned within ± 1.0 ºF (0.6ºC) accuracy in the lab.

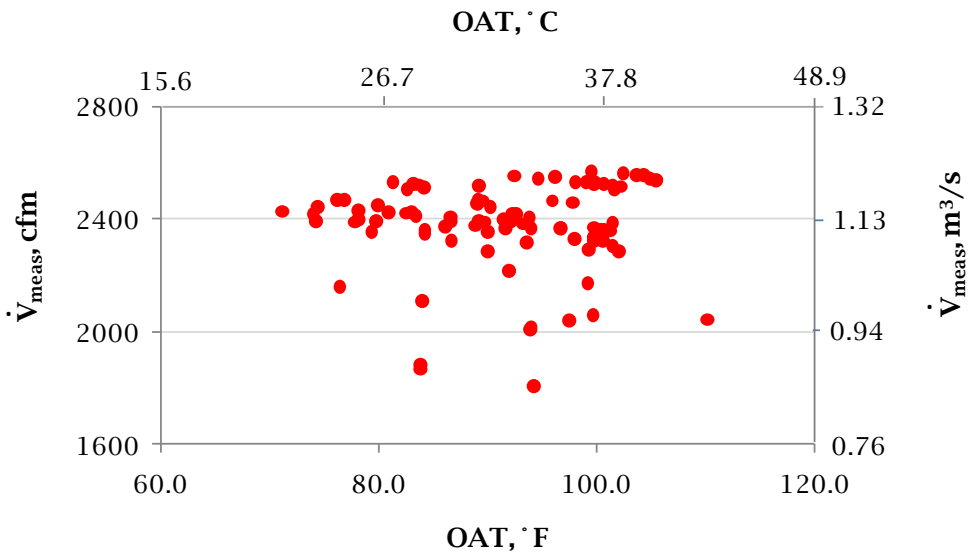

Figure 23: Experimental settings in the cooling mode

Experimental results: The involved direct measurements and indirect results for evaluating the cooling-based SCFM meter are elaborated below.

- ***Direct measurements***

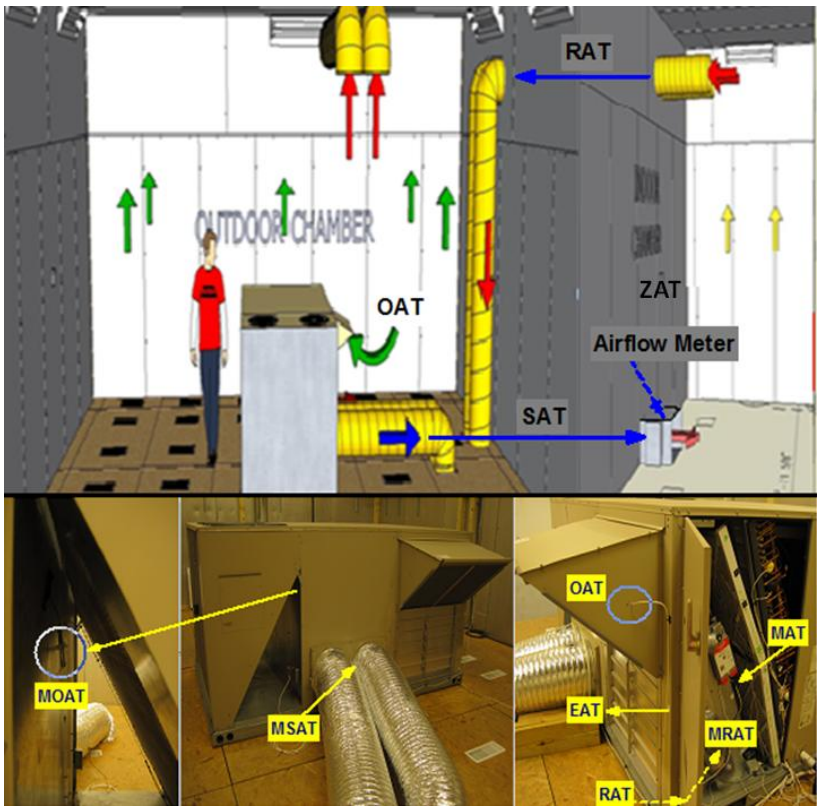

Figure 24: Lab sensors' layout

Outside air temperature (OAT) It is found, the manufacturer-preinstalled OAT (MOAT) sensor in Figure 24 is fixed beside the evaporator coils, and the measurements are not reliable due to improper heat gain and poor temperature distribution. To supplement it for an accurate OAT, another air temperature sensor with ± 0.1 ºF (0.6ºC) uncertainty is mounted at the RTU outside air inlet (Figure 24). In this experiment, average reading of the lab-installed OAT sensor instead of MOAT sensor is used.

Supply air temperature (SAT) Based on the study by Yu et al. (2011), an manufacturer-preinstalled SAT (MSAT) sensor (Figure 24) in RTUs could predict the true values in cooling mode. Therefore, average reading of the MSAT sensor with ± 0.1 ºF (0.6ºC) uncertainty is adopted here.

Return air temperature (RAT) In order to calculate MAT accurately, obtaining the true value of RAT is also important. In the lab, a RAT sensor with ± 0.1 ºF (0.6ºC) uncertainty installed right at the return air duct outlet (Figure 24) is utilized to verify the accuracy of the manufacturer-preinstalled RAT (MRAT) sensor. In the case, average reading of the lab-installed RAT sensor is proved trustable and then used.

Outside air relative humidity (OARH), zone air relative humidity (ZARH) and zone air temperature (ZAT) Besides, in an attempt to calculate the parameter of MAT_{wb}, average readings of lab-installed OARH sensor in the outdoor chamber (Figure 22), ZARH and ZAT sensors in the indoor chamber are collected accordingly.

Measured SCFM ($\dot{V}_{meas}$) An airflow station (pressure transducer) offering ± 1% full scale accuracy is permanently mounted in supply air duct in the lab. The airflow station was calibrated by the manufacturer before it was installed. It serves as the airflow reference $\dot{V}_{meas}$ in this study.

- ***Indirect results***

Virtual mixed air temperature (MAT_{vir}) Since there is no pre-installed physical MAT sensor available in our study, we adopted the method proposed by Yang and Li (2011) with an acceptable uncertainty of ±1.0ºF (0.6ºC). The specific details are provided in Section 3.4.2 about measuring and processing MAT.

Virtual mixed air wet bulb temperature ($MAT_{wb,vir}$) Since mixed air wet bulb temperature could not be metered directly, an mass balance equation by using the direct measurements of OAT, OARH, ZAT, ZARH and a correlated virtual outside air ratio sensor β (Yang and Li 2011) is computed to obtain the values , namely, $MAT_{wb,vir}$ with an uncertainty of ±1.0ºF (0.6ºC) in this study.

Supply fan temperature rise (ΔT_{fan}) Additionally, the supply fan temperature rise ΔT_{fan} is calculated using the heat loss from the fan and checked with actual measurements using the method presented by Wichman and Braun (2009) under conditions where neither mechanical cooling nor heating is operating. The result of it in the lab is 1.7 ºF (0.9 ºC) with an uncertainty of ±0.2 ºF (0.1ºC). Since it is a CAV RTU, the uncertainty of the fan temperature rise is relatively small.

Based on the experimental results acquired from the extensive laboratory testing, uncertainty analysis is thereby performed at the first place, and then experimental evaluation is conducted to evaluate the effectiveness of the cooling-based approach.

3.1.2.2 Uncertainty analysis of cooling-based SCFM meter

The root sum square method of uncertainty calculation is applied to the variables of OAT, $MAT_{vir,}$ $MAT_{wb,vir,}$ SAT and ΔT_{fan}. The random uncertainty is expressed as Equation (29):

$$\delta \dot{V}_{C,model} = [(\frac{\partial \dot{V}}{\partial OAT}\delta OAT)^2 + (\frac{\partial \dot{V}}{\partial MAT_{vir}}\delta MAT_{vir})^2 + (\frac{\partial \dot{V}}{\partial MAT_{wb,vir}}\delta MAT_{wb,vir})^2 + (\frac{\partial \dot{V}}{\partial SAT}\delta SAT)^2 + (\frac{\partial \dot{V}}{\partial \Delta T_{fan}}\delta \Delta T_{fan})^2]^{1/2} \quad (29)$$

Where δOAT , δMAT_{vir}, $\delta MAT_{wb,vir,}$ δSAT and $\delta \Delta T_{fan}$ are inputs uncertainties.

The 110 sets of extensive laboratory tests for the 7.5 ton RTU in cooling mode collected by Yang and Li (2010) are used in the analysis. Table 3 summarizes the uncertainties of independent variables as inputs, as well as the calculated uncertainties of $\dot{V}_{C,model}$ as outputs. Uncertainties of temperature measurements are ±1.0ºF (0.6ºC). It is found that, due to the complex cooling process and multiple variables, the absolute uncertainty of $\dot{V}_{C,model}$ can be up to 13.8%.

In field applications, the best practice of a physical airflow meter could have a theoretical accuracy close to ±1%, but the actual uncertainty of the meter might be enlarged to some extent, owing to a variety of practical factors, such as uneven air distribution, gradual drifting, faulty installation, or adverse duct work surroundings. In general, ±10% uncertainty of airflow measurement can be regarded good for most thermal control applications in HVAC, while a better uncertainty is always desired. The uncertainty (±13.8%) of a cooling-based virtual SCFM meter is slightly high.

Table 3: Uncertainty analysis of cooling-based SCFM meter

Variables	Inputs					Output
	OAT,°F (°C)	MAT_{vir},°F (°C)	$MAT_{wb,vir}$,°F (°C)	SAT,°F (°C)	ΔT_{fan},°F (°C)	$\dot{V}_{C,model}$
Uncertainty	±1.0 (0.6)	±1.0 (0.6)	±1.0 (0.6)	±1.0 (0.6)	±0.2(0.1)	±13.8%

3.1.2.3 Experimental evaluation of cooling-based SCFM meter

Direct SCFM measurements acquired from the 110 sets of cooling tests (Yang and Li 2010) are also used to evaluate the accuracy of the cooling-based SCFM meter. The relative error $e_{C,eva}$ between the measured SCFM $\dot{V}_{meas}$ and $\dot{V}_{C,model}$ is defined as follows,

$$e_{C,eva} = \frac{\dot{V}_{C,model} - \dot{V}_{meas}}{\dot{V}_{meas}} \tag{30}$$

In Table 4, results show that the maximum relative error is as high as 16.4%, and the minimum low to -16.2%. The absolute average of these errors is 7.8% with a standard deviation 8.9%. It can be seen that these actual errors are a little bit higher than those values obtained from prior uncertainty analysis, which is fully anticipated, because in the prior uncertainty analysis, the uncertainty from the model regression of gross sensible cooling capacity in Equation (18) which is about 5% (Yang and Li 2010), was not considered. These factors lead to certain difficulty (complex cooling process and multiple variables), and slight inaccuracy (uncertainty is ±13.8% and relative error is -16.2~16.4%) in developing the virtual SCFM meter for cooling mode.

Table 4: Experimental evaluation of cooling-based SCFM meter

	Maximum	Minimum	Absolute average	Standard deviation
$e_{C,eva}$	16.4%	-16.2%	7.8%	8.9%

3.2 Modeling and evaluations of heating-based approach

In heating mode, gas burnt in furnace transmits heat into conditioned air and causes air temperature to increase. An obvious advantage of utilizing heating energy transmission is that the process generally doesn't have mass transfer involved across the furnace. The measurement of conditioned air energy change relies purely on the air dry bulb temperature. The modeling and evaluation of the heating-based approach are explored in the following subsections.

3.2.1 Modeling of heating-based approach

Referring to ASHRAE handbook of fundamental 2009 Chapter 4, for heat exchangers, to calculate the heating transfer rate, mean temperature difference analysis and number of transfer units (NTU)-effectiveness (ε) analysis are used. The former method involves trial-and-error calculations unless inlet and outlet fluid temperatures are known for both fluids. NTU-ε method is adopted in the study.

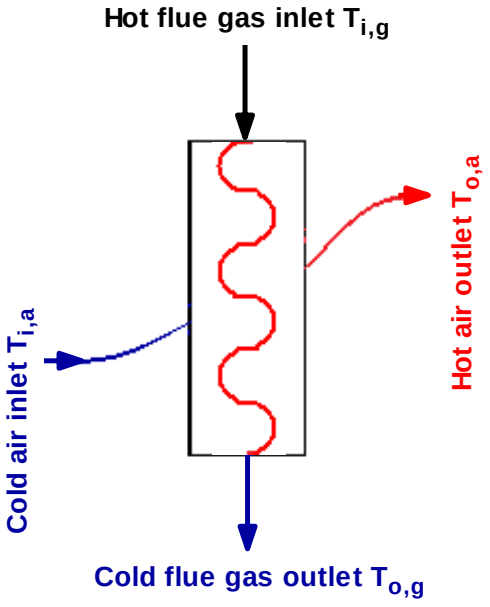

Figure 25: Heat transfer of a heat exchanger

Figure 25 shows the configuration of a counterflow heat exchanger. $T_{i,a}$ and $T_{o,a}$ are the air temperature at the inlet and outlet of heat exchanger respectively. $T_{i,g}$ and $T_{o,g}$ are the flue gas temperatures of inlet and outlet of heat exchanger. The maximum possible heat transfer rate $\dot{Q}_{H,max}$ occurs when the hot fluid enters at $T_{i,g}$ and leaves at the entering temperature of the cold fluid $T_{i,a}$:

$$\dot{Q}_{H,max} = C_{min} \times (T_{i,g} - T_{i,a}) \tag{31}$$

Where C_{min}= min (C_g,C_a), C_{max}= max (C_g,C_a), wherein C_g [$(\dot{m} \times C_P)_g$] and C_a [$(\dot{m} \times C_P)_a$] are fluid capacity rates, Btu/(hr·°F) (kW/K).

The actual heating capacity $\dot{Q}_H$ can be calculated as:

$$\dot{Q}_H = \dot{Q}_{H,max} \times \varepsilon = \frac{\dot{Q}_{H,d}}{\varepsilon_d} \times \varepsilon \tag{32}$$

According to NTU-ε method, in a counterflow heater, ε is determined by,

$$\varepsilon = \frac{1 - exp[-NTU(1 - C_r)]}{1 - C_r \times exp[-NTU(1 - C_r)]} \quad (C_r < 1) \tag{33}$$

Where $C_r = C_{min}/C_{max}$ as a capacity ratio.

Therefore, by combining Equation (32) and (33), $\dot{Q}_H$ can be expressed as,

$$\dot{Q}_H = \frac{\dot{Q}_{H,d}}{\varepsilon_d} \times \frac{1 - exp[-NTU(1 - C_r)]}{1 - C_r \times exp[-NTU(1 - C_r)]} \tag{34}$$

Observed from Equation (14), the intermediate variables C_r and NTU are required to make $\dot{Q}_H$ work. The following four steps are thus needed in order to analyze the heating capacity and capture the heating-based virtual SCFM meter. Data from a 7.5 ton RTU is adopted for illustration purposes.

Step 1: Determination of C_r

To determine C_r, the knowns and assumptions are listed below:

- The design heating capacity and design heat exchanger effectiveness are: $\dot{Q}_{H,d}$ = 130,000 Btu/hr (38.1 kW); ε_d = 80%.
- The design airflow rate and design flue gas flow rate are: $\dot{V}_{a,d}$ = 144,000 ft^3/hr (2400 cfm; 1.13m^3/s), $\dot{V}_g$ = 1,800 ft^3/hr (30.0 cfm; 0.014m^3/s).
- The density and specific heat of air are: ρ_a = 0.070lb/ft^3 (1.200 kg/m^3); $C_{P,a}$ =0.240 Btu/(lbm·ºF) (1.005 kJ/(kg·K)).
- It is a sufficient combustion process in the gas furnaces. The density and specific heat of flue gas are: ρ_g = 0.077lb/ft^3 (1.240 kg/m^3); $C_{P,g}$ =0.295 Btu/(lbm·ºF) (1.230 kJ/(kg·K)).

Since with similar specific heat on both sides the flow rate on the air side is several degrees of magnitude higher than that on the flue gas side, $C_g << C_a$, then according to C_{min} and C_{max} definition, we have C_{min} equals C_g and C_{max} equals C_a.

(1) $C_{min} = C_g$. With flue gas flow rate known, the value of C_g can be obtained as,

$$C_g = \rho_g \times C_{P,g} \times \dot{V}_g \tag{35}$$

In this case, C_g is 40.36 Btu/(hr·ºF) (0.021 kW/K) as calculated.

(2) $C_{max} = C_a$. With design airflow rate known, C_a can be derived from Eq. (16):

$$C_a = \rho_a \times C_{P,a} \times \dot{V}_{a,d} \tag{36}$$

The result is C_a = 2419 Btu/(hr·ºF) (1.423 kW/K) under design conditions.

Since C_a is significantly greater than C_g, the assumption holds for wide range airflow rate and we have,

$$C_r = \frac{C_{min}}{C_{max}} = \frac{C_g}{C_a} \tag{37}$$

Step 2: Correlating NTU

As shown in Table 5, based on ASHRAE handbook of fundamental 2009, with the knowns of $\dot{V}_a$ and $\dot{V}_g$, the NTU of a heat exchanger can be applied through Equation (38) to (47).

Table 5: Calculation of NTU of a heat exchanger

Equations		
NTU	**UA, C_{min}**	**$h_a \leftarrow Nu_a \leftarrow Re_a \leftarrow V_a \leftarrow \dot{V}_a$; $h_g \leftarrow Nu_g \leftarrow Re_g \leftarrow V_g \leftarrow \dot{V}_g$**
$NTU=UA/C_{min}$ Equation (38)	$\frac{1}{UA}=\frac{1}{h_a A_a}+\frac{li(D_a/D_g)}{2\pi kL}+\frac{1}{h_g A_g}$ Eq. (39) C_{min}=Minimum(C_a ,C_g)	$h_a=\frac{k_a}{D_a}Nu_a$ Equation (40) $Nu_a=0.3+\frac{0.62\,Re_a^{1/2}\,Pr_a^{1/3}}{[1+0.4/Pr_a)^{2/3}]^{1/4}}[1+(\frac{Re_a}{282{,}000})^{1/2}$ *(10,000<Re_a<40,000)* Equation (41) $Re_a=V_aD_a/v_a$ Equation (42) $\boldsymbol{V_a=\dot{V}_a/A_a}$ Equation (43) $h_g=\frac{k_g}{D_g}Nu_g$ Equation (44) $Nu_g=0.023\,Re_g^{4/5}\,Pr_g^{0.4}$ *(Re_g>10,000)* Equation (45) $Re_g=\rho V_g D_g/\mu_g$ Equation (46) $\boldsymbol{V_g=\dot{V}_g/A_g}$ Equation (47)

Symbols	
A = area, ft^2 (m^2)	Pr = Prandtl number
C = heat air capacity rate, Btu/(hr·ºF) (kW/K)	Re = duct Reynolds number
D = duct diameter, in (m)	U = heat transfer coefficient, Btu/(hr·ºF·ft²) (kW/(m^2·K))
k = thermal conductivity, Btu/(h·ft·ºF) (kW/(m·K))	v = kinematic viscosity, ft^2/s(m^2/s)
L = duct length, ft (m)	V = linear velocity, ft/s(m/s)
NTU = number of transfer units	$\dot{V}$ = flow rate, ft^3/s (m^3/s)
Nu = Nusselt number	ρ = density, lbm/ft^3(kg/m^3)
μ = absolute viscosity, lbm/ft·s ((N·s)/m^2)	

Step 3: Obtaining $\dot{Q}_H$

With the intermediate parameters C_r (C_g, C_a) and NTU obtained, for different operations, $\dot{Q}_H$ then can be calculated through Equation (34). However, observed from the calculation of C_g (Equation (35)),

C_a (Equation (36)) and NTU, it is found that $\dot{Q}_H$ is essentially derived from and mainly effected by two parameters, the air side flow rate $\dot{V}_a$ and the flue gas flow rate $\dot{V}_g$. Therefore, fundamentally, we determine the $\dot{Q}_H$ as Equation (48) in this study,

$$\dot{Q}_H = f(\dot{V}_a, \dot{V}_g) \tag{48}$$

Step 4: Modeling heating-based virtual SCFM meter $\dot{V}_{H,model}$

Besides, considering the effect of supply fan heat loss in heating mode and no moisture related mass change in the air, the energy balance expressed in Equation (24) can be reduced to Equation (49) in heating mode,

$$\dot{V}_H = \frac{\dot{Q}_H}{C_P \times (SAT - MAT - \Delta T_{fan})} v \tag{49}$$

Combining Equation (48) and (49), we could formulate the heating-based SCFM meter as follows,

$$\dot{V}_{H,model} = f(\dot{V}_g, \Delta T_{fan}, SAT, MAT) \tag{50}$$

It can be seen from Equation (50) that the heating-based approach requires reliable values of $\dot{V}_g$ and three air temperature inputs to get SCFM, wherein $\dot{V}_g$ and ΔT_{fan} are nearly constant. $\dot{V}_g$ possess a low uncertainty of ±1% because the natural gas regulator holds a high accuracy of pressure control (ASHRAE handbook of fundamental 2009). ΔT_{fan} has also a low uncertainty of ±0.2 ºF (0.1ºC) in a constant air volume (CAV) RTU (Yu et al. 2011). Therefore, the uncertainty of $\dot{V}_{H,model}$ is mainly determined by the uncertainty of two temperature measurements (SAT and MAT).

3.2.2 Evaluations of heating-based SCFM meter

3.2.2.1 Experiment preparation of heating-based SCFM meter

System description: Experiments for evaluating the heating-base virtual SCFM meter were also performed in the 7.5 ton RTU in Figure 22 equipped with two-stage gas heating. The design total heating capacity is 130,000 Btu/hr (38.1kW) and the first stage is 84,500 Btu/hr (24.8kW).

Experimental designs: Data used for evaluation here are adopted from the study by Yu et al. (2011). Table 6 collects experimental configurations and results. Sixteen tests named with different scenario ID were performed with different heating running stages (1 and 2), OADst (0% and 30%), a wide span of OAT (34.1~50.0 ºF [1.3~10.0ºC]) and measured SCFM (1829~2272 cfm [0.86~1.07 m^3/s]) to cover the most real operation combinations. Similarly to the cooling mode, each test was conducted around 20 minutes preparation, followed by 10 to 15 minutes steady status data. Average readings of each test were collected and utilized in the evaluation. All temperature sensors have been tuned within ± 1.0 ºF (0.6ºC) accuracy.

Table 6: Experimental designs and results of heating-based SCFM meter

Scenario ID	Running Mode	Hstage	OADst	OAT, ºF(ºC)	RAT, ºF(ºC)	$\dot{V}_{meas}$, cfm(m^3/s)	SAT, ºF(ºC)	$SAT_{mfr,cal}$, ºF(ºC)	MAT_{vir}, ºF(ºC)
H-1	Heating	2	0%	36.0(2.2)	59.1(15.1)	1848(0.87)	120.1(48.9)	108.0(42.2)	54.2(12.3)
H-2	Heating	2	0%	42.9(6.1)	63.9(17.7)	2045(0.97)	120.0(48.9)	108.3(42.4)	59.5(15.3)
H-3	Heating	2	0%	44.1(6.7)	58.4(14.7)	1857(0.88)	121.5(49.7)	108.9(42.7)	55.4(13.0)
H-4	Heating	2	0%	50.0(10.0)	59.4(15.2)	1829(0.86)	124.0(51.1)	111.8(44.3)	57.4(14.1)
H-5	Heating	2	30%	34.4(1.3)	55.5(13.1)	2076(0.98)	99.9(37.7)	93.0(33.9)	44.9(7.2)
H-6	Heating	2	30%	44.3(6.8)	60.7(15.9)	2269(1.07)	104.5(40.3)	96.7(35.9)	52.5(11.4)
H-7	Heating	2	30%	43.3(6.3)	57.0(13.9)	2037(0.96)	106.1(41.2)	99.2(37.3)	50.2(10.1)
H-8	Heating	2	30%	49.1(9.5)	58.6(14.8)	2040(0.96)	109.9(43.3)	102.7(39.3)	53.8(12.1)
H-9	Heating	1	0%	35.6(2.0)	65.6(18.7)	1853(0.87)	99.4(37.4)	94.7(34.8)	59.3(15.2)
H-10	Heating	1	0%	45.9(7.7)	65.0(18.3)	2051(0.97)	98.1(36.7)	93.2(34.0)	61.0(16.1)
H-11	Heating	1	0%	44.4(6.9)	65.3(18.5)	1849(0.87)	100.8(38.2)	96.4(35.8)	60.9(16.1)
H-12	Heating	1	0%	49.2(9.6)	65.6(18.7)	1831(0.86)	102.6(39.2)	99.6(37.6)	63.7(17.6)
H-13	Heating	1	30%	34.1(1.2)	63.1(17.3)	2081(0.98)	82.6(28.1)	80.4(26.9)	48.6(9.2)
H-14	Heating	1	30%	42.9(6.1)	62.9(17.2)	2272(1.07)	83.2(28.4)	82.1(27.8)	52.9(11.6)
H-15	Heating	1	30%	43.1(6.2)	63.8(17.7)	2059(0.97)	87.5(38.3)	85.5(29.7)	53.4(11.9)
H-16	Heating	1	30%	48.4(9.1)	64.4(18.0)	2046(0.97)	90.8(32.7)	88.7(31.5)	56.4(13.6)

Experimental results: Experimental results for evaluating the heating-based virtual SCFM meter are collected in Table 6 respectively. The methods to obtain the direct measurements (OAT, RAT, and $\dot{V}_{meas}$) and the indirect results (MAT_{vir} and ΔT_{fan}) are the same as the cooling mode, excepting the SAT values:

Calibrated MSAT ($SAT_{mfr, cal}$) Based on the study by Yu et al. (2011), direct measurements of an MSAT sensor are incorrect in heating mode with gas furnaces equipped in RTUs. There exists unacceptable erratic measurement errors (e.g., in a 7.5 ton RTU, the errors are from 1.0 ºF [0.6ºC] to 12.6ºF [7.0ºC]) due to severe temperature stratification and high thermal radiation. The traditional calibration method can hardly overcome the defect. The methodology of virtual calibration of an MSAT sensor is innovated with good accuracy by Yu et al (2011). This method is adopted in this study and MSAT is calibrated as $SAT_{mfr, cal}$ in Table 4 with uncertainty ± 1.2 ºF (0.7ºC). For more information about the virtual calibration of an MSAT sensor in RTUs, please refer to the section 3.4.2.

Based on the experimental results in the 7.5 ton RTU in the heating mode, uncertainty analysis and experimental evaluation are thereby conducted to evaluate the effectiveness of the heating-based approach.

3.2.2.2 Uncertainty analysis of heating-based SCFM meter

Based on Equation (50), uncertainty of heating-based approach calculation is conducted with the independent variables of $\dot{V}_g$, ΔT_{fan}, $SAT_{mfr,cal}$ and MAT_{vir}. The root sum square is used as Equation (51):

$$\delta \dot{V}_{H,model} = [(\frac{\partial \dot{V}_{H,model}}{\partial \dot{V}_g} \delta \dot{V}_g)^2 + (\frac{\partial \dot{V}_{H,model}}{\partial \Delta T_{fan}} \delta \Delta T_{fan})^2 + (\frac{\partial \dot{V}_{H,model}}{\partial SAT_{mfr,cal}} \delta SAT_{mfr,cal})^2 + (\frac{\partial \dot{V}_{H,model}}{\partial MAT_{vir}} \delta MAT_{vir})^2]^{1/2} \quad (51)$$

Where $\delta \dot{V}_g$, $\delta \Delta T_{fan}$, $\delta SAT_{mfr,cal}$ and δMAT_{vir} are inputs uncertainties.

The results of sixteen experiments in heating mode preformed in the 7.5 ton RTU are used to analyze the uncertainty of heating-based approach. As shown in Table 7, $\dot{V}_g$ is 30.0 cfm (0.014m^3/s) for

the testing RTU with an uncertainty of ±1%. ΔT_{fan} is 1.7 ºF (0.9 ºC) obtained in the CAV RTU with an uncertainty of ±0.2 ºF (0.1ºC). The uncertainties of $SAT_{mfr,cal}$ and MAT_{vir} are ±1.2ºF (0.7ºC) and ±1.0ºF (0.6ºC), respectively. It is found that uncertainty of heating-based SCFM meter is within ±6.9%. This means we are 93.1% confident with the true value of SCFM in heating mode.

Table 7: Uncertainty analysis of heating-based SCFM meter

Independent variables	**Inputs**	**Uncertainty**
Flue gas flow rate, $\dot{V}_g$, cfm (m^3/s)	30.0 (0.014)	±1%
Supply fan temperature rise, ΔT_{fan}, ºF (ºC)	1.7 (0.9)	±0.2(0.1)
Supply air temperature, $SAT_{mfr,cal}$, ºF (ºC)	The results of $SAT_{mfr,cal}$ in Table 4	±1.2(0.7)
Mixed air temperature, MAT_{vir}, ºF (ºC)	The results of MAT_{vir} in Table 4	±1.0(0.6)

Dependent variable	Uncertainty of heating-based approach, $\dot{V}_{H,model}$							
Scenario ID	H-1	H-2	H-3	H-4	H-5	H-6	H-7	H-8
Uncertainty	±3.6%	±4.0%	±3.7%	±3.6%	±4.1%	±4.4%	±4.0%	±4.0%
Scenario ID	H-9	H-10	H-11	H-12	H-13	H-14	H-15	H-16
Uncertainty	±5.7%	±5.8%	±6.3%	±6.9%	±6.3%	±6.3%	±5.7%	±5.8%

3.2.2.3 Experimental evaluation of heating-based SCFM meter

Experimental evaluation of the heating-based virtual SCFM meter by using the sixteen sets of lab tests is given in this section. The relative error $e_{H,eva}$ between the measured SCFM $\dot{V}_{meas}$ and $\dot{V}_{H,model}$ is defined as follows,

$$e_{H,eva} = \frac{\dot{V}_{H,model} - \dot{V}_{meas}}{\dot{V}_{meas}} \tag{52}$$

As shown in Table 8, it is found the maximum absolute relative error $e_{H,eva}$ is 7.6%. This demonstrates the virtual SCFM meter in heating mode accurately predicts the true value of SCFM in the RTU.

Table 8: Experimental evaluation of heating-based SCFM meter

Scenario ID	**$\dot{V}_{H,model}$, cfm(m^3/s)**	**$\dot{V}_{meas}$, cfm(m^3/s)**	**$e_{H,eva}$**	**Scenario ID**	**$\dot{V}_{H,model}$, cfm(m^3/s)**	**$\dot{V}_{meas}$, cfm(m^3/s)**	**$e_{H,eva}$**
H-1	1854(0.87)	1848(0.87)	0.3%	H-9	1896(0.89)	1853(0.87)	2.3%
H-2	2076(0.98)	2045(0.97)	1.5%	H-10	2123(1.00)	2051(0.97)	3.5%

H-3	1866(0.88)	1857(0.88)	0.5%	H-11	1890(0.89)	1849(0.87)	2.2%
H-4	1834(0.87)	1829(0.86)	0.3%	H-12	1969(0.93)	1831(0.86)	7.6%
H-5	2174(1.03)	2076(0.98)	4.7%	H-13	2204(1.04)	2081(0.98)	5.9%
H-6	2399(1.13)	2269(1.07)	5.7%	H-14	2443(1.15)	2272(1.07)	7.5%
H-7	2125(1.00)	2037(0.96)	4.3%	H-15	2181(1.03)	2059(0.97)	5.9%
H-8	2132(1.01)	2040(0.96)	4.5%	H-16	2164(1.02)	2046(0.97)	5.7%

To here, both cooling- and heating-based approaches to develop a virtual SCFM meter are presented. Finally, the comparisons and conclusions of the two approaches are explored in the next subsection.

3.3 Comparisons and conclusions of cooling- and heating-based approaches

Comparing the cooling and heating-based approaches, we could reach the following conclusions:

- *Uncertainty of $\dot{V}_{C,model}$ is much higher than the uncertainty of $\dot{V}_{H,model}$*

$\dot{V}_{H,model}$ is correlated with the inputs of $\dot{V}_g$,ΔT_{fan}, $SAT_{mfr,cal}$ and MAT_{vir}, wherein $\dot{V}_g$ and ΔT_{fan} are quite stable with very low uncertainties. Uncertainty of $\dot{V}_{H,model}$ is low, within ±6.9%. In contrast, $\dot{V}_{C,model}$ is calculated by five parameters of OAT, MAT_{vir}, $MAT_{wb,vir}$, SAT and ΔT_{fan} with more difficulties of implementation and higher risk of uncertainties (±13.8 %, in this case). The heating-based SCFM meter, with the feature of "less uncertainty", is considered simple, stable and could accurately predict the SCFM in RTUs.

- *The relative error $e_{C,eva}$ between $\dot{V}_{meas}$ and $\dot{V}_{C,model}$ is high, while $e_{H,eva}$ in heating mode is low*

Owing to the uncertainty generated by the model regression of $\dot{Q}_{C,sens}$ in Equation (18), as well as the uncertainty associated with the multiple measurements of $\dot{V}_{C,model}$ in Equation (28), the relative errors $e_{C,eva}$ between $\dot{V}_{meas}$ and $\dot{V}_{C,model}$ are high (-16.2~16.4%, in this case). However, $\dot{V}_{H,model}$, with simple and reliable inputs, is much close to $\dot{V}_{meas}$ as evaluated through laboratory tests.

- *Robustness of $\dot{V}_{H,model}$ is better than $\dot{V}_{C,model}$*

Although the manufacturer-data based cooling capacity model proposed by Yang and Li (2010) could work well when the system operates normally or only air side faults are present (e.g. improper supply airflow rates), it could not work in the presence of the faults developed at refrigerant side (e.g. low refrigerant charge). However, it is notorious that the refrigerant side of RTUs is plagued by various common degraded faults due to its complexity (Proctor and Downey, 1995; Cowan, 2004; Li and Braun 2007a, 2007b, 2009a). This fact causes more difficulties and limitations when implementing and accurately monitoring the cooling-based SCFM meter in practice. However, in heating mode, the gas side is simple and its gas flow rate is accurately controlled by a sophisticated gas regulator. Although the gas side could fail occasionally, degraded faults associated with the gas side have been rarely reported. It is easy to identify complete failure and thus to avoid using the flow meter. With the good-fault free property, heating-based SCFM meter performs robustly most of the time.

- *Relative humidity measurement of inlet air is required for cooling mode, but not for heating mode*

According to Equation (28), MAT_{wb} is critical to calculate the SCFM for cooling mode. Installing relative humidity sensor is needed to collect the measurement of wet bulb temperature. However, no measurement on the air humidity is required in the heating-based approach. Only easy-to-obtain measurements (dry bulb temperatures) are left in Equation (50) as unknown dependent variables. As we know, RTUs may not have relative humidity sensors mounted by manufacturers. Comparing to temperature sensors, relative humidity sensors are costly. Additional costs entail with procurement, installation and maintenance of relative humidity sensors. Moreover, a relative humidity sensor is notorious for its accuracy drifting and saturation under high humidity levels.

The above comparisons between cooling- and heating-based approaches reveals that utilizing heating mode to develop a virtual SCFM meter is worthy of confidence. Therefore, the implementation issues of a heating-based virtual SCFM meter, covering detailed measuring and processing the parameters and an implementation flowchart, are introduced in the following section.

3.4 Implementation issues

This part is dedicated to provide an instruction of using this virtual SCFM meter in practice. Except for the stable input of $\dot{V}_g$ of the heat exchanger, implementation issues of three temperature measurements SAT, MAT and ΔT_{fan}, are described.

To ensure the robustness and reliability of this virtual meter, a steady-status detector presented by Li and Braun (2003b) is referred to filter out the transient data of all temperature measurements related to Equation (38).

3.4.1 Measuring and processing SAT

3.4.1.1 Background of direct measurements of SAT in RTUs

Accurate SAT measurements would directly influence the performance of the virtual SCFM meter. In the field, there is a manufacturer-preinstalled SAT sensor (MSAT) widely used in most light commercial RTUs and it is not difficult to collect the readings. However, a common practice by RTU manufacturers is to pre-install the MSAT sensor right after the gas-fired heating coil in a compact chamber. Owing to the following two inherent problems under this arrangement, the accuracy and reliability of the MSAT sensor are notoriously difficult to attain in heating mode (ASHRAE fundamental, 2009):

- *Poor air temperature distribution*

With gas-fired heating coil mounted in a crowded housing, RTUs have an extremely uneven air temperature distribution where the onboard SAT temperature sensor is located. According to ASME PTC 19.3-1974, aspiration method involving passing a high-velocity stream of air over the temperature sensor is improbable to be applied.

- *Intensive thermal radiation of gas heating*

The MSAT sensor is bathed in an adverse hot air chamber. Measurements can be affected by radiation from surrounding surfaces (ASHRAE fundamental, 2009). Strong thermal radiation from gas

burners causes a dramatic rise in air temperature measurement. Even with the shielding suggested by Parmelee and Huebscher (1946), the radiation impact on the MSAT sensor can hardly be eliminated. Meanwhile, the RTU's compact structure makes it improper for shielding.

Consequently, manufacturers recommend that the MSAT sensor should be relocated to the supply air duct on site, particularly if the supply air temperature control functions were used (Lennox, 2007). However, relocating the MSAT sensor would run into a series of problems.

First of all, repositioning the MSAT sensor to the supply air duct could be very costly in a situation where all other installations of a system are completed. It is greatly in excess of the original budget planned for an economy packaged unit. Second, RTUs are usually set up right upon the roof of the served zones in light commercial buildings (e.g., big-box retail stores), the supply air duct, if there is one, is too short to meet the minimum requirements by manufacturers or to achieve a balanced air temperature distribution.

As a result, a lot of building operators either do not bother to relocate the MSAT sensor, which will cause unreliable supply air temperature related control functions, or completely disable the MSAT sensor related functions.

Instead of repositioning the MSAT sensor to supply air duct or directly using the MSAT measurements, we proposed an innovative virtual calibration method to solve the dilemma (Yu et al. 2011). The main merit of this method is that a general linear model to offset the MSAT errors is created through a one-time algorithm development. This virtual calibration technique is very cost-effective, accurate, stable, easy-to-use and generic for all RTUs with similar construction of gas furnaces and can be implemented for long-term use.

The study begins with the evaluation of two groups of direct measurements: the single onboard MSAT sensor-based measurement and further a measuring grid-based measurement. It is found neither method can provide the real time true value of SAT. There are unstable changing errors in both of them, which rules out the possibility of using regular calibration. Then, a virtual calibration algorithm for the MSAT sensor is proposed based on lab data, and also the modeling and implementation procedures are

summarized for easy-to-use implementation. Uncertainty analysis and additional experimental evaluation are carried out over a wide range of controlled tests later on. The study concludes that the virtually calibrated MSAT sensor can accurately predict the true value and is adopted to develop a virtual SCFM meter in RTUs.

3.4.1.2 Evaluation of direct measurements of SAT in RTUs

Direct measurements are conventionally used for air temperature in all kinds of forced air systems. In this section, the 7.5 ton RTU equipped with gas heating is evaluated in terms of direct SAT measuring of two methods: the MSAT sensor-based measurement and a measuring grid-based measurement.

The assessment starts with the single onboard MSAT sensor under both cooling and heating mode. To further understand the nature of inaccuracy in direct measurement, an additional method, termed multi-sensor measuring grid, is applied. The measurements for them are performed simultaneously in the same experimental series to ensure the consistency and comparability of the results. To keep it simple, only the necessary experimental results and the deduction are debriefed right below.

- **MSAT sensor-based measurement**

A group of parametric tests are implemented to the two-stage cooling and two-stage gas heating 7.5 ton RTU for the evaluation of the MSAT sensor derived measurements. Both cooling and heating mode are offered with stage 1 and 2. OADst is modulated at 0% and 30% for the different runs, since in cooling and heating mode, RTUs bring in minimum outside air flow for ventilation and 30% is usually the upper limit for a minimum damper position (ASHRAE Standard 62.1, 2007). Besides the data point given in the section 3.1.2.1 and 3.2.2.1, there is an additional lab-installed SAT sensor ($SAT_{lab,meas}$) to verify the MSAT measurement in the lab. Each experiment assigned a scenario ID is conducted around 20 minutes for preparation, and followed by 10 to 15 minutes under steady status (Li and Braun 2003b). Instant readings for each sensor are sampled every 15 seconds and the mean of the samples is then used to represent the corresponding measurement result.

In Table 9, experiment settings and results are provided. The error e accounts for the difference between the average measurements of the MSAT sensor ($SAT_{mfr,meas}$) and the additional lab-installed SAT sensor ($SAT_{lab,meas}$):

$$e = SAT_{lab,meas} - SAT_{mfr,meas} \tag{53}$$

From the results, we can see,

- *In cooling mode, the direct measurements are considered reliable with e less than 2.0 °F (1.1°C).*
- *However, in heating mode, direct measurements with both sensors lose credibility since e widely varies from 21.0 °F (11.7 °C) to 34.6 °F (19.2 °C).*

Therefore, further analysis to evaluate the MSAT sensor-based measurement in heating mode is carried out by comparing $SAT_{mfr,meas}$ to the predicted theoretical true value of SAT ($SAT_{th,pred}$) as e_H:

$$e_H = SAT_{mfr,meas} - SAT_{th,pred} \tag{54}$$

Where $SAT_{th,pred}$ is derived from an energy balance shown as Equation (55).

$$SAT_{th,pred} = \frac{\dot{Q}_H}{C_P \times \dot{V}_{meas}} v + MAT + \Delta T_{fan} \tag{55}$$

The procedures of measuring the parameters in Equation (54) to (55) are addressed in detail in the section 3.1.2.1. As given in Table 9, e_H is found unstable with the MSAT sensor-based measurement. It alters in a wide range from 1.0 °F (0.6 °C) to 12.6°F (7.0 °C) when test condition varies. It is obviously improper to directly use $SAT_{mfr,meas}$ in heating mode as the true value of SAT in the RTU. The results also demonstrate that a regular calibration with a fixed offset based on the MSAT sensor-based direct measurement would fail.

Table 9: Evaluation of direct SAT measurement under both cooling and heating mode

Running Mode	Running Stage	OADst	Scenario ID	$SAT_{lab,meas}$,°F(°C)	$SAT_{mfr,meas}$,°F(°C)	*e* ,°F(°C)
Cooling	2	0%	C-1	48.2(9.0)	46.2(7.9)	***2.0(1.1)***
Cooling	2	0%	C-2	38.8(3.8)	36.8(2.7)	***2.0(1.1)***
Cooling	2	30%	C-3	51.2(10.7)	49.4(9.7)	***1.8(1.0)***
Cooling	2	30%	C-4	50.4(10.2)	48.4(9.1)	***1.9(1.1)***
Cooling	1	0%	C-5	62.3(16.8)	61.3(16.3)	***1.0(0.6)***
Cooling	1	0%	C-6	56.4(13.6)	55.8(13.2)	***0.5(0.3)***

Cooling	1	30%	C-7	66.4(19.1)	65.9(18.8)			***0.5(0.3)***	
Cooling	1	30%	C-8	66.0(18.9)	64.6(18.1)			***1.4(0.8)***	
Running Mode	**Running Stage**	**OADst**	**Scenario ID**	**$SAT_{lab,meas}$,°F(°C)**	**$SAT_{mfr,meas}$, °F(°C)**	**$\dot{V}_{meas}$, cfm(m^3/s)**	**$SAT_{th,pred}$, °F(°C)**	**MAT, °F(°C)**	**e_H , °F(°C)**	**e , °F(°C)**
Heating	2	0%	H-1	151.4(66.3)	120.1(48.9)	1848(0.87)	108.0(42.2)	54.2(12.3)	***12.1(6.7)***	***31.3(17.4)***
Heating	2	0%	H-2	151.3(66.3)	120.0(48.9)	2045(0.97)	108.3(42.4)	59.5(15.3)	***11.7(6.5)***	***31.3(17.4)***
Heating	2	0%	H-3	152.5(66.9)	121.5(49.7)	1857(0.88)	108.9(42.7)	55.4(13.0)	***12.6(7.0)***	***31.0(17.2)***
Heating	2	0%	H-4	155.1(68.4)	124.0(51.1)	1829(0.86)	111.8(44.3)	57.4(14.1)	***12.2(6.8)***	***31.1(17.3)***
Heating	2	30%	H-5	134.4(56.9)	99.9(37.7)	2076(0.98)	93.0(33.9)	44.9(7.2)	***6.9(3.8)***	***34.5(19.2)***
Heating	2	30%	H-6	138.5(59.2)	104.5(40.3)	2269(1.07)	96.7(35.9)	52.5(11.4)	***7.8(4.3)***	***34.1(18.9)***
Heating	2	30%	H-7	140.5(60.3)	106.1(41.2)	2037(0.96)	99.2(37.3)	50.2(10.1)	***7.0(3.9)***	***34.4(19.1)***
Heating	2	30%	H-8	144.4(62.4)	109.9(43.3)	2040(0.96)	102.7(39.3)	53.8(12.1)	***7.2(4.0)***	***34.6(19.2)***
Heating	1	0%	H-9	120.4(49.1)	99.4(37.4)	1853(0.87)	94.7(34.8)	59.3(15.2)	***4.6(2.6)***	***21.1(11.7)***
Heating	1	0%	H-10	119.1(48.4)	98.1(36.7)	2051(0.97)	93.2(34.0)	61.0(16.1)	***4.9(2.7)***	***21.0(11.7)***
Heating	1	0%	H-11	122.1(50.1)	100.8(38.2)	1849(0.87)	96.4(35.8)	60.9(16.1)	***4.3(2.4)***	***21.4(11.9)***
Heating	1	0%	H-12	124.1(51.2)	102.6(39.2)	1831(0.86)	99.6(37.6)	63.7(17.6)	***3.0(1.7)***	***21.4(11.9)***
Heating	1	30%	H-13	106.1(41.2)	82.6(28.1)	2081(0.98)	80.4(26.9)	48.6(9.2)	***2.2(1.2)***	***23.5(13.1)***
Heating	1	30%	H-14	106.4(41.3)	83.2(28.4)	2272(1.07)	82.1(27.8)	52.9(11.6)	***1.0(0.6)***	***23.3(12.9)***
Heating	1	30%	H-15	111.0(43.9)	87.5(38.3)	2059(0.97)	85.5(29.7)	53.4(11.9)	***2.0(1.1)***	***23.5(13.1)***
Heating	1	30%	H-16	114.8(46.0)	90.8(32.7)	2046(0.97)	88.7(31.5)	56.4(13.6)	***2.1(1.2)***	***24.0(13.3)***

- **Measuring grid-based measurement**

A measuring grid in the inlet of supply air duct and right out of the RTU is also constructed for the experiments. Since the grid is not located in the chamber, the radiation influence from the gas burner can be attenuated to some extent. The multi-point measurements employed in a measuring grid are also supposed to improve the overall measurement accuracy with less stratification impact. Eight temperature sensors are positioned in the duct work after the RTU, as depicted in Figure 26. With eight sensors the duct section representative locations are well covered.

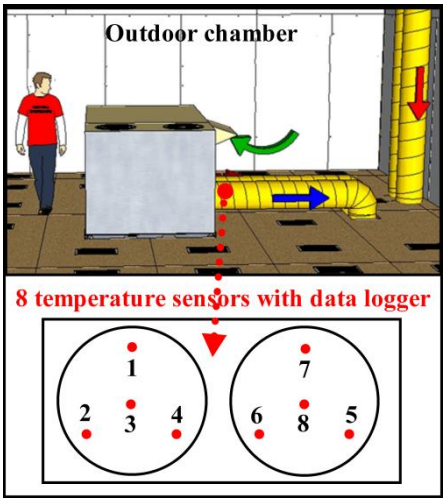

Figure 26: Illustration of measuring grid and numbered sensors

Average values of each sensor from 1 to 8 ($SAT_{G,C}$ for cooling mode and $SAT_{G,H}$ for heating mode), the MSAT sensor-based $SAT_{mfr,meas}$, and the calculated $SAT_{th,pred}$, are plotted in Figure 27 for comparison. The horizontal axis is for different sensor ID and the vertical axis is for air temperatures in Fahrenheit and Celsius degrees. To get a clear view, results of all cooling scenarios and half of all 16 heating scenarios are given.

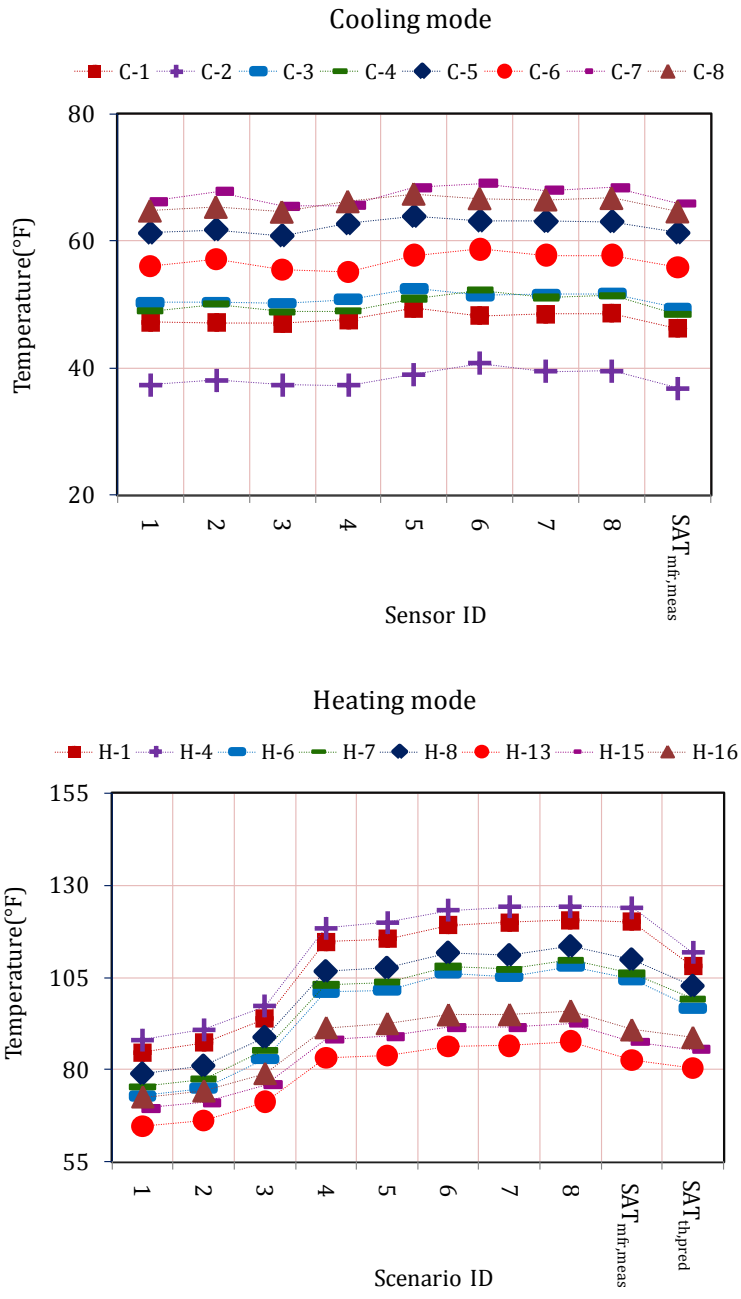
Cooling mode
C-1
C-2
C-3
C-4
C-5
C-6
C-7
C-8
Temperature(°F)
80
60
40
20
1
2
3
4
5
6
7
8
SAT mfr,meas
Sensor ID
Heating mode
H-1
H-4
H-6
H-7
H-8
H-13
H-15
H-16
Temperature(°F)
155
130
105
80
55
1
2
3
4
5
6
7
8
SAT mfr,meas
SAT th,pred
Scenario ID

(a)

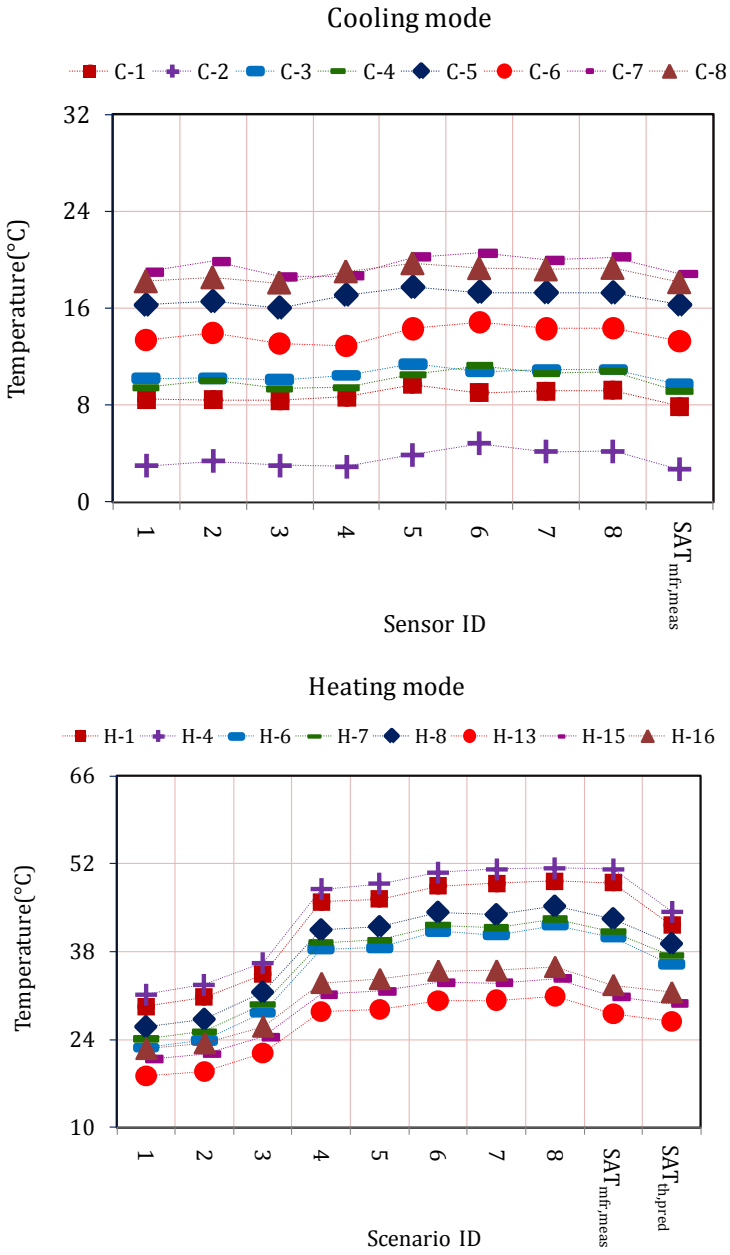

(b)

Figure 27: Evaluation of measuring grid under both cooling and heating mode: (a) IP units and (b) SI units.

The results of cooling mode illustrate that measurements of eight $SAT_{G,C}$ are close to those of $SAT_{mfr,meas}$. In all cooling scenarios, the error between the mean of eight $SAT_{G,C}$ and $SAT_{mfr,meas}$ is about 1.5 ºF (0.8 °C) or less. It is consistent with the previous evaluation for the MSAT sensor-based direct measurement. Both MSAT sensor and measuring grid in cooling mode are trustable for using.

From the heating mode plot, the following points can be observed:

- *Temperature distribution of eight $SAT_{G,H}$ is irregular*

Combining Figure 26 and 27, relationships of eight $SAT_{G,H}$ and their location in heating mode are erratic. Temperature values of sensors 1 to 4 are lower than those of the corresponding sensors 5 to 8. It is unsuitable to calculate the true value of SAT by averaging eight $SAT_{G,H}$.

- *Big temperature difference exists between $SAT_{mfr,meas}$ and the average eight $SAT_{G,H}$*

In scenario H-7, for example, $SAT_{mfr,meas}$ is 106.1°F (41.2 °C) ; $SAT_{G,H}$ sensors 1 to 8 give the lowest reading as 74.4 °F (23.6 °C), the highest as 108.7 °F (42.6°C). It makes the differential temperature between $SAT_{mfr,meas}$ and the average eight $SAT_{G,H}$ 8.9 °F (4.9 °C). In all heating scenarios, the error between $SAT_{mfr,meas}$ and the mean of eight $SAT_{G,H}$ varies from 3.0 ºF (1.7 °C) to 12.2 ºF (6.8 °C) .

- *Various temperature difference stands between $SAT_{th,pred}$ and the mean of eight $SAT_{G,H}$*

The temperature difference between $SAT_{th,pred}$ and the mean of eight $SAT_{G,H}$ varies in different scenarios. Like in scenario H-7, with Hstage 2 and OADst 30%, the mean of eight $SAT_{G,H}$ is 95.2 °F (35.1°C) while the true value $SAT_{th,pred}$ is 99.2 °F (37.3 °C) [with 4.0 °F (2.2 °C) temperature difference]. However, in scenario H-16 with Hstage 1 and OADst 30%, the mean of eight $SAT_{G,H}$ is 85.9°F (29.9 °C) while the true value $SAT_{th,pred}$ is 88.7 °F (31.5 °C) [with 2.8 °F (1.6 °C) temperature difference]. As presented in this case, the measuring grid does not indicate the true value of SAT.

In summary, the evaluation of measuring grid further testifies that the offset error for MSAT in heating mode varies. Controls in RTUs related to MSAT sensor direct measurements in heating mode can be far from the intended operation and lead to inferior system performance. What is more, using measuring grid does not help obtain the true value of SAT in RTUs. It could not be used for the verification of the predicted true value of SAT as well. An innovative calibration algorithm is needed to fill in the gap.

3.4.1.3 Development of a virtual calibration model for a SAT sensor in RTUs

- **Algorithm development**

As analyzed above, direct measurement, either the single MSAT sensor-based or the measuring grid-based cannot catch the true value of SAT. The measuring grid method in a location out of the RTU merely provides closer but still mediocre prediction. Besides, additional construction, costs, maintenance and sources for uncertainty are incurred by using the measuring grid. It is not a practical tool in real applications.

Variables in the experiments thus are reinvestigated to identify the algorithm that might be useful to predict the offset for the calibration of the MSAT sensor-based measurement.

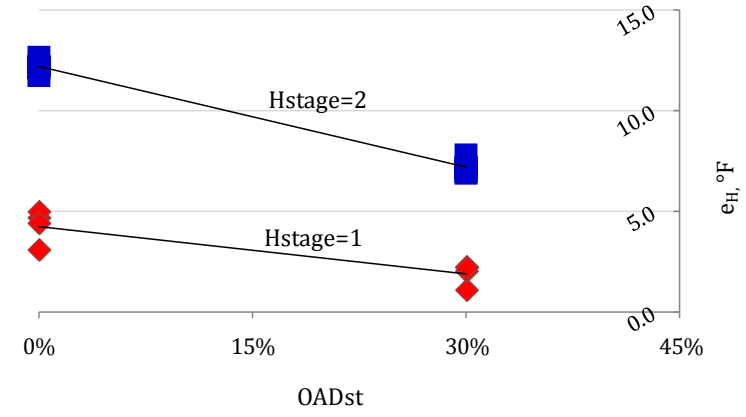

(a)

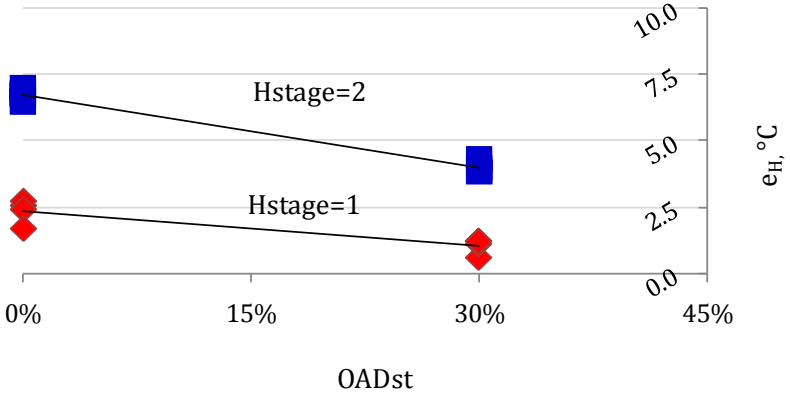

(b)

Figure 28: e_H vs OADst in different Hstage: (a) IP units and (b) SI units.

As shown in Figure 28, the error e_H is a strong function of heating stages (Hstage) and OADst. A liner model can be fitted to represent the relationship between e_H, Hstage and OADst in RTUs. As shown in Equation (56), the model can be used to estimate the calibration error (e_{cal}) of the MSAT sensor under certain Hstage and OADst. Verification through more lab tests is explored in later sections.

$$e_{cal} = a + b \times Hstage + c \times Hstage^2 + d \times OADst + f \times OADst^2 + g \times Hstage \times OADst \quad (56)$$

Once such an offset e_{cal} expression is obtained for a given type of RTU, it can be utilized to correct the MSAT sensor-based measurement for the true value in RTUs. The equation for the calibrated MSAT sensor ($SAT_{mfr,cal}$) is given below:

$$SAT_{mfr,cal} = SAT_{mfr,meas} - e_{cal} \quad (57)$$

For this 7.5 ton rooftop unit with 130,000 Btu/hr (38.1 kW) gas heating capacity, the coefficients for the linear model are obtained with the experimental data. The results are listed in Table 10, with R-square 0.98.

Table 10: Linear model coefficients for the example RTU

IP units	**Coefficient**	**a**	**b**	**c**	**d**	**f**	**g**
	Value	1.0900	0.6905	2.4200	0.5484	0.1166	-8.5000
SI units	**Coefficient**	**a**	**b**	**c**	**d**	**f**	**g**
	Value	0.6056	0.3836	1.3444	0.3047	0.0648	-4.7222

Equations (56) and (57) jointly constitute the model of the virtual calibration that can be directly transplanted to different RTUs.

3.4.1.4 Uncertainty analysis

The virtual calibration algorithm of an MSAT sensor obtains $SAT_{mfr,cal}$ as the prediction of SAT true value. In this section, uncertainty sensitivity of $SAT_{mfr,cal}$ to relative $\dot{Q}_H$, $\dot{V}_{meas}$, MAT and ΔT_{fan} is raised. The root sum square method of uncertainty calculation is applied to the variables. The random uncertainty is expressed in units °F (°C) as Equation (58):

$$\delta SAT_{mfr,cal} = [(\frac{\partial SAT_{mfr,cal}}{\partial \dot{Q}_H}\delta \dot{Q}_H)^2 + (\frac{\partial SAT_{mfr,cal}}{\partial \dot{V}_{meas}}\delta \dot{V}_{meas})^2 + (\frac{\partial SAT_{mfr,cal}}{\partial MAT}\delta MAT)^2 + (\frac{\partial SAT_{mfr,cal}}{\partial \Delta T_{fan}}\delta \Delta T_{fan})^2]^{1/2} \quad (58)$$

Where $\delta \dot{Q}_H$, $\delta \dot{V}_{meas}$, δMAT and $\delta \Delta T_{fan}$ are sensor uncertainties.

Table 11 summarizes the uncertainties of independent variables as inputs to Equation (55), as well as the calculated uncertainties of $SAT_{mfr,cal}$ as outputs. As can be seen, the absolute uncertainty of virtual calibrated SAT is lower than 1.2 °F (0.7 °C). It is in the range of acceptable error for temperature uncertainties in the HVAC industry.

Table 11: Uncertainty analysis of $SAT_{mfr,cal}$

Independent variables			**Inputs**			**Uncertainty**		
Gas heating capacity, $\dot{Q}_H$, Btu/hr (kW)			Gas heating stage 1: 84,500 (24.8) Gas heating stage 2: 130,000 (38.1)			±2%		
Measured supply air flow rate, $\dot{V}_{meas}$, cfm (m^3/s)			Default data in Table 1			±1%		
Mixed air temperature, MAT, °F (°C)			Default data in Table 1			±1.0°F (0.6 °C)		
Supply fan temperature rise, ΔT_{fan}, °F (°C)			1.7°F (0.9 °C)			±0.2°F (0.1 °C)		
Dependent variable	Calibrated manufacturer-installed SAT sensor, $SAT_{mfr,cal}$, °F (°C)							
Scenario ID	H-1	H-2	H-3	H-4	H-5	H-6	H-7	H-8
Uncertainty (°F)	1.2(0.7)	1.1(0.6)	1.2(0.7)	1.2(0.7)	1.1(0.6)	1.1(0.6)	1.1(0.6)	1.1(0.6)
Scenario ID	H-9	H-10	H-11	H-12	H-13	H-14	H-15	H-16
Uncertainty (°F)	1.1(0.6)	1.1(0.6)	1.1(0.6)	1.1(0.6)	1.1(0.6)	1.1(0.6)	1.1(0.6)	1.1(0.6)

The accuracy of virtual calibrated MSAT ($SAT_{mfr,cal}$) in Equation (56) and (57) is further evaluated by using energy balance under both cooling (forward) and heating (backward) mode as elaborated in Appendix B. It demonstrates $SAT_{mfr,cal}$ can be trusted as the true value of SAT in RTUs. The virtual calibration method for measuring and processing MSAT measurement is adopted to develop a virtual SCFM meter in this study.

3.4.2 Measuring and processing MAT

Accurate direct MAT measurements are notoriously difficult to obtain in RTUs due to space constraints and the use of small chambers for mixing outdoor and return air (ANSI/ASME Standard PTC 19.3, 1974). As presented previously, Wichman and Braun (2009) proposed and demonstrated an economical scheme for adjusting a single-point measurement of MAT (a smart MAT sensor) in RTUs that is based on in-situ measurements and self calibration. The approach is achieved by correlating the bias error in terms of OADst and temperature difference between outdoor and return-air. Extensive lab

testing demonstrates that the smart mixed air temperature sensor performs very well and the overall root-mean-squared error is 0.57ºF (0.3ºC). The smart MAT sensor proposed overcomes a typical technical barrier of using costly measurement grids or simulation software.

However, a physical MAT sensor is not typically installed in light commercial RTUs due to its bad performance. So this smart MAT sensor cannot be implemented without adding a new MAT sensor. To further simplify this technique, Yang and Li (2011) proposed an alternative method which eliminates the need of a physical MAT sensor and instead constructs a virtual MAT sensor to estimate MAT using OAT, RAT and a correlated virtual outdoor air ratio sensor β as follows,

$$MAT = \beta \times OAT + (1-\beta) \times RAT \tag{59}$$

Both laboratory and field testing demonstrate an acceptable uncertainty of ±1.0 ºF (0.6 ºC). Since there is no pre-installed physical MAT sensor available in our study, we adopted this method.

With accurate parameters accomplished, a graphical flowchart is explored accordingly to sum up the implementation procedures of a virtual SCFM meter in RTUs.

3.4.3 Implementation flowchart of the virtual SCFM meter

The virtual SCFM meter in RTUs can be implemented through the following procedures in Figure 29:

Step 1: Check the steady-status;

Step 2: Check the heating and cooling status;

Step 3: Check the availability of direct MSAT, OAT and RAT measurements;

Step 4: Virtually calibrate MSAT measurement; compute virtual MAT values;

Step 5: Run the virtual SCFM meter in Equation (50).

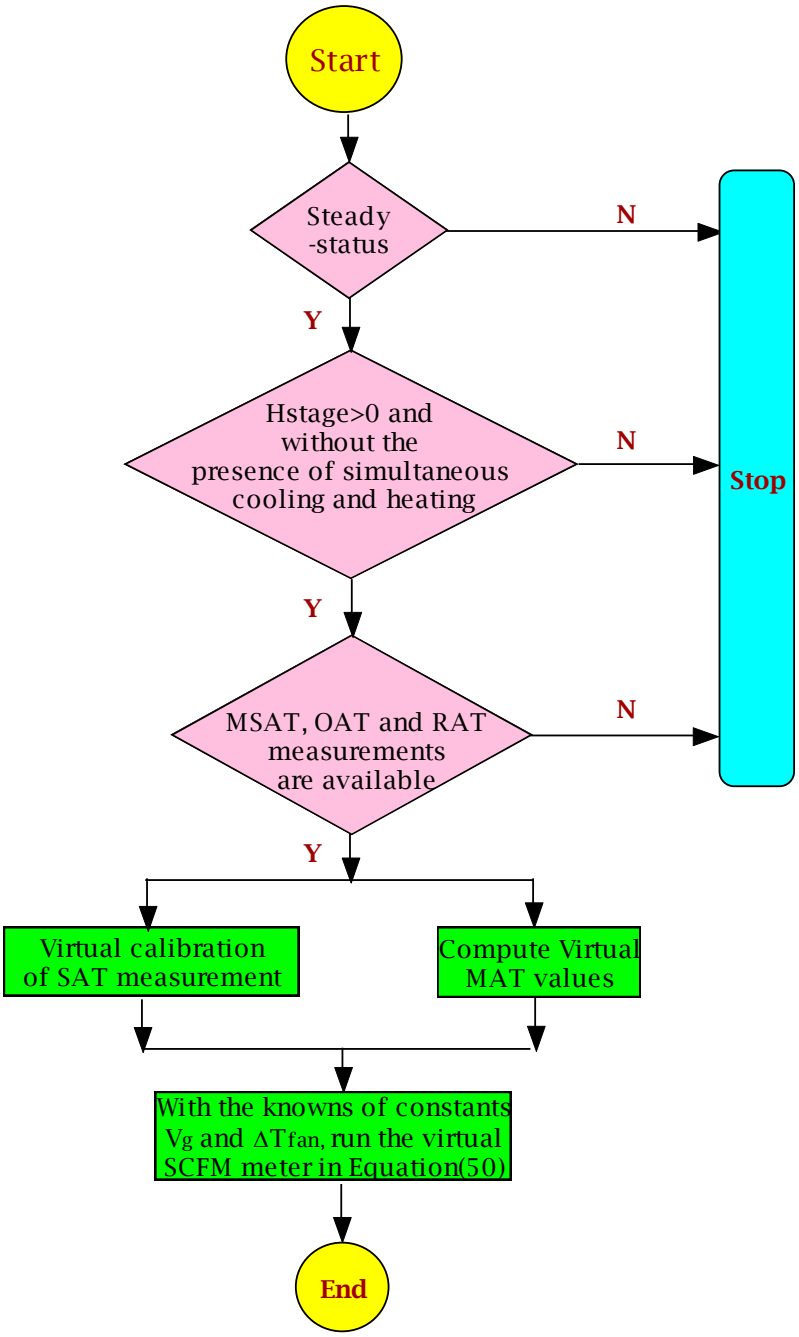

Figure 29: An implementation flowchart of a virtual SCFM meter in RTUs

Chapter 4 FUTURE RESEARCH NEEDS AND CONCLUTION

4.1 Future needs for virtual sensing technology and its application in building systems

4.1.1 Future needs for virtual sensing technology in building systems

There is significant research and development that is needed before virtual sensors become commonplace within buildings. In addition to the need for specific virtual sensor developments, there is a need for standard methods to evaluate virtual sensor performance and approaches for information management of networks of virtual sensors that can share sensor inputs and outputs.

According to Underwood (1997), the performance of physical sensors is evaluated in terms of range, repeatability, sensitivity and accuracy. These same performance parameters are important for virtual sensors. However, the performance of a single virtual sensor can be dependent on the accuracy of multiple physical sensor inputs and a model that uses those inputs to predict the virtual sensor output. Standard approaches for calibrating and evaluating the performance of virtual sensors over a wide range of operating conditions do not exist but are needed. Furthermore, the model used within a virtual sensor can be based on a physical process that changes over time due to the development of faults. As a result, virtual sensor performance evaluations need to consider the robustness of sensor outputs with respect to the development of physical faults.

Another important issue is information management for networks of virtual sensors that are massively deployed within a building system. This problem can be described as systemization of virtual sensors (SoVS), which has been an active area of research in other fields

for more than a decade (Hardy and Maroof 1999; Gu et al. 2004; Chin et. al, 2005; Bose et al. 2007). Figure 30 presents a proposed hierarchy for SoVS that could be applied to virtual sensors in buildings. Two classes of virtual sensor are proposed: basic and derived virtual sensors. Basic virtual sensors are created by using information from a group of physical sensors, empirical coefficients, and user specifications. They can be viewed as extensions of physical sensors that are used as low-cost replacements or backups for physical sensors or to estimate new quantities that cannot be physically measured. Conversely, a derived virtual sensor is a sensor model built in a combination with physical, basic and/or other derived virtual sensor measurements. They could be used to provide higher level system information for performance monitoring, fault identification and advanced control.

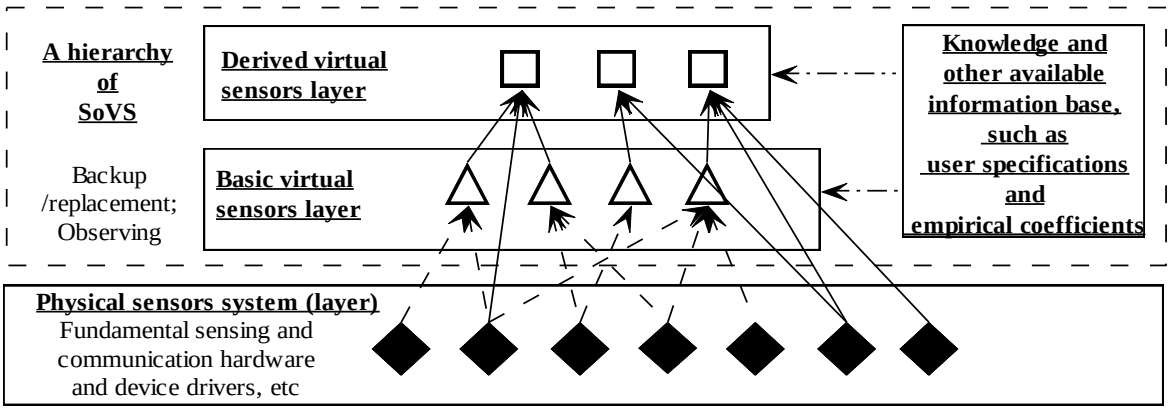

Figure 30: A hierarchy scheme of SoVS

4.1.2 Future steps for development of an improved virtual SCFM meter in RTUs

Based on the above study of development and deployment an FP based virtual SCFM meter in RTUs, we find that it needs further research about its model implementation and fault diagnostics.

The FP based virtual SCFM meter relies heavily on indirect measurements of a virtually calibrated supply air temperature ($SAT_{mfr,cal}$) sensor (Yu. et al. 2011a) and a virtual mixed air temperature (MAT_{vir}) sensor (Yang and Li 2011). Owing to the drifts and other changes of data

during routine operations and during system renovation (e.g., serious damages of physical sensors), there is often no objective measurement to reassess the virtual or virtually calibrated sensors. Moreover, multiple parameters of the virtual meter (e.g., OAT, RAT, SAT and β) periodically require traditional calibration or virtual calibration (Yang et al. 2011) before they can be used since the accuracy and reliability of the fragile physical sensors often cannot be guaranteed (e.g., exposed to hostile environment for a long time).

In the meantime, since the FP based virtual SCFM meter is proposed by utilizing an energy balance in combination with accurate $SAT_{mfr,cal}$ and MAT_{vir} measurements across heating coils, it cannot be used to develop a virtual heating capacity meter inversely for further automated FDD applications.

Therefore, further simplification of implementation and maintenance and enhancement of fault diagnosing capability for the virtual SCFM meter in RTUs is necessary. The attempt of using grey-box or black-box based modeling method could be one of solutions for the future development of an improved virtual SCFM meter in RTUs.

4.1.3 Future steps for development of an improved virtually calibrated SAT sensor in RTUs

The existing virtual calibration model for a SAT sensor proposed by Yu et al (2011) has several deficiencies practically in the following aspects:

- *Low accuracy under a wide range of operating conditions*

Due to the limitations of experimental configurations from Yu et al. (2011), the correlated model of the virtual calibration method exposes greater errors (e.g., relative error is ±4.0 ˚F [2.2˚C]) under a wide range of operating conditions (e.g., OAT is lower than 35˚F[1.67˚C] and the SCFM degradation is higher than 20%) .

- *Poor performance in fault diagnostics*

The low credibility of virtually calibrated MSAT measurements directly causes relatively poor performance in fault diagnostics. A classic example is the FP based virtual SCFM meter, which could raise a higher uncertainty.

- *Limited fault-tolerance in the presence of faults.*

The current virtual calibration model for an MSAT sensor functions well only under conditions in which the RTU performance is not significantly degraded [e.g., supply airflow rate should not be lower than 80% of nominal SCFM level].

Therefore, to overcome the inadequacies of the existing virtual calibration method for an MSAT sensor in RTUs, further research is needed to develop an improved calibration model with well-designed laboratory experiments under a wider span of operation conditions and in the presence of faults (e.g., substantially enhanced SCFM degradation of 50%).

4.2 Conclusion

Virtual sensing has the potential for providing high value information with low cost measurements and models that has been successfully applied in other fields. The benefits for buildings could be even greater than those for other applications because of the cost sensitivity of the industry and the current lack of real-time information on building performance. Virtual sensors could be embedded in practically every device within a building, providing a wealth of component performance information that when combined would provide subsystem and overall system level performance. In addition to smart mechanical and electrical devices (pumps, fans, compressors, lights, etc.), structural and passive devices such as windows, skylights, walls, etc. could have embedded intelligence for providing virtual sensor outputs for energy flows, daylighting, etc. The widespread development and application of virtual sensors within buildings could play a part in revolutionizing the industry and enabling the vision of intelligent and high performance buildings that includes real-time performance monitoring, automated diagnostics, and optimized controls.

This study has reviewed developments and approaches within other fields that could be helpful to product developers and researchers for building applications. Some recent examples of virtual sensors developed for buildings were presented, but for the most part the landscape for future developments is wide open. The virtual sensors developed for buildings are based on very simple steady-state models. More robust and accurate virtual sensors are undoubtedly possible using dynamic models and techniques that have been applied in other fields. Ultimately, manufacturers' of building devices and systems must embrace the concept of embedding virtual sensors within their products before significant progress towards intelligent buildings will be made.

As for development of a virtual SCFM meter for RTUs, the importance and necessity of monitoring SCFM are obvious for control effectiveness, energy conservation and IAQ in building systems. Using direct SCFM meters in RTUs has long been retarded due to the relatively high price and practical problems. An innovative virtual SCFM meter in RTUs only using noninvasive temperature measurements is then proposed in this study.

Modeling and evaluations of both cooling- and heating-based approaches are studied before selecting the algorithm. According to the guiding principles for developing a virtual SCFM meter as the authors suggested, it is found that heating-based SCFM meter possesses the following features: (1) *using a simple while reliable mechanism*; (2) *characteristic of small uncertainty and robust against faults*; (3) *easy-to-obtain parameters or measurements*. The otherwise hard-to-measure SAT and MAT are solved by using the existing research results.

In conclusion, the innovative methodology demonstrates that the virtual SCFM meter in RTUs

- *Is robust enough against various operation conditions;*
- *Has a good accuracy rate (uncertainty is ± 6.9%);*
- *Is relatively easy to implement and economical for use;*

- *Is generic for all RTUs with gas heating.*

As for applications, the virtual SCFM meter can facilitate maintenance and real-time automated FDD in RTUs by:

1. Serving as part of permanently installed control or monitoring system to indicate the real time SCFM and automatically detect and diagnose improper readings

2. Detecting RTU air side faults such as dirty indoor filters and slipping supply fan belt, which lead to decreased SCFM in RTUs

Besides, regarding the SAT parameter used in the virtual SCFM meter, it is found that the single MSAT sensor-based direct measurement is conventionally used in RTUs to obtain SAT. But the accuracy and reliability is greatly compromised in heating mode due to the severe temperature stratification and high thermal radiation in RTUs. The single onboard MSAT sensor- and measuring grid-based measurements are evaluated through a set of tests in a lab. The experiments are designed to cover representative operations in both cooling and heating mode. It is found that, although direct measurements have reasonably good accuracy in cooling mode, there are unacceptable erratic errors in heating mode and a regular calibration can hardly overcome the defect.

An easy-to-use virtual calibration methodology of an MSAT sensor in RTUs is then proposed. A general linear model relying on available operation information (OADst, Hstage) and direct temperature measurements ($SAT_{mfr,meas}$) is derived to acquire the various offsets. Further experimental evaluation and uncertainty analysis are conducted to prove the performance of this innovative method. The study indicates that the virtual calibration of an MSAT sensor in RTUs is robust against multi-variable operating conditions, is easy to implement and economical for use, and is generic in RTUs with the same construction of gas furnaces. Knowledge of accurate SAT values in RTUs would also benefit to real-time automated control, FDD and other advance applications. For instance,

- *It could improve the energy efficiency and obtain better reliability of the SAT based sequencing control*
- *It could serve as part of a permanently installed control or monitoring system to ensure the accuracy in SAT measurement.*
- *It could help find the heating stage failure fault in RTUs by evaluating the differential temperature across the gas furnaces.*
- *It also could be utilized to develop a virtual supply airflow rate meter which is vital for improving energy management, sustaining indoor air quality, and facilitating real-time automated control and FDD in RTU*

References

ACCA. 1995. Manual S. Residential Equipment Selection. Washington, D.C.: Air Conditioning Contractors of America.

ANSI/ARI Standard 540-1999. Positive Displacement Refrigerant Compressors and Compressor Units, American National Standards Institute, New York, NY 10036/Air-Conditioning and Refrigeration Institute, Atlanta, GA 30329, 2003 Ashok N. Srivastava, Nikunj C. Oza and Julienne Stroeve. 2005. Virtual Sensors: Using Data Mining Techniques to Efficiently Estimate Remote Sensing Spectra. *IEEE TRANSACTIONS* ON GEOSCIENCE AND REMOTE SENSING, 43 (3): 590-600

ASHRAE 1999. *ASHRAE Standard* 52.2 . 1999. Method of Testing General Ventilation Air-Cleaning Devices for Removal Efficiency by Particle Size. Atlanta: American Society of Heating, Refrigerating and Air-conditioning Engineers, Inc.

ASHRAE 1992. *ASHRAE Standard* 52.1. 1992, Gravimetric and Dust Spot Procedures for Testing Air Cleaning Devices Used in General Ventilation for Removing Particulate Matter. Atlanta: American Society of Heating, Refrigerating and Air-conditioning Engineers, Inc.

ASHRAE. 2009. *2009 ASHRAE Handbook –Fundamentals*. Atlanta: American Society of Heating, Refrigerating and Air-conditioning Engineers, Inc.

ASHRAE. 1987. *ASHRAE Standard 41.2-1987, Standard Methods for Laboratory Airflow Measurement.* Atlanta: American Society of Heating, Refrigerating and Air-conditioning Engineers, Inc.

ASHRAE. 1995. *ASHRAE Standard 110-1995, Method of Testing Performance of Laboratory Fume Hoods.* Atlanta: American Society of Heating, Refrigerating and Air-conditioning Engineers, Inc.

ASHRAE. 2007. *ASHRAE Standard 62.1-2007, Ventilation for Acceptable Indoor Air Quality.* Atlanta: American Society of Heating, Refrigerating and Air-conditioning Engineers, Inc.

ASME. 1974. *ANSI/ASME Standard PTC 19.3-1974 (R1998), Temperature measurement instruments and apparatus.* American Society of Mechanical Engineers, New York.

Avery, G. 2002. Do averaging sensors average? ASHRAE Journal 44(12):42–43.

Bishop, C. M. 1995. Neural networks for pattern recognition. USA: Oxford University Press.

Bonne, D., and Jorgensen, S. B. 2004. Data-drivenmodeling of batch processes. In Proceedings of 7th international symposium on advanced control of chemical processes, ADCHEM.

Bose, Raja; Helal, Abdelsalam; Sivakumar, Vishak and Lim, Shinyoung. 2007. Virtual sensors for service oriented intelligent environments. *The 3rd IASTED International Conference on Advances in Computer Science and Technology, ACST 2007*: 165-170

Braun, R.H. 1986. Problem and solution to plugging of a finned-tube cooling coil in an air handler. *ASHRAE Transactions, 92(2)*

Breuker, M.S. 1997. Evaluation of a statistical, rule-based detection an diagnosis method for vapor compression air conditioners. Master's thesis, School of Mechanical Engineering, Purdue University, West Lafayette. IN.

Breuker, M.S., and Braun, J.E. 1998a. Common faults and their impacts for rooftop air conditioners. *International Journal of Heating, Ventilating, Air Conditioning and Refrigerating Research* 4(3):303-318.

Breuker, M.S., and Braun, J.E. 1998b. Evaluating the performance of a fault detection and diagnostic system for vapor compression equipment. *International Journal of Heating, Ventilating, Air Conditioning and Refrigerating Research* 4(4):401-425.

C.P. Underwood. 1997. HVAC Control Systems: Modeling, Analysis and Design. Spon Press, ISBN-13: 978-0419209805

Canale, M.; Fagiano, L.; Ruiz, F.; Signorile, M.C.. 2008a. On the design of linear virtual sensors for low cost vehicle stability control. *17th IEEE International Conference on Control Applications 2008*: 1-6

Canale, M.; Fagiano, L.; Ruiz, F.; Signorile, M.C. 2008b. A study on the use of virtual sensors in vehicle control. *47th IEEE Conference on Decision and Control*: 4402-4407

Carling, P., and P. Isakson. 1999. Temperature measurement accuracy in an air-handling unit mixing box. *Proceedings of the 3rd International Symposium on HVAC, ISHVAC '99, Shenzhen, China.*

Casali, A., Gonzalez, G., Torres, F., Vallebuona, G., Castelli, L., & Gimenez, P. 1998.Particle size distribution soft-sensor for a grinding circuit. Powder Technology, 99(1), 15–21.

CEC, 2008, Strategic Plan to Reduce the Energy Impact of Air Conditioners, June 2008, CEC-400-2008-010

Champagne, M., Dudzic, M., Inc, T., & Temiscaming, Q. 2002. Industrial use of multivariate statistical analysis for process monitoring and control. In Proceedings of the 2002 American control conference (vol. 1).

Chastain, J.P. 1987. Pressure gradients and the location of the neutral pressure axis for low-rise structures under pure stack conditions. Unpublished M.S. thesis. University of Kentucky, Lexington.

Cisco, 2005, Cisco Connected Real Estate, http://www.builconn.com/downloads/CCRE-WP2.pdf

Cowan, A. 2004. Review of recent commercial rooftop unit field studies in the Pacific Northwest and California. Northwest Power and Conservation Council and Regional Technical Forum, October 8, Portland, OR.

Devogelaere, D., Rijckaert, M., Leon, O. G., & Lemus, G. C. 2002. Application of feedforward neural networks for soft sensors in the sugar industry. In Proceedings of the VII Brazilian symposium on neural networks, 2002 (SBRN 2002) (pp. 2–6).

DeWolf, S., Cuypers, R. L. E., Zullo, L. C., Vos, B. J., & Bax, B. J. 1996. Model predictive control of a slurry polymerisation reactor. Computers and Chemical Engineering, 20, 955–961.

Doyle, F. J. 1998. Nonlinear inferential control for process applications. Journal of Process Control, 8(5–6), 339–353.

Engdahl, F. and Johansson, D. 2003. Optimal supply air temperature with respect to energy use in a variable air volume system. *Energy and Buildings*, 36(3): 205-18.

Etheridge, D.W. 1977. Crack flow equations and scale effect. Building and Environment 12:181.

Federspiel, C. 2000. Predicting the Frequency and Cost of Hot and Cold Complaints in Buildings. *HVAC&R Research 6(4):* 289-305

Fortuna, Luigi; Graziani, Salvatore; Rizzo, Alessandro; Xibilia, M. Gabriella, 2007, Soft Sensors for Monitoring and Control of Industrial Processes, Springer-Verlag, ISBN 978-1-84628-479-3

Frank, I. E., and Friedman, J. H., 1993. A statistical view of some chemometrics regression tools. *Technometrics*, 35(2): 109–135.

Friedman, G.2004. Too Hot Too Cold Diagnosing Occupant Complaints. *ASHRAE Journal, 46(1):* S157-S158, S160-S163

Gawthrop, Peter J.. 2005. Virtual actuators with virtual sensors. *Proceedings of the Institution of Mechanical Engineers Part I: Journal of Systems and Control Engineering*: 370-377.

Gomez, E., Unbehauen, H., Kortmann, P., and Peters, S. 1996. Fault detection and diagnosis with the help of fuzzy-logic and with application to a laboratory turbogenerator. In Proceedings of the 13th IFAC World Congress (Vol. N) (pp. 175–180).

Gonzalez, G. D., 1999. Soft sensors for processing plants. *In Proceedings of the second international conference on intelligent processing and manufacturing of materials,*1999.

Gosset,W. S. 1908. The probable error of a mean. Biometrika, 6(1), 1–25.

Guopeng Liu, Mingsheng Liu and Gang Wang. 2007a. Development of a pump water flow station in HVAC systems. *2007 Energy Sustainability Conference*

Guopeng Liu, Mingsheng Liu, Gang Wang. 2007b. Optimized pump speed control using pump water flow station for HVAC systems. *ASHRAE Transactions, 113(2)*:362-367

Gustafsson, M. Drevö, U. Forssell, M. Löfgren, N. Persson, and H. Quicklund. 2001. Virtual sensors of tire pressure and road friction. *Society f Automotive Engineers (SAE), Inc.*

Gustafsson, F. 1997. Slip-based estimation of tire-road friction. *Automatica, 33 (6)*:1087-1099

Gustafsson, F. 1998. Estimation and change detection of tire-road friction using the wheel slip. *IEEE Control System Magazine, 18(4):* 42-49

Han, C., and Lee, Y. H., 2002. Intelligent integrated plant operation system for six sigma. Annual Reviews in Control, 26(1), 27–43.

Hardy, Nigel and Maroof, Aftab Ahmad. 1999. ViSIAr - a virtual sensor integration architecture. *Robotica, 17(6):* 635-647

Hardy, Nigel; Ahmad, Aftab. 1999. De-Coupling for Re-Use in Design and Implementation Using Virtual Sensors. Autonomous Robots 6:265-280

Hassan Shraim, Bouchra Ananou, Leonid Fridman, Hassan Noura and Mustapha Ouladsine. 2006. Sliding Mode Observers for the Estimation of Vehicle Parameters Forces and States of the Center of Gravity. Proceedings of the 45th IEEE Conference on Decision & Control: 1635-1640

Hastie, T., Tibshirani, R., and Friedman, J. 2001. The elements of statistical learning: Data mining, inference, and prediction. Springer.

Healy, W., 2010, Building Sensors and Energy Monitoring Systems, Building America Meeting on Diagnositic Measurement and Performance Feedback for Residential Space Conditioning Equipment, National Institute of Standards and Technology, April 26, 2010, Gaithersburg, MD

Hotelling, H. 1931. The generalization of student's ratio. The Annals of Mathematical Statistics, 2(3), 360–378.

Ian B.D. Mclntosh, John W. Mitchell and William A. Beckman. 2000. Fault Detection and Diagnosis in Chillers-Part I: Model Development and Application. ASHRAE Transaction 106: 268-282

Ik-Seong Joo; Mingsheng Liu; Guopeng Liu.2007. Application of Fan Airflow Stations In Air-Handling Units. *Energy engineering, 104(2):* 66-80

J. Ph. Lauffenburger, B. Bradai, A. Herbin and M. Basset. N.2007. Navigation as a Virtual Sensor for Enhanced Lighting Preview Control. *2007 IEEE Intelligent Vehicles Symposium, Istanbul, Turkey*: 1-6

J.S.Y. Chin et. al, 2005. Virtual Appliances for Pervasive Computing: A Deconstructionist, Ontology based, Programming-by-example Approach, the 2005 IEE. International Workshop on Intelligent Environments.

J. Stephant, A. Charara and D. Meizel. 2004a. Experimental validation of vehicle sideslip angle observers. *2004 IEEE Intelligent Vehicles Symposium, Parma, Italy:* 150-155

J. Stephant, A. Charara and D. Meizel. 2004b. Virtual sensor: application to vehicle sideslip angle and transversal forces. *IEEE Transactions on Industrial Electronics, 51(2)*: 278-289

J. Stephant, A. Charara and D. Meizel. 2007. Evaluation of sliding mode observer for vehicle sideslip angle. Control Engineering Practice.15: 803-812

Jackson, J. E., and Mudholkar, G. S. 1979. Control procedures for residuals associated with principal component analysis. Technometrics, 21(3), 341–349.

James, S., Legge, R., and Budman, H. 2002. Comparative study of black-box and hybrid estimation methods in fed-batch fermentation. Journal of Process Control, 12(1), 113–121.

Jang, J. S. R., Sun, C. T., and Mizutani, E. 1997. Neuro-fuzzy and soft computing. Upper Saddle River, NJ: Prentice Hall.

Jolliffe, I. T. 2002. Principal component analysis. Springer.

Jos de Assis, A., and Maciel Filho, R. 2000. Soft sensors development for on-line bioreactor state estimation. Computers and Chemical Engineering, 24(2), 1099–1103.

Kadlec, Petr; Gabrys, Bogdan; Strandt, Sibylle , 2009, Data-driven Soft Sensors in the process industry, Computers and chemical engineering 33 (4): 795–814,

Kampjarvi, P., Sourander, M., Komulainen, T., Vatanski, N., Nikus, M., & Jms-Jounela, S. L. 2008. Fault detection and isolation of an on-line analyzer for an ethylene cracking process. Control Engineering Practice, 16(1), 1–13.

Katipamula, S. and Brambley, M. R. 2005. Methods for Fault Detection, Diagnostics, and Prognostics for Building Systems—A Review, Part I. *HVAR&R Research*, 11(1): 3-25.

Kestell, C.D.; Hansen, C.H.; Cazzolato, B.S. 2001. Virtual sensors in active noise control. *Acoustics Australia, 29(2):* 57-62

Kohonen, T. 1997. Self-organizing maps. Secaucus, NJ, USA: Springer-Verlag New York, Inc.

Kourti, T. , 2002. Process analysis and abnormal situation detection: From theory to practice. Control Systems Magazine, *IEEE*, 22 (5):10–25.

Kresta, J.V., Marlin,T. E.,&MacGregor, J. F. 1994.Development of inferential process models using PLS. Computers and Chemical Engineering, 18(7), 597–611.

Kronvall, J. 1980. Correlating pressurization and infiltration rate data—Tests of an heuristic model. Lund Institute of Technology, Division of Building Technology, Lund, Sweden.

L. Dorst, A.G. Hoekstra, J.M. van den Akker, M. Bergman, F.C.A. Groen, J.M. Lagerberg, A. Visser, H. Yakali, L.O. Hertzberger, 1998. Evaluation Automatic Debiting Systems by Modeling and Simulation of Virtual Sensors. *IEEE Instrumentation and Measurement*, 1:118-25

Larry Palmiter and Paul Francisco. 2000. Development of a Simple Device for Field Airflow Measurement of Residential Air Handling Equipment, Phase I and Phase II. Ecotope Final Report for DOE 2000.

Lee, P.S., and A.L. Dexter. 2005. A fuzzy sensor for measuring the mixed air temperature in air-handling units. Measurement 37(1):83–93.

Lennox, 2007. "M1-7 VERSION 5.02 INTEGRATED MODULAR CONTROLLER (IMC)". *Lennox technical publications*, 2007

Li. H. 2004. A DECOUPLING-BASED UNIFIED FAULT DETECTION AND DIAGNOSIS APPROACH FOR PACKAGED AIR CONDITIONERS. A thesis submitted to the faculty of Purdue University.

Li, H., and J.E. Braun. 2002. On-line models for use in automated fault detection and diagnosis for HVAC&R equipment, in: Proceedings of the 2002 ACEEE Conference on Energy Efficiency in Buildings, Monterey, CA, USA.

Li, H., and J.E. Braun. 2003a. A survey of field service costs for rooftop air conditioners. Internal report, Ray W. Herrick Laboratories, Purdue University, West Lafayette, IN.

Li, H., and J.E. Braun. 2003b. An improved method for fault detection and diagnosis applied to packaged air conditioners. ASHRAE Transactions 109(2):683-92.

Li, H. and Braun, J.E. 2007a. Decoupling Features and Virtual Sensors for Diagnosis of Faults in Vapor Compression Air Conditioners. *International Journal of Refrigeration, 30(3):* 546-564

Li, H. and Braun, J.E. 2007b. A Methodology for Diagnosing Multiple-Simultaneous Faults in Vapor Compression Air Conditioners. *HVAC&R Research, 13(2):* 369-395

Li, H., and J.E. Braun. 2007c. Economic Evaluation of Benefits Associated with Automated Fault Detection and Diagnosis in Rooftop Air Conditioners. *ASHRAE Transactions, 113(2):* 200-210

Li, H., and J.E. Braun. 2009a. Development, Evaluation, and Demonstration of a Virtual Refrigerant Charge Sensor. *HVAC&R Research,15(1)*:117-136

Li, H., and J.E. Braun. 2009b. Virtual Refrigerant Pressure Sensors for Use in Monitoring and Fault Diagnosis of Vapor-Compression Equipment. *HVAC&R Research, 15(3):*597-616

Li, H., and J.E. Braun. 2009c. Decoupling features for diagnosis of reversing and check valve faults in heat pumps *International Journal of Refrigeration,* 32(2009): 316-326

Li, H., Yu, D., and J. E. Braun. 2011. A Review of Virtual Sensing Technology and Application in Building Systems. *HVAC&R Research*, under review

Lin, C., and Lee, C. 1996. Neural fuzzy systems: A neuro-fuzzy synergism to intelligent systems. Upper Saddle River, NJ, USA: Prentice-Hall, Inc.

Matthias Röckl, Jan Gacnik, Jan Schomerus. 2008. Integration of Car-2-Car Communication as a Virtual Sensor in Automotive Sensor Fusion for Advanced Driver Assistance Systems. *2008 Springer Automotive Media (FISITA) World Automotive Congress*

Meleiro, L. A. C., & Finho, R. M. 2000. A self-tuning adaptive control applied to an industrial large scale ethanol production. Computers and Chemical Engineering, 24(2–7), 925–930.

Milanese, Mario; Regruto, Diego; Fortina, Andrea. 2007. Direct Virtual Sensor (DVS) design in vehicle sideslip angle estimation. *2007 American Control Conference*: 3654-3658

Moustapha Doumiati, Alessandro Victorino, Ail Charara and Daniel Lechner. 2009. Virtual sensors, application to vehicle tire-road normal forces for road safety. *2009 American Control Conference*: 3337-3343

Nomikos, P., & MacGregor, J. F. 1995. Multivariate SPC charts formonitoring batch processes. Technometrics, 37(1), 41–59.

Oosterom, M.; Babuška, R. 2000. Virtual sensor for fault detection and isolation in flight control systems - fuzzy modeling approach. *Proceedings of the IEEE Conference on Decision and Control*, 3: 2645-2650,

Ottney, TC. 1993. Particle management for HVAC systems. *ASHRAE Journal 5(l):6.*

Oza, Nikunj C.;Srivastava, Ashok N.; Stroeve, Julienne. 2005. Improvements in virtual sensors: Using spatial information to estimate remote sensing spectra. *International Geoscience and Remote Sensing Symposium (IGARSS)*, 8: 5606-5609

Pablo H. Ibarg¨uengoytia, Alberto Reyes, Mario Huerta and Jorge Hermosillo. 2008. Probabilistic Virtual Sensor for On-Line Viscosity Estimation. Proceedings of the 2008 Seventh Mexican International Conference on Artificial Intelligence: 377-382

Park, S., and Han, C. 2000. A nonlinear soft sensor based on multivariate smoothing procedure for quality estimation in distillation columns. Computers and Chemical Engineering, 24(2–7): 871–877.

Parmelee, G.V. and Huebscher, R.G. 1946. The shielding of thermocouples from the effects of radiation. *ASHRAE Transactions*, 52:183

Poggio, T., and Girosi, F. , 1990. Regularization algorithms for learning that are equivalent to multilayer networks. Science, 247(4945): 978–982.

Prasad, V., Schley, M., Russo, L. P., & Wayne Bequette, B. 2002. Product property and production rate control of styrene polymerization. Journal of Process Control, 12(3), 353–372.

Principe, J. C., Euliano, N. R., and Lefebvre, W. C. 2000. Neural and adaptive systems. New York: Wiley.

Proctor, J., and T. Downey. 1995. Heat pump and air conditioner performance. *Affordable Comfort Conference*, March 26–31, Pittsburgh, PA.

Qin, S. J. 1997. Neural networks for intelligent sensors and control—Practical issues and some solutions. Neural Systems for Control, 213–234.

Qin, S. J., and McAvoy, T. J. 1992. Nonlinear PLS modeling using neural networks. Computers & Chemical Engineering, 16(4), 379–391.

Raveendranathan, N. Loseu, V. Guenterberg, E. Giannantonio, R. Gravina, R. Sgroi, M. Jafari, R. Implementation of Virtual Sensors in Body Sensor Networks with the SPINE Framework. Industrial Embedded Systems, 2009. SIES '09: 124-127

Radhakrishnan, V. R., and Mohamed, A. R. 2000. Neural networks for the identification and control of blast furnace hot metal quality. Journal of Process Control, 10(6), 509–524.

R.H. Howell and H.J. Sauer. 1990a. Field measurements of air velocity: pitot traverse or vane anemometer, *ASHRAE Journal* 32 (3): 46–52.

R.H. Howell and H.J. Sauer. 1990b. Airflow measurements at coil faces with vane anemometers, ASHRAE Transactions 1990; 96(1):502-511.

Rossi, T.M. 1995. Detection, diagnosis, and evaluation of faults in vapor compression cycle equipment. Ph.D. thesis, School of Mechanical Engineering, Purdue University, West Lafayette, Indiana.

Rossi, T.M., and J.E. Braun. 1997. A statistical rule-based fault detection and diagnostic method for vapor compression air conditioners. *HVAC&R Research* 3(1): 19-37.

Rotem, Y., Wachs, A. and Lewin, D. R. 2000. Ethylene compressor monitoring using model-based PCA. *AIChE Journal*, 46(9), 1825–1836.

Robinson, K.D. 1999. Mixing effectiveness of AHU combination mixing/filter box with and without filters. ASHRAE Transactions 105(1):88–95.

S. Kabadayi, A. Pridgen, C. Julien, 2006. Virtual Sensors: Abstracting Data from Physical Sensors, *Proceedings of the 2006 International Symposium on World of Wireless, Mobile and Multimedia Networks*, Buffalo, NY.

Said, Eyad Haj; Homaifar, Abdollah; Grossberg, Michael, 2009. Creating virtual sensors using learning based super resolution and data fusion. IEEE Aerospace Conference Proceedings.

Schulte, R., et. al. 2005. Continuous IAQ Monitoring. *ASHRAE Journal 47(5):* 38-40, 42, 44, 46

Seo, Donghyun; Huang, Joe; Krarti, Moncef. 2008. Development of models for hourly solar radiation prediction. *ASHRAE Transactions, 114(1):* 392-403

Serneels, S., and Verdonck, T. 2008. Principal component analysis for data containing outliers and missing elements. Computational Statistics and Data Analysis, 52(3),1712–1727.

Shengwei Wang and Jingtan Cui. 2006. A Robust Fault Detection and Diagnosis Strategy for Centrifugal Chillers. *HVAC& R Research;* 12(3):407-427.

Stanimirova, I., Daszykowski, M., and Walczak, B. 2007. Dealing with missing values and outliers in principal component analysis. Talanta, 72(1), 172–178.

T.A. Wenzel; K.J. Burnham; M.V. Blundell; R.A. Williams. 2007. Kalman filter as a virtual sensor: applied to automotive stability systems. Transactions of the Institute of Measurement and Control 29(2): 95-115

T. Agami Reddy.2007a. Formulation of a Generic Methodology for Assessing FDD Methods and Its Specific Adoption to Large Chillers. HVAC&R Research, 113(2): 334-342

T. Agami Reddy. 2007b. Development and Evaluation of a Simple Model-Based Automated Fault Detection and Diagnosis (FDD) Method Suitable for Process Faults of Large Chillers. ASHRAE Transactions, 113(2): 27-39

T. Gu, H. K. Pung, D. Q. Zhang, 2004. Towards an OSGibased Infrastructure for Context-aware Applications, Pervasive Computing.

Tan, H., and A.L. Dexter. 2005. Improving the accuracy of sensors in building automation systems. Proceedings of the 16th IFAC World Congress, Prague, Czech Republic.

Tan, H., and A.L. Dexter. 2006. Automated commissioning of a cooling coil using a smart mixed-air temperature sensor. Proceedings of the 7th International Conference on System Simulation in Buildings (SSB 2006), Paper P14, Liege, Belgium.

Takeyasu, Taguchi. 1997. Tire air pressure detecting device. *EP783982. Nippon Denso Co.*

U. Holmberg and M. Hellring. 2003. A simple virtual sensor for combustion timing. *Journal of dynamic systems, measurement, and control, 125(3):* 462-467

Vapnik, V. N. 1998. Statistical learning theory. NewYork: Wiley.

Venkatasubramanian, V.; Rengaswamy, S.; Yin, K.; Kavuri , 2003a, A review of process fault detection and diagnosis Part I: Quantitative model-based methods, Computers and chemical engineering 27 (3): 293–311

Venkatasubramanian, V.; Rengaswamy, S.; Yin, K.; Kavuri , 2003b, A review of process fault detection and diagnosis Part II: Qualitative models and search strategies, Computers and chemical engineering 27 (3): 313–326

Venkatasubramanian, V.; Rengaswamy, S.; Yin, K.; Kavuri , 2003c, A review of process fault detection and diagnosis Part III: Process history based methods, Computers and chemical engineering 27 (3): 327–346

W. P. Mihelc and S. J. Citron, 1984. "An on-line engine roughness measurement technique," SAE Tech. paper 840136.

Walczak, B., and Massart, D. L. 1995. Robust principal components regression as a detection tool for outliers. Chemometrics and Intelligent Laboratory Systems, 27(1),41–54.

Ward, Matthew and Siegel, Jeffrey. 2005. Modeling filter bypass: Impact on filter efficiency: *ASHRAE Transactions, 111(1):* 1091-1100

Walker, I.S., D.J. Wilson., and M.H. Sherman. 1997. A comparison of the power law to quadratic formulations for air infiltration calculations. Energy and Buildings 27(3).

Warne, K., Prasad, G., Rezvani, S., &Maguire, L., 2004. Statistical and computational intelligence techniques for inferential model development: A comparative evaluation and a novel proposition for fusion. Engineering Applications of Artificial Intelligence, 17(8), 871–885.

Wichman, A. 2007. Evaluation of fault detection and diagnosis methods for refrigeration equipment and air-side economizers. Masters thesis, Ray W. Herrick Laboratories, School of Mechanical Engineering,Purdue University, West Lafayette, IN.

Weiss, S., and Kulikowski, C. 1991. Computer systems that learn: Classification and prediction methods from statistics, neural nets, machine learning, and expert systems. San Francisco, CA, USA: Morgan Kaufmann Publishers Inc.

Westphalen, D., and S. Koszalinski. 2001. Energy Consumption Characteristics of Commercial Building HVAC Systems: Volume I – Chillers, Refrigerant Compressors, and Heating Systems. Final Report to the Department of Energy (Contract No. DE-AC01-96CE23798)

Wichman, A and J.E. Braun. 2009. A Smart Mixed-Air Temperature sensor. *HVAR&R Research, 15(1)*: 101-115

Wold, S., Sjstrm, M., and Eriksson, L. 2001. PLS-regression: A basic tool of chemometrics. Chemometrics and Intelligent Laboratory Systems, 58(2), 109–130.

Wray, C., I. Walker, J. Siegel, and M. Sherman. 2002. Practical Diagnostics for Evaluating Residential Commissioning Metrics. Lawrence Berkeley National Laboratory Report LBNL–45959

Yang, M., Yu,D., Xiong,J. and Li, H. 2011, A Methodology of Virtual Calibration and Its Applications in Building Sytems. *HVAC&R Research*, under review.

Yang, H., and Li, H. 2010. A Generic Rating-Data-Based DX Coil Modeling Method, *HVAC&R Research* 16(3): 331–353

Yang, M., and Li, H. 2011. A virtual outside air ratio in packaged air conditioners. *HVAC&R Research,* under review.

Yu, D., Li, H., Yu, Y., and Xiong, J. 2011. Virtual Calibration of A Supply Air Temperature Sensor in Rooftop Air Conditioning Units. *HVAC &R Research,* 17(1): 31.

Yu, D., Li, H., and Yang, M. 2010. A Virtual Supply Airflow Meter for Rooftop Air Conditioning Units. *Building and environment,* 46 (6): 1292-1302.

Yoshihiro, Nishikawa. 1998. Tire air pressure detecting device. *EP832768, US 5982279. Denso Corp, Nippon Soken*

Zhang, Wei; Ding, Nenggen; Yu, Guizhen; Zhou, Wei. 2009. Virtual Sensors Design in Vehicle Sideslip Angle and Velocity of the Centre of Gravity Estimation. Electronic Measurement & Instruments, 9th International Conference 2009: 3-652

Appendix A

Calculation procedure of virtual cooling capacity sensor and its calculation case (Yang and Li 2010)

1. Calculate SHR values for the 192 sets of manufacturer' rating data, i.e., $SHR = \dot{Q}_{C,s} / \dot{Q}_C$

2. Determine $\dot{Q}_C = f(MAT_{wb}, \dot{V}_C, OAT)$ function for wet-coil condition from manual data.

a. First, filter out the dry-coil condition data (i.e., SHR = 1) from the manufacturer's rating data, and then take the average $\dot{Q}_C$ for the remaining data with different MAT values but with the same $(MAT_{wb}, \dot{V}_C, OAT)$. In fact, $\dot{Q}_C$ at different MAT only has a slight difference.

b. Second, use the above data as regression data to obtain the two polynomial-order regression equation (including the cross-terms), i.e.,

$$\dot{Q}_C = -2.07941376E+02 + 2.96627293E + 00 \cdot \dot{V}_C - 5.09934779E-03 \cdot \dot{V}_C^{\,2} - 2.80837085E+00 \cdot OAT - 1.20456417E-02 \cdot OAT^2 + 1.13374693E+01 \cdot MAT_{wb} - 8.90324909E-02 \cdot MAT_{wb}^{\,2} + 3.31590430E-03 \cdot \dot{V}_C \cdot OAT - 3.25207538E-02 \cdot \dot{V}_C \cdot MAT_{wb} + 5.95485478E-02 \cdot OAT \cdot MAT_{wb}.$$

3. Determine $SHR = f(MAT, MAT_{wb}, \dot{V}_C, OAT)$ function for wet-coil condition from manual data.

a. First, using all of the manufacturer's rating data (including the dry- and wet-coil condition data) as regression base data to obtain the two polynomial-order regression equation (including the cross-terms), i.e.,

$SHR_0 = f_0(MAT, MAT_{wb}, \dot{V}_C, OAT)$, Calculated

$SHR_0 = \min(f_0[MAT, MAT_{wb}, \dot{V}_C, OAT], 1)$

SHR_0 = 2.06138630E+00 + 4.86175823E–03 · $\dot{V}_C$ – 2.31885687E–05 · $\dot{V}_C^2$ – 6.03107125E–03 · OAT – 3.47628104E–06 · OAT^2 – 2.12623314E–02 · MAT_{db} – 6.23810658E–04· MAT_{db}^2 + 1.42567593E-03· MAT_{wb} – 1.70365679E–03 · MAT_{wb}^2 + 5.08243110E–06 · $\dot{V}_C$ · OAT– 7.18371002E–05 · $\dot{V}_C$ · MAT_{db} + 8.47359069E–05 · $\dot{V}_C$ · MAT_{wb} + 2.65979398E–05 · OAT· MAT_{db} + 8.21949015E–05 · OAT · MAT_{wb} + 2.16712122E–03 · MAT_{db} · MAT_{wb}

b. Second, calculate the relative error Rel_{SHR0}= *(real SHR – Calculated* SHR_0*) / real SHR* for all data. If the absolute ABS (Rel_{SHR0}) < 0.04 for all data, then SHR_0 is the needed SHR, i.e., SHR = $SHR_0 = f_0(MAT, MAT_{wb}, \dot{V}_C, OAT)$. However, the case has the maximum Rel_{SHR0} at 11%, so the following step (one more trial run) is needed.

c. Otherwise, select both the wet-coil data and the dry-coil data with their SHR_0 (i.e., filter out the dry-coil condition data with their $SHR_0 \geq 1$) as the regression base data to obtain the two polynomial-order regression equation (including the cross-terms), i.e., $SHR_1 = f_1(MAT, MAT_{wb}, \dot{V}_C, OAT)$. Then calculate the relative error Rel_{SHR1} = *(real SHR – Calculated* SHR_1*) / real SHR* for all data. If the absolute ABS(Rel_{SHR1}) < 0.04 for all data, then SHR_1 is the needed SHR. If not, then repeat step 3 to obtain SHR_i (i > 1) until ABS(Rel_{SHR1}) < 0.04 where SHR_i is the needed SHR. The case has the following SHR_1 equation and its maximum Rel_{SHR1} is 7.9%, so one more trial run is needed.

SHR_1 = 9.15278278E–01 + 9.81014645E–03 · $\dot{V}_C$ – 1.65320650E–05 · $\dot{V}_C^2$ – 3.17794263E–03 · OAT + 3.91291794E–06 · OAT^2 + 1.14217256E–02 · MAT_{db}– 5.74152410E–04 · MAT_{db}^2– 1.58296172E–02 · MAT_{wb} – 6.72975815E–04 · MAT_{wb}^2 + 3.44307387E–05 · $\dot{V}_C$ ·

OAT + 7.48326342E–05 · $\dot{V}_C$ · MAT_{db} – 2.08790216E–04 · $\dot{V}_C$ · MAT_{wb} + 1.86863800E–04 · OAT · MAT_{db} – 1.93730853E–04· OAT · MAT_{wb} + 1.21717851E–03 · MAT_{db} · MAT_{wb}

d. Filter out the dry-coil data with their $SHR_1 \geq 1$ and use the remaining data as the regression base data to obtain the two polynomial-order regression equation (including the cross-terms), i.e., $SHR_2 = f_2(MAT, MAT_{wb}, \dot{V}_C, OAT)$ and then its corresponding Rel_{SHR2}. The maximum Rel_{SHR2} is 4%, so SHR_2 is the needed SHR.

SHR_2 = 8.13491256E–01 + 1.12900295E–02 · $\dot{V}_C$ – 1.05332286E–05 · $\dot{V}_C^2$ – 5.14903396E–03 · OAT + 1.62786936E–05 · OAT^2 + 5.17463820E–02 · MAT_{db} – 3.97020976E–04 · MAT_{db}^2 – 6.07627777E–02 · MAT_{wb} + 4.18798335E–04 · MAT_{wb}^2 + 3.91372605E–05 · $\dot{V}_C$ · OAT + 1.20515835E–04 · $\dot{V}_C$ · MAT_{db} – 2.98347811E–04 · $\dot{V}_C$ · MAT_{wb} + 2.70113976E–04 · OAT · MAT_{db} – 2.97676815E–04· OAT · MAT_{wb} + 8.76128835E–05 · MAT_{db} · MAT_{wb}

e. If there is no ABS(Rel_{SHRi}) < 0.04 after several runs, we can choose the SHR_i whose max value or average value of ABS(Rel_{SHRi}) is minimal among these trial runs. Fortunately, we generally can obtain the SHR function before the third trial run for our case calculations, that is, SHR_2 or SHR_1 is the right solution.

4. Determine MAT^0_{wb}.

a. For a fixed ($MAT, \dot{V}_C, OAT$), the equation $SHR = f(MAT, MAT_{wb}, \dot{V}_C, OAT)$ is actually a quadratic equation of MAT_{wb}, i.e., $SHR = a \times MAT_{wb}^2 + b \times MAT_{wb} + c$, where (a, b, c) are constants at a fixed $MAT, \dot{V}_C, OAT$. Given SHR = 1, the MAT_{wb}^0 can be easily solved from the following equation:

$$a \times MAT_{wb}^2 + b \times MAT_{wb} + c - 1 = 0$$

$$\text{i.e., } MAT_{wb}{}^{0} = \frac{-b - \sqrt{b^2 - 4 \times a \times (c-1)}}{2 \times a}$$

All coefficients of the case follow:

a = 4.18798335E–04

b = –6.07627777E–02 – 2.98347811E–04 · $\dot{V}_C$ – 2.97676815E–04 · OAT + 8.76128835E–05 · MAT_{db}

c = 8.13491256E–01 + 1.12900295E–02 · $\dot{V}_C$ – 1.05332286E–05 · $\dot{V}_C{}^2$ – 5.14903396E–03· OAT + 1.62786936E–05 · OAT^2 + 5.17463820E–02 · MAT_{db} – 3.97020976E–04 · $MAT_{db}{}^2$+ 3.91372605E–05 · $\dot{V}_C$ · OAT + 1.20515835E–04· $\dot{V}_C$ · MAT_{db} + 2.70113976E–04 · OAT · MAT_{db}

5. Having obtained $\dot{Q}_C$ = f(MAT_{wb}, $\dot{V}_C$, OAT), SHR = f(MAT_{wb}, MAT_{db}, OAT, $\dot{V}_C$), and $MAT_{wb}{}^{0}$, we can quickly determine the coil's condition and its cooling capacity for any operating driving inputs (MAT_{db}, MAT_{wb}, $\dot{V}_C$, OAT) using Equation (18).

Appendix B

Experimental evaluation of the virtual calibration method for a SAT sensor in RTUs

Measurements description

There are another more than seven indispensable air temperature sensors to accomplish the study are listed below:

Measurements of additional six air temperature sensors Figure 31 depicts the installation of six air temperature sensors at the supply air duct outlet to the indoor chamber. Measurements under both cooling ($SAT_{O,C}$) and heating ($SAT_{O,H}$) mode of these six air temperature sensors are collected.

Measurement of lab-installed temperature sensor at the supply air duct outlet The sensor is referred to as lab-installed temperature sensor at the supply air duct outlet ($SAT_{O,lab}$). The function is to verify the additional six temperature sensors at the supply air duct outlet in Figure 31.

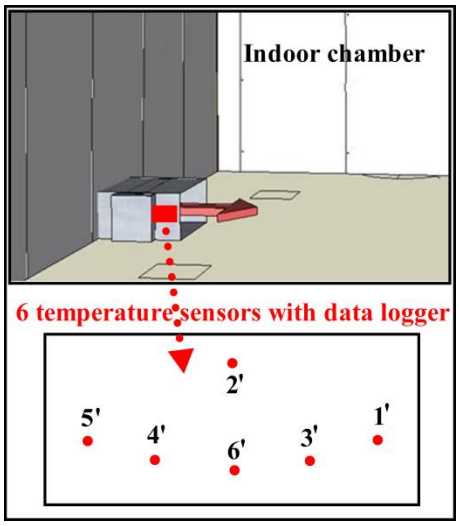

Figure 31: Sensors layout of additional six air temperature sensors

Evaluation of $SAT_{O,C}$ and $SAT_{O,H}$

Observed from Figure 32, in cooling mode, the average error between $SAT_{O,lab}$ and the mean of six $SAT_{O,C}$ is less than 1ºF (0.6°C). In the meantime, in heating mode, the error between $SAT_{O,lab}$ and the mean of six $SAT_{O,C}$ is lower 3 ºF (1.7°C). As expected, at the cross-section close to the outlet, air is well mixed and temperature distribution is fairly balanced. So in this study the mean of six $SAT_{O,C}$ and the mean of six $SAT_{O,H}$ are used in the verification process.

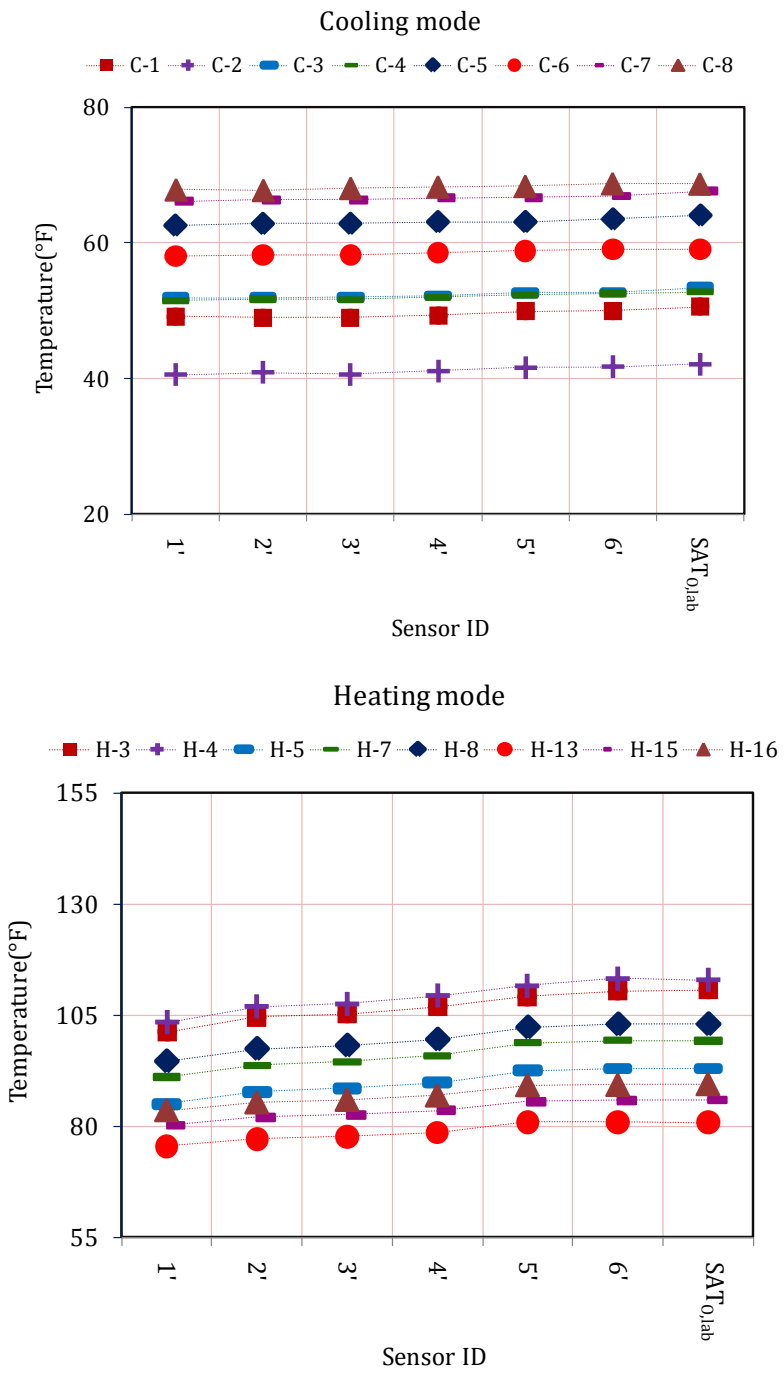
Cooling mode
C-1
C-2
C-3
C-4
C-5
C-6
C-7
C-8
80
60
40
20
Temperature(°F)
1'
2'
3'
4'
5'
6'
SAT O,lab
Sensor ID
Heating mode
H-3
H-4
H-5
H-7
H-8
H-13
H-15
H-16
155
130
105
80
55
Temperature(°F)
1'
2'
3'
4'
5'
6'
SAT O,lab
Sensor ID

(a)

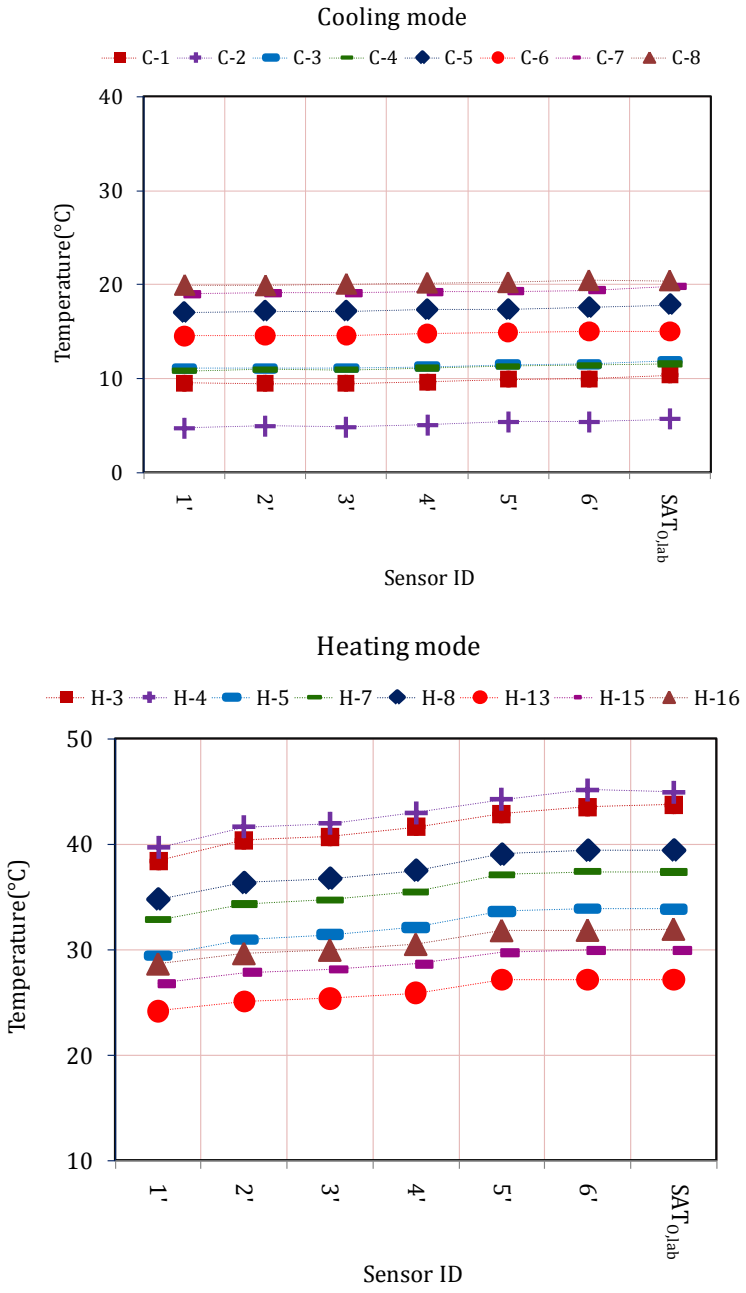

(b)

Figure 32: Evaluation of additional six temperature sensors under both cooling and heating mode: (a) IP units and (b) SI units.

Experimental evaluation of virtually calibrated SAT measurement

Evaluation is presented here to validate the accuracy of virtually calibrated MSAT measurement. There is no direct way but an indirect method to evaluate the accuracy of virtual

calibration method in RTUs. This goal is achieved by carefully designing an experiment in a laboratory environment.

- **Evaluation layout**

Figure 33 depicts the experiment evaluation procedures of the virtual calibration methodology for an MSAT sensor presented in this study. The idea of using energy balance under both cooling (forward) and heating (backward) mode is innovatively conducted.

The verification is implemented by comparing $SAT_{mfr,cal}$ in Equation (57) to experimentally calculated true value of SAT ($SAT_{exp,eva}$). $SAT_{exp,eva}$ is obtained based on an energy balance of the heat loss through the duct work. It is a counterpart of $SAT_{mfr,cal}$ but used for evaluation purposes only. To calculate $SAT_{exp,eva}$, the knowns and assumptions are listed as follows:

- The mean of eight $SAT_{G,C}$ is regarded as the true value of SAT in cooling mode.
- Based on the supportive analysis previously, measurements of six air temperature sensors at the supply air duct outlet are reliable under both heating ($SAT_{O,H}$) and cooling mode ($SAT_{O,C}$). The average of six $SAT_{O,H}$ and the average of six $SAT_{O,C}$ are used in the calculation.
- UA of the supply air duct work from the measuring grid to the outlet is assumed to be constant under both cooling and heating mode.
- Supply air flow rate ($\dot{V}_{meas}$) and additional temperature measurements are taken in the location where the air is well mixed.

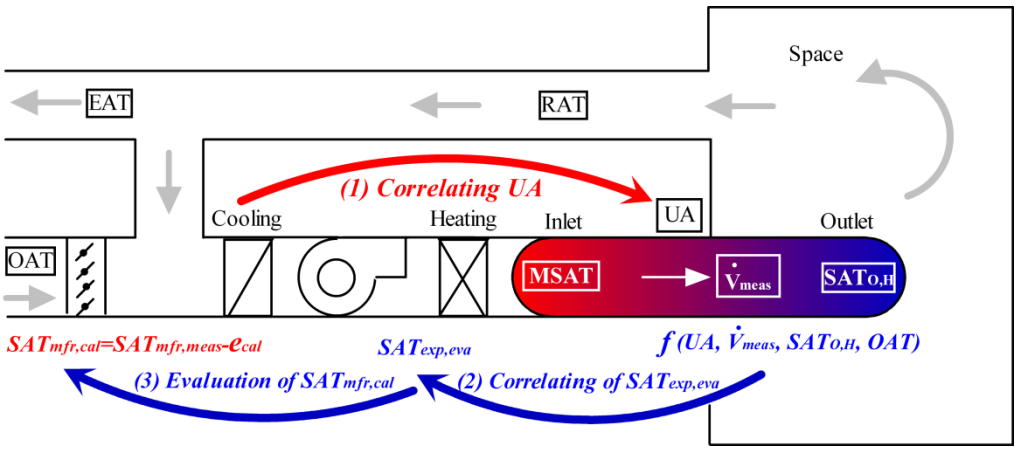

Figure 33: The experiment evaluation procedures of the virtual calibration methodology

- **Evaluation implementation**

Three main steps of evaluation in sequence are included as follows:

Step (1): Correcting UA in cooling mode

Heat loss in cooling mode ($Q_{loss,C}$) through the duct work leads to the air temperature change from the measuring grid cross-section to the outlet in the duct. Heat transfer surface (A) and heat transfer coefficient (U) of the duct work are constants; therefore, UA could be deduced with $\dot{V}_{meas}$, OAT, $SAT_{G,C}$ and $SAT_{O,C}$.

Step (2): Correlating $SAT_{exp,eva}$

Similarly, $SAT_{exp,eva}$ in heating mode should be acquired while UA, $\dot{V}_{meas}$, $SAT_{O,H}$ and OAT are known.

Step (3): Verification of $SAT_{mfr,cal}$

Finally, $SAT_{mfr,cal}$ in heating mode is evaluated after $SAT_{exp,eva}$ is derived from experiments.

Step (1): Correcting UA in cooling mode

The goal here is to estimate the constant UA in the lab environment with the data points collected in the experiment series in cooling mode. To investigate the UA, it is assumed that (1)

the overall heat transfer coefficient is constant, (2) the specific heat of air is constant, and (3) the supply air flow rate is constant because a fixed-fan speed is incorporated in the RTU.

In cooling mode, with $\dot{V}_{meas}$, OAT, $SAT_{G,C}$ and $SAT_{O,C}$ known, $Q_{loss,C}$ can be calculated:

$$Q_{loss,C} = \frac{\dot{V}_{meas} \times C_p \times (SAT_{O,C} - SAT_{G,C})}{v} \tag{60}$$

Meanwhile, $Q_{loss,C}$ also can be expressed as:

$$Q_{loss,C} = UA(OAT - \frac{SAT_{O,C} + SAT_{G,C}}{2}) \tag{61}$$

Combining the two expressions, we get:

$$\frac{\dot{V}_{meas} \times C_p \times (SAT_{O,C} - SAT_{G,C})}{v} = UA(OAT - \frac{SAT_{O,C} + SAT_{G,C}}{2}) \tag{62}$$

Put variable ΔT_C as follows:

$$\Delta T_C = OAT - \frac{SAT_{O,C} + SAT_{G,C}}{2}$$

So, Equation (61) can be further simplified to the equation below:

$$Q_{loss,C} = UA \times \Delta T_C \tag{63}$$

Eight sets of $\dot{V}_{meas}$, OAT, $SAT_{G,C}$ and $SAT_{O,C}$, as well as the intermediate value $Q_{loss,C}$ and ΔT_C, are listed in Table 12.

Table 12: Correcting UA in cooling mode

Scenario ID	$\dot{V}_{meas}$, cfm (m^3/s)	$SAT_{O,C}$,°F(°C)	$SAT_{G,C}$,°F(°C)	OAT,°F(°C)	$Q_{loss,C}$, Btu/hr(kW)	ΔT_C,°F(°C)
C-1	1931(0.9)	49.4(9.7)	48.0(8.9)	81.8(27.7)	2982(0.87)	33.1(18.4)
C-2	2328(1.1)	41.1(5.1)	38.6(3.7)	87.8(31.0)	6311(1.85)	47.9(26.6)
C-3	2084(1.0)	52.3(11.3)	51.1(10.6)	82.3(27.9)	2566(0.75)	30.6(17.0)
C-4	2595(1.2)	51.9(11.1)	50.3(10.2)	87.0(30.6)	4596(1.35)	35.9(19.9)
C-5	1874(0.9)	63.0(17.2)	62.5(16.9)	79.6(26.4)	1154(0.34)	16.9(9.4)
C-6	2251(1.1)	58.5(14.7)	57.0(13.9)	81.8(27.7)	3792(1.11)	24.1(13.4)
C-7	2026(1.0)	66.5(19.2)	66.0(18.9)	81.9(27.7)	1094(0.32)	15.7(8.7)
C-8	2526(1.2)	68.2(20.1)	67.4(19.7)	86.4(30.2)	2373(0.70)	18.7(10.3)

Figure 34 shows that $Q_{loss,C}$ and ΔT_C have a positive linear correlation. Data points scatter closely beside a line. The slope of the linear-regressed line, which is 115.47, can be used as the value of UA for the duct work. In other words, UA is found as115.47 Btu/hr·°F (0.06 kW/K). As physical characteristics of the duct work, this value remains unchanged when gas heating is operating.

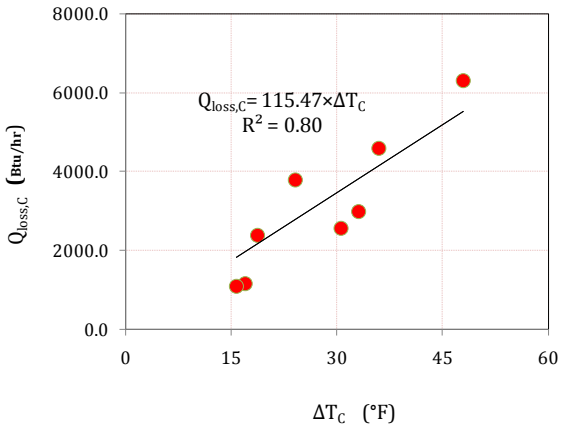

(a)

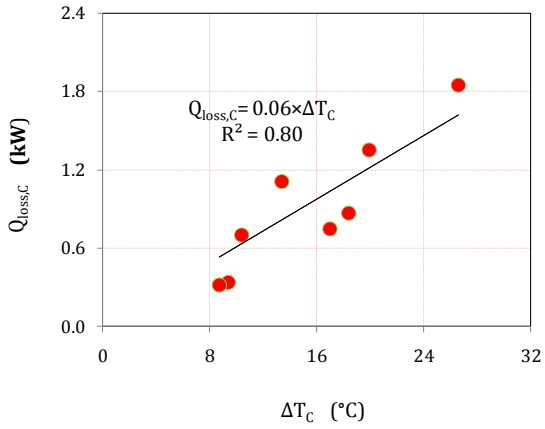

(b)

Figure 34: UA linear regression: (a) IP units and (b) SI units.

Step (2): Correlating $SAT_{exp,eva}$

As pointed out previously, with UA, $\dot{V}_{meas}$, $SAT_{O,H}$ and OAT known, $SAT_{exp,eva}$ could be obtained by jointly solving Equation (64) and (65),

$$Q_{loss,H} = \frac{\dot{V}_{meas} \times C_p \times (SAT_{exp,eva} - SAT_{O,H})}{v} \quad (64)$$

$$Q_{loss,H} = UA(OAT - \frac{SAT_{exp,eva} + SAT_{O,H}}{2}) \quad (65)$$

Then results of $SAT_{exp,eva}$ are summarized in Table 13. From this point on, $SAT_{exp,eva}$ can be used to evaluate the accuracy of $SAT_{mfr,cal}$.

Step (3): Evaluation of $SAT_{mfr,cal}$

To estimate the accuracy of $SAT_{mfr,cal}$, the error e_{eva} between $SAT_{mfr,cal}$ and $SAT_{exp,eva}$ given as Equation (66) is to be analyzed:

$$e_{eva} = SAT_{mfr,cal} - SAT_{exp,eva} \quad (66)$$

The results are gathered in Table 13. The error e_{eva} is within the range of ±1.1 °F (0.6 °C). Thus $SAT_{mfr,cal}$ is demonstrated credible and can be trusted as the true value of SAT in RTUs.

Table 13: Results of evaluation of $SAT_{mfr,cal}$

Scenario ID	$SAT_{exp,eva}$, °F (°C)	$\dot{V}_{meas}$,cfm (m^3/s)	$SAT_{mfr,cal}$, °F (°C)	e_{eva} , *°F (°C)*
H-1	108.6(42.6)	1848(0.87)	108.0(42.2)	***-0.6(-0.3)***
H-2	108.8(42.7)	2045(0.97)	108.3(42.4)	***-0.5(-0.3)***
H-3	110.1(43.4)	1857(0.88)	108.9(42.7)	***-1.1(-0.6)***
H-4	112.3(44.6)	1829(0.86)	111.8(44.3)	***-0.5(-0.3)***
H-5	92.4(33.6)	2076(0.98)	93.0(33.9)	***0.6(0.3)***
H-6	95.9(35.5)	2269(1.07)	96.7(35.9)	***0.7(0.4)***
H-7	98.4(37.3)	2037(0.96)	99.2(37.3)	***0.7(0.4)***
H-8	101.9(39.3)	2040(0.96)	102.7(39.3)	***0.8(0.4)***
H-9	95.2(35.1)	1853(0.87)	94.7(34.8)	***-0.5(-0.3)***
H-10	93.9(34.4)	2051(0.97)	93.2(34.0)	***-0.6(-0.3)***
H-11	96.7(35.9)	1849(0.87)	96.4(35.8)	***-0.3(-0.2)***
H-12	98.8(37.1)	1831(0.86)	99.6(37.6)	***0.8(0.4)***
H-13	80.8(27.1)	2081(0.98)	80.4(26.9)	***-0.4(-0.2)***
H-14	81.1(27.3)	2272(1.07)	82.1(27.8)	***1.0(0.6)***
H-15	85.5(29.7)	2059(0.97)	85.5(29.7)	***0.0(0.0)***
H-16	88.9(31.6)	2046(0.97)	88.7(31.5)	***-0.2(-0.1)***